In presenting the dissertation as a partial fulfillment of the requirements for an advanced degree from the Georgia Institute of Technology, I agree that the Library of the Institute shall make it available for inspection and circulation in accordance with its regulations governing materials of this type. I agree that permission to copy from, or to publish from, this dissertation may be granted by the professor under whose direction it was written, or, in his absence, by the Dean of the Graduate Division when such copying or publication is solely for scholarly purposes and does not involve potential financial gain. It is understood that any copying from, or publication of, this dissertation which involves potential financial gain will not be allowed without written permission.

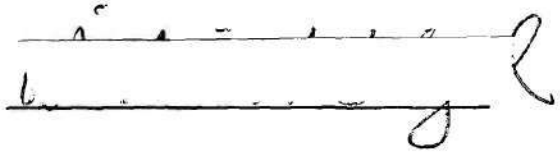

7/25/68

A STUDY OF THE VELOCITY PROFILE IN THE ENTRANCE REGION OF A MAGNETOHYDRODYNAMIC CHANNEL

A THESIS

Presented to

The Faculty of the Division of Graduate

Studies and Research

by

William Malcolm Flegal

In Partial Fulfillment

of the Requirements for the Degree

Doctor of Philosophy

in the School of Mechanical Engineering

Georgia Institute of Technology

December, 1970

A STUDY OF THE VELOCITY PROFILE

IN THE ENTRANCE REGION

OF A MAGNETOHYDRODYNAMIC CHANNEL

Approved:

Chairma

Date approved by Chairman: 2/16/70

ACKNOWLEDGEMENTS

It is with much appreciation that the assistance rendered to the author during the course of this work is acknowledged.

To Dr. W. O. Carlson, who has served as academic counselor as well as thesis advisor, the author expresses his thanks for the encouragement, advice, and support which he has given. The author is indebted to Dr. J. C. Wu and Dr. P. V. Desai who so graciously agreed to serve on the reading committee. Thanks are also extended to the School of Mechanical Engineering for the financial support which it has given this project. The assistance of Professor H. O. Foster in the acquisition of equipment is appreciated.

The author wishes to thank Messrs. J. W. Davis, R. G. Grim, L. A. Cavalli, B. L. Wallace, and H. J. Carr for their help in fabricating the experimental apparatus. A special note of thanks is due Mr. J. G. Doyal for his assistance in constructing the test stand and in procuring materials for the test apparatus.

The most heart-felt thanks also go to the author's parents for their love, encouragement, and support through these years of study. And a very special "thank you" goes to the author's wife, Penny, for her understanding, sacrifice, and love through all of this.

TABLE OF CONTENTS

TABLE OF CONTENTS (CONTINUED)

LIST OF ILLUSTRATIONS

LIST OF ILLUSTRATIONS (CONTINUED)

NOMENCLATURE

a	half-width of channel
A	cross-sectional area of channel, or parameter in series
b	half-height of channel
B	parameter in series
$\vec{B}$	magnetic induction
B_o	component of magnetic induction in z direction
C	parameter in series
C_1	parameter in series
C_m	constant in Fourier series
C_n	constant in Fourier series
C_{mn}	constant in Fourier series
dA	differential element of area
D	parameter in series
E_1	sum of series
E_2	sum of series
$\vec{E}$	electric field
Ex, Ey, Ez	components of electric field
F_1	sum of series
F_2	sum of series
$Ha=aB(\sigma/\eta)^{\frac{1}{2}}$	Hartmann number

I	magnet current
I_1	function of β
I_2	function of β
I_1'	non-dimensional function of β
I_2'	non-dimensional function of β
K	ratio of electric field to open-circuit electric field
m	integer
n	integer
P	pressure
r	integer
$Re_a = \frac{\bar{U}a}{\nu}$	Reynolds number based on channel half-width
S_1	sum of series
S_2	sum of series
S_3	sum of series
T_1	sum of series
u, v, w	velocity components in x, y, z directions
$\bar{U}$	average or entrance velocity
V	linear velocity
x, y, z	spatial coordinates
x', y', z'	non-dimensional axial coordinates
β	function of x
γ	aspect or width-to-height ratio

δ	boundary layer thickness
η	viscosity
η_o	reference viscosity
$\nu=\eta/e$	kinematic viscosity
e	density
e_o	reference density
σ	electrical conductivity
ω	angular velocity

SUBSCRIPTS

fd	fully developed
o	value evaluated a centerline
t_1	tangential directions in material 1
t_2	tangential direction in material 2

SUMMARY

The change in the velocity profile of a conducting fluid as it flows through a rectangular channel in the presence of electric and magnetic fields was investigated both analytically and experimentally for channels with height-to-width ratios of 6-to-1 and 4-to-1. The influence of the Hartmann number on the development of the velocity profile was studied also.

The analytical investigation involved linearizing the differential equation of motion, expressing the velocity as a Fourier series in two variables, substituting this series in the differential equation, and solving for the Fourier constants. An unknown function of axial position, which was introduced in the linearization process and which appears in the series solution for the velocity, was evaluated by integrating across the channel cross-section and then solving the resultant differential equation in the axial variable. Numerical results were obtained by using a high-speed digital computer.

An experimental investigation was conducted for two rectangular channels, using potassium chloride solution as the working fluid. Tests were run at four different Hartmann numbers for each channel. The maximum Hartmann numbers attainable were 2.0 for the 6-to-1 channel and 2.9 for the 4-to-1 channel.

The agreement of the experimental data with the analytical results was quite good, being within approximately 5% to 8% at all times. The influence of the Hartmann number and channel aspect ratio on the velocity profile development

was observed. It was found that the rate of velocity development increases for a given channel with increasing Hartmann number. At a given Hartmann number, the velocity profile developed more slowly for the 4-to-1 channel than for the 6-to-1 channel. The electric field strength was found to have no measurable influence on the velocity profile or its development.

CHAPTER I

INTRODUCTION

Whenever a viscous fluid enters a duct, it is subjected to forces which tend to retard portions of the flow and to accelerate others. These forces consist of the viscous shear force, the pressure gradient, the inertia force, and, in some cases, the Lorentz force. Eventually, if the channel is of sufficient length for a given set of flow parameters, all of the forces listed above will come into balance and the fluid will assume a velocity profile across the duct which does not change with respect to the direction of motion. Such flow is called fully developed flow. The region in which the flow adjusts from its initial profile to the fully developed one is called the hydrodynamic entrance region. In this region, the friction factor and wall shear stress are also functions of distance along the duct axis unlike in the fully developed region where they are constant.

A study of the velocity field and friction factor in the entrance region of a duct is of practical importance and has been a subject of investigation for many years. In general, the purpose of these investigations is to obtain expressions for the velocity distribution at any cross-section of the duct, the friction factor for the entrance region, and the value of the axial position where fully developed flow is attained. A knowledge of these quantities is important for the proper design of flow devices which contain ducts or pipes in which the entrance

region covers a significant portion of the total duct length.

With the increased interest in magnetohydrodynamics (MHD) in the last decade, it was only natural that attention be directed to the entrance region in MHD channels. Several considerations dictate that generating channels be kept as short as possible. Thus it seems likely that fully developed flow may never be attained, making the entrance region of prime importance.

Although the governing differential equations for the entrance region may be easily written, their exact solutions have so far not been found. The development of the boundary layer theory by Prandtl simplified the equations of motion for the entrance region considerably. Unfortunately, no exact solution to these simplified equations has been found either. It has been necessary to turn to approximate methods in order to obtain solutions for the entrance flow problem. These approximate methods are described in the following section. Experimental work has been conducted for a number of geometries and compares well with the analytical results.

Scientific Background

The entrance region has been a subject of investigation for over a century. Hagenback (1), in 1860, attempted to predict the total pressure drop involved in the passage of a fluid from a place of negligible velocity in a reservoir to the place where the velocity profile becomes parabolic. In 1890 and 1891, Boussinesq (2) published an analysis of this flow problem. It was some forty years later, when several German scientists began investigating the problem, that significant progress was made. These investigators, faced with the task of

trying to solve the equations of motion, began to look for approximate methods which would yield satisfactory results. From their efforts, and those of later investigators, four distinct methods emerged, all yielding suprisingly similar results. These approximate solutions may be classified as the momentum integral, matching, linearization and finite difference methods. While each of these methods was originally applied to a non-MHD flow, they have been modified to provide a description of the entrance region in an MHD channel as well. In addition to analytical studies, some attempts have been made to measure experimentally velocity profiles and pressure gradients in the entrance regions.

Analytical Studies

The momentum integral method of analysis was first applied by Schiller (3) in 1922 for flow in a circular tube. In this method, the flow is divided into a boundary layer part near the wall and a potential flow part in the central core. A velocity profile of some appropriate shape is assumed in the boundary layer and is joined with the velocity profile of the central core which is assumed to be that of a potential flow. In general, solutions are found by integrating the equations of motion in two steps: first, in the direction normal to the wall using the assumed velocity distribution and then secondly, in the flow direction where a new dependent variable, the boundary layer thickness, arises as a result of the first integration. The results depend a great deal on the velocity profile which is assumed for the boundary layer. Siegel (4) reworked Schiller's solution using both a cubic and a quartic representation for the velocity profile in the boundary layer. Shapiro, Siegel and Kline (5) allowed for velocity profile variations with pressure gradient.

Campbell and Slattery (6) repeated Schiller's calculations but obtained the pressure at each cross section from a consideration of a mechanical energy balance on all the fluid in the tube, taking into account the energy loss due to viscous dissipation. The entrance problem in a flat duct was treated in the same manner by Gupta (7). McComas (8) developed a method to estimate the entrance length in a duct of arbitrary cross-section which requires only a knowledge of the fully developed velocity profile. This method is approximate and predicts entrance lengths shorter than those of other methods. The entrance length and the velocity development coefficient (K) may be found by this method.

Application of the momentum integral method to MHD flows has been made by a number of authors, all for the parallel-plate channel case. Moffatt (9) utilized a boundary layer profile similar to that profile which exists in fully developed Hartmann flow. Maciulaitis and Loeffler (10) extended Moffatt's work to include variation of the free-stream velocity in the flow direction. They also treated the case of a nonmagnetically fully developed profile at the channel entry plane. Tan (11) also used a Hartmann-like velocity distribution in his analysis. A summary of results from this method for linear, parabolic, cubic, and Hartmann profiles is given by Zalosh (12). An extension of this method to account for Reynolds stresses in turbulent flow has been developed by Schwirian (13). The validity of the momentum integral method as applied to MHD channel flows has been investigated by Heywood and Moffatt (14). Their conclusion was that under proper interpretation, the momentum integral method yields results that compare favorably with analytical solutions obtained by other methods.

The second method of solution involves matching two series solutions, each series being derived for a particular region of the flow. Schlichting (15) developed this method for a flat duct. In the section near the inlet, a boundary layer formulation of equations is used and a solution is developed in a series of stream functions with Blasius functions as coefficients. Downstream, the flow field is assumed to be described by a series solution representing a perturbation on the fully developed velocity profile. The flow development throughout the entrance region is found by patching together the upstream and downstream solutions at some intermediate location. Further development of this method was carried out by Collins and Schowalter (16) who carried more terms in the expansion. Roidt and Cess (17) applied this method to the MHD entrance problem.

The third method of analysis involves a linearization of the inertia terms in the equations of motion. With this approach, a boundary layer model is not necessary. Instead, velocity solutions are obtained which are continuous over the cross section and along the channel length all the way from the duct entrance to the fully developed region. Langhaar (18) was the first to utilize this method. He replaced the inertia term in the Navier-Stokes equation for the axial direction in a tube by a linear relationship which made it possible to obtain a closed-form solution for the velocity. Han (19) extended the method to flow through a rectangular duct. Sparrow, Lin and Lundgren (20) linearized the momentum equation by introducing a weighting function for the mean velocity, an undetermined function that includes the pressure gradient and the residual of the inertia terms, and a new stretched coordinate in the direction of the flow. Fleming (21) used this method

to obtain velocity profiles and pressure drops for rectangular ducts of five to one and two to one aspect ratio. Snyder (22) extended this method to the MHD flow case with a uniform velocity at the channel entrance. Goins (23) considered the case of parabolic entrance profile and utilized this method. Snyder and Eraslan (24) added the influence of the Hall effect in their solution utilizing the linearization technique.

With the development of electronic digital computers, several investigators utilized numerical techniques to obtain solutions to the entrance flow problem. Bodia and Osterle (25) reduced the continuity and momentum equations to finite difference equations and solved these numerically for a uniform entrance profile. Wang and Longwell (26) solved the Navier-Stokes equations numerically after introducing the stream function and vorticity into the equations. Finite difference techniques were first applied to the MHD entrance flow problem by Shohet, Osterle, and Young (27). They also obtained temperature profiles in the entrance region. Hwang and Fan (28) have solved the same problem by finite difference techniques. Brandt and Gillis (29) have solved the problem of an incompressible fluid with constant properties and uniform entrance velocity in the Reynolds number range from 0 to 500. The complete equations are solved numerically without any approximating assumptions. The case of incompressible, constant property flow with a parabolic velocity at the entrance was treated by Hwang, Li, and Fan (30). As might be expected, the entrance length for a parabolic velocity profile is larger than that for the uniform entrance profile at the higher Hartmann numbers.

Shercliff (31) developed an approximate method for solving the MHD entry

problem in circular pipes which does not involve any of the previously mentioned methods. He did not arrive at velocity profiles explicitly. The method is not precise and has not been pursued further.

So far, all the works reviewed have involved incompressible flow. Hale and Kerrebrock (32) considered compressible flow with a variable conductivity in an accelerator. Many restrictions were assumed for obtaining a similar solution. Hwang, Fan, and Hwang (33) presented an analysis of two dimensional, steady-state, laminar compressible flow in a duct. The compressible boundary layer equations are reduced to ordinary differential equations which are solved simultaneously by numerical integration. Flow characteristics investigated include growth of the boundary layers, development of velocity and temperature profiles, the skin friction, and the heat transfer.

Experimental Studies

In 1922, Schiller (3) investigated the entrance region experimentally. He found friction factors in the entrance region of a tube. Schiller and Kirsten (34) used a pitot tube to experimentally determine velocity profiles at various axial stations along a tube. Shapiro and Smith (35) investigated the friction factor in the inlet region of smooth, round tubes in the range of Reynolds numbers from 31,000 to 590,000 using water and air at low Mach number as the working fluids. Deissler (36) studied the development of turbulent flow in an adiabatic, smooth tube. Velocity profiles in supersonic flow in a tube were measured by Kaye, Brown, Dieckmann, and Sziklas (37) using an impact probe. For ducts of rectangular and triangular cross section, Irvine and Eckert (38) used wall pressure taps to determine friction

factors in developing flow. Olsen and Sparrow (39), using static-pressure measurements, investigated the entrance length in tubes and annuli with square or rounded entrances in the Reynolds number range from 16,000 to 70,000. For the Reynolds number range from 200 to 600, McComas and Eckert (40) determined experimentally the pressure drop in the entrance region of an abrupt inlet circular tube. In addition, the friction factor was also obtained. Berman and Santos (41) have investigated flow development in a tube at low Reynolds number using a laser. They obtained velocity profiles for various axial positions along the tube. Velocity profiles in a tube were measured by Atkinson, Kemblowski, and Smith (42) using neutral density particles and a photographic technique.

Flow development in rectangular ducts has been investigated in two separate works. Sparrow, Hixon, and Shavit (43) investigated the entrance region in rectangular channels of aspect ratio five to one and two to one. They used air as the working fluid and pitot tubes to measure velocity. They also obtained static pressure measurements along the channel axis. Goldstein and Kreid (44) utilized a laser-Doppler flowmeter to measure velocity profiles in a square channel. Their working fluid was water with small polystyrene particles added to obtain the Doppler shift.

Hartmann and Lazarus (45) performed experiments in 1937 involving the flow of mercury through rectangular ducts in the presence of a magnetic field. They measured pressure drops for various Reynolds numbers and various Hartmann numbers. Murgatroyd (46) investigated the flow of mercury in a rectangular channel with a magnetic field imposed. He measured pressures at the wall and obtained

friction factors and pressure gradients. He investigated the turbulent regime. Maciulaitis, Loeffler, and Calcanes (47) have studied friction factors at high Reynolds and Hartmann numbers in the entrance region up to the fully developed region of a tube, using mercury as a working fluid. Khozhainov (48) also used mercury in his study of the development of the velocity profile in a square channel using Hall probes. No velocity profiles were actually measured, however. Snyder and Eraslan (24), using a potassium chloride solution, attempted to obtain velocity profiles in the entrance region. They attempted to use a pitot tube as their velocity measuring device. Due to the very slow response time of their micromanometer, they were able to obtain only a few static pressure measurements along the channel, none in the presence of a magnetic field.

The purpose of this investigation was to obtain data in the entrance region of a rectangular channel under the influence of magnetic and electric fields. This situation has not been investigated previously. In addition, it was necessary to develop an approximate solution for the entrance region which took into account the finite width of the channel, an effect that has been neglected in all other solutions for the MHD case. The experimental results agreed well with this solution.

CHAPTER II

AN ANALYTICAL STUDY OF MHD CHANNEL FLOW

In all MHD entrance flow solutions which have been reviewed, the assumption has been made that the channel is of infinite extent in the direction perpendicular to the applied magnetic field. This assumption was necessary to reduce the problem from a three-dimensional to a two-dimensional one. With the channel aspect ratio defined as the ratio of the width to the height, an infinite height channel has an aspect ratio of zero. In practice, an aspect ratio of zero cannot be realized. Thus, it was necessary to seek an analytical solution which would take into account the finite height of the channel. Han (19) developed a technique for the entrance region of channels with non-zero aspect ratios in the absence of the Lorentz force. By extending this work to include the Lorentz force, it is possible to obtain an approximate solution for the finite height MHD channel. Figure 1 shows the duct configuration to be investigated.

In order to simplify the problem as much as possible, a number of assumptions have been made. The fluid is assumed to be incompressible and to have constant physical properties. The Hall parameter and magnetic Reynolds number are taken to be small. This latter assumption makes it possible to neglect the induced magnetic field. The validity of these assumptions for the flow situation under investigation will be discussed more fully in Chapter III. It is also assumed that the applied electric field is in the direction perpendicular to the applied

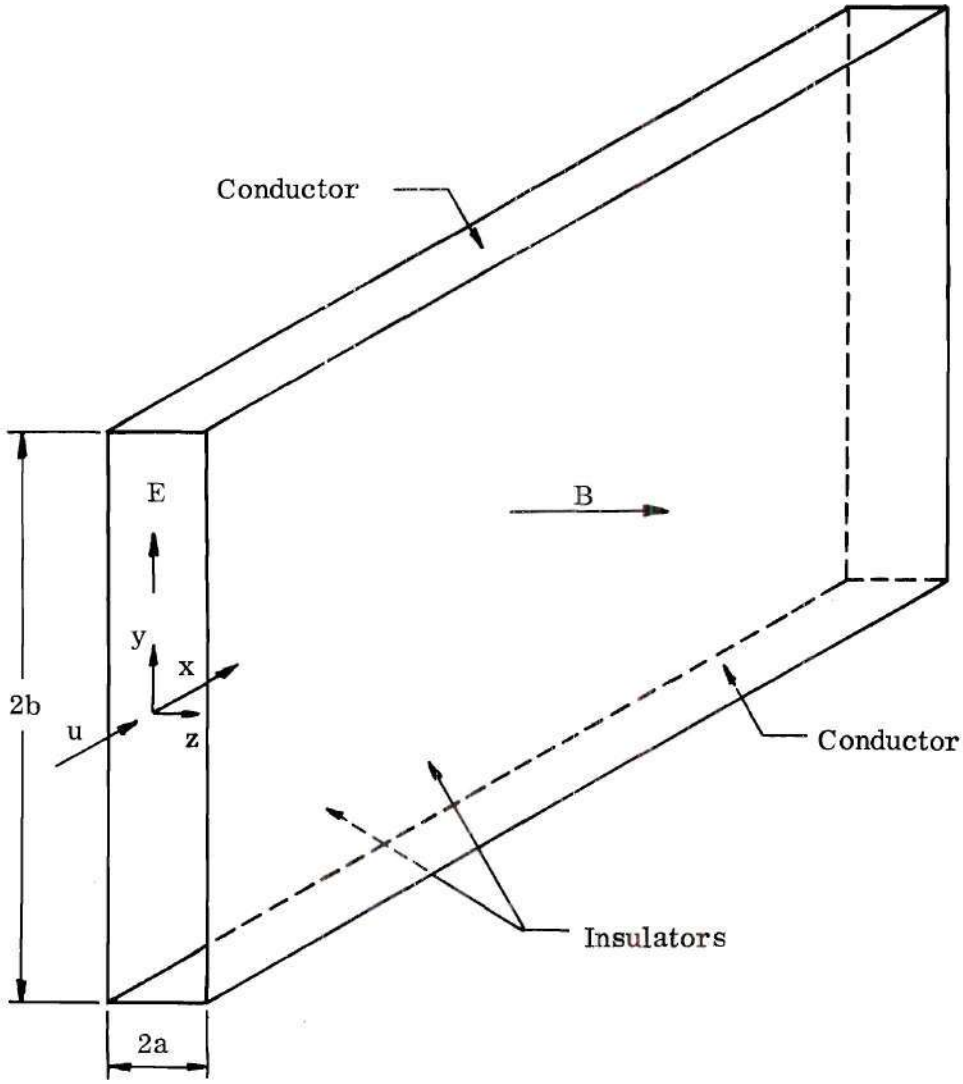

Figure 1. Channel Geometry.

magnetic field and it is shown in Appendix A that this field is constant across the channel.

The equation of motion in the axial direction is

$$u\frac{\partial u}{\partial x}+v\frac{\partial u}{\partial y}+w\frac{\partial u}{\partial z}=-\frac{1}{\rho}\frac{\partial P}{\partial x}+\nu\left(\frac{\partial^2 u}{\partial x^2}+\frac{\partial^2 u}{\partial y^2}+\frac{\partial^2 u}{\partial z^2}\right)+\frac{\sigma B_o}{\rho}(E_y-uB_o) \qquad (1)$$

where the additional assumption of steady flow has been made and Ohm's Law has been incorporated into the Lorentz force. As in the analyses of Langhaar (18), Han (19), and Fleming (21), the following simplifications are introduced:

1. The term $\frac{\partial^2 u}{\partial x^2}$ may be dropped in comparison to the terms $\frac{\partial^2 u}{\partial y^2}$ and $\frac{\partial^2 u}{\partial z^2}$.

2. The pressure gradient $\frac{\partial P}{\partial x}$ is independent of cross-sectional coordinates and is a function of x only.

Despite these simplifications, an exact solution to equation (1) has not been found, mainly due to the presence of the non-linear inertia terms on the left hand side. Langhaar (18) proposed that these terms be replaced by the linear expression

$$u\frac{\partial u}{\partial x}+v\frac{\partial u}{\partial y}+w\frac{\partial u}{\partial z}=\nu\beta^2 u \qquad (2)$$

where β is a function of x only. The equation of motion may now be written

$$\nu\beta^2 u=-\frac{1}{\rho}\frac{\partial P}{\partial x}+\nu\left(\frac{\partial^2 u}{\partial y^2}+\frac{\partial^2 u}{\partial z^2}\right)+\frac{\sigma B_o}{\rho}(E_y-uB_o) \qquad (3)$$

The use of equation (2) can be partially justified on theoretical grounds.

It is obvious that for $\beta = 0$ the equation of motion reduces to that for a fully developed flow. Equation (2) is also satisfied for all values of β at points on the channel boundaries since u, v, and w all must vanish at these surfaces. If it is assumed that the laminar state is attained by the development of a boundary layer in the transition length, it follows that equation (2) is satisfied at all points in the undisturbed central core. This conclusion is based on the fact that the derivatives $\frac{\partial u}{\partial y}$ and $\frac{\partial u}{\partial z}$ vanish over the flat portions of the velocity profiles and equation (2) reduces to

$$\frac{\partial u}{\partial x} = \nu \beta^2 \tag{4}$$

Since u is a function of x alone in the core, β is likewise a function of x alone in that region, and it follows that equation (4) is valid. Finally, it may be concluded that equation (2) is valid over the entrance section since the depth of the boundary layer reduces to zero at this point. Thus there is considerable justification for the use of equation (2).

Determination of Velocity

In order to get an explicit relation for the velocity, it is convenient to rewrite equation (3) as

$$\nu \beta^2 u + \frac{1}{e} \frac{\partial P}{\partial x} = \nu \left(\frac{\partial^2 u}{\partial y^2} + \frac{\partial^2 u}{\partial z^2} \right) - \frac{\sigma B_o^2}{e} (u - K\bar{U}) \tag{5}$$

where

$$K = Ey/\bar{U}B_o \tag{6}$$

and $\bar{U}$ is the space-average or entrance velocity. The velocity may now be expressed as

$$u = \sum_{m \text{ odd}}^{\infty} \sum_{n \text{ odd}}^{\infty} C_{mn} \cos\left(\frac{m\pi z}{2a}\right)\cos\left(\frac{n\pi y}{2b}\right) \tag{7}$$

where C_{mn} are constants to be determined. Since the velocity u is to satisfy the condition of zero velocity on $z = \pm a$ and $y = \pm b$, the even-valued terms of the Fourier series have been omitted as they would violate this condition. Now, it is shown in Appendix C that

$$\sum_{m \text{ odd}}^{\infty} \sum_{n \text{ odd}}^{\infty} \left(\frac{1}{mn}\right)(-1)^{\frac{m+n}{2}-1} \cos\left(\frac{m\pi z}{2a}\right) \cos\left(\frac{n\pi y}{2b}\right) = \pi^2/16 \tag{8}$$

Using equation (8), the terms $\frac{1}{e}\frac{\partial P}{\partial x}$ and $\frac{\sigma B_o^2}{e} K\bar{U}$ in equation (5) may be written

$$\frac{1}{e}\frac{\partial P}{\partial x} = \frac{16}{\pi^2}\left(\frac{1}{e}\frac{\partial P}{\partial x}\right) \sum_{m \text{ odd}}^{\infty} \sum_{n \text{ odd}}^{\infty} \left(\frac{1}{mn}\right)(-1)^{\frac{m+n}{2}-1} \cos\left(\frac{m\pi z}{2a}\right)\cos\left(\frac{n\pi y}{2b}\right) \tag{9}$$

and

$$\frac{\sigma B_o^2}{e} K\bar{U} = \frac{16}{\pi^2}\left(\frac{\sigma B_o^2 K\bar{U}}{e}\right) \sum_{m \text{ odd}}^{\infty} \sum_{n \text{ odd}}^{\infty} \left(\frac{1}{mn}\right)(-1)^{\frac{m+n}{2}-1} \cos\left(\frac{m\pi z}{2a}\right)\cos\left(\frac{n\pi y}{2b}\right) \tag{10}$$

Substituting equations (7), (9), and (10) into equation (5) yields

$$\sum_{m\ \text{odd}}^{\infty} \sum_{n\ \text{odd}}^{\infty} \left\{ C_{mn}\left[\nu\beta^2 + \nu\left(\frac{m\pi}{2a}\right)^2 + \nu\left(\frac{n\pi}{2b}\right)^2 + \frac{\sigma B_o^2}{e} \right] + \left(\frac{1}{e}\frac{\partial P}{\partial x} - \frac{\sigma B_o^2}{e} K\bar{U}\right)\left(\frac{16}{\pi^2}\right)\left(\frac{1}{mn}\right)\left(-1\right)^{\frac{m+n}{2}-1} \right\} \cos\left(\frac{m\pi z}{2a}\right) \cos\left(\frac{n\pi y}{2b}\right) = 0 \tag{11}$$

For the sum above to be identically zero for all y and z, the quantity in the bracket must be identically zero. Therefore,

$$C_{mn} = \frac{-\left(\frac{1}{e}\frac{\partial P}{\partial x} - \frac{\sigma B_o^2}{e} K\bar{U}\right)\left(16/\pi^2\right)\left(\frac{1}{mn}\right)\left(-1\right)^{\frac{m+n}{2}-1}}{\nu\left[\beta^2 + \left(\frac{m\pi}{2a}\right)^2 + \left(\frac{n\pi}{2b}\right)^2 + \frac{\sigma B_o^2}{\eta}\right]} \tag{12}$$

By using the continuity expression

$$\int_A u\, dA = 4ab\bar{U} \tag{13}$$

it is possible to eliminate the pressure gradient and electric field from the expression for the velocity. Integrating u over the cross section yields

$$\bar{U} = \frac{4}{\pi^2} \sum_{m\ \text{odd}}^{\infty} \sum_{n\ \text{odd}}^{\infty} C_{mn}\left(\frac{1}{mn}\right)\left(-1\right)^{\frac{m+n}{2}-1} \tag{14}$$

Dividing u by $\bar{U}$ yields

$$\frac{u}{\bar{U}} = \frac{\pi^2}{4} \quad \frac{\sum_{m\ \text{odd}}^{\infty} \sum_{n\ \text{odd}}^{\infty} \frac{(-1)^{\frac{m+n}{2}-1} \cos\left(\frac{m\pi z}{2a}\right) \cos\left(\frac{n\pi y}{2b}\right)}{\left[\left(\frac{2\beta a}{\pi}\right)^2 + m^2 + \gamma^2 n^2 + (2Ha/\pi)^2\right]}}{\sum_{m\ \text{odd}}^{\infty} \sum_{n\ \text{odd}}^{\infty} \frac{1}{m^2 n^2 \left[m^2 + \gamma^2 n^2 + \left(\frac{2\beta a}{\pi}\right)^2 + (2Ha/\pi)^2\right]}} \tag{15}$$

where

$$\gamma = \frac{a}{b} \tag{16}$$

is the aspect ratio and

$$Ha = aB_o(\sigma/\eta)^{\frac{1}{2}} \tag{17}$$

is the Hartmann number. By manipulating these series it is possible to reduce them from doubly infinite series to singly infinite series. The details of this procedure are given in Appendix B. The result is

$$u/\bar{U} = F_1/F_2 \tag{18}$$

where

$$F_1 = \left[\frac{1}{(\beta a)^2 + Ha^2}\right]\left[\frac{\cosh\{[(\beta a)^2 + Ha^2]^{\frac{1}{2}} z/a\}}{\cosh\{[(\beta a)^2 + Ha^2]^{\frac{1}{2}}\}} - 1\right]$$

$$+\frac{16}{\pi^3}\sum_{m\ \text{odd}}^{\infty}\frac{(-1)^{\frac{m-1}{2}}\cos\left(\frac{m\pi z}{2a}\right)\cosh\left\{\frac{\pi}{2\gamma}\left[\left(\frac{2\beta a}{\pi}\right)^2+\left(\frac{2Ha}{\pi}\right)^2+m^2\right]^{\frac{1}{2}}\frac{y}{b}\right\}}{m\left[\left(\frac{2\beta a}{\pi}\right)^2+\left(\frac{2Ha}{\pi}\right)^2+m^2\right]\cosh\left\{\frac{\pi}{2\gamma}\left[\left(\frac{2\beta a}{\pi}\right)^2+\left(\frac{2Ha}{\pi}\right)^2+m^2\right]^{\frac{1}{2}}\right\}} \tag{19}$$

and

$$F_2=\left[\frac{1}{(\beta a)^2+Ha^2}\right]\left[\frac{\tanh\left\{\left[(\beta a)^2+Ha^2\right]^{\frac{1}{2}}\right\}}{\left[(\beta a)^2+Ha^2\right]^{\frac{1}{2}}}-1\right]$$

$$+\frac{32}{\pi^4}\sum_{m\ \text{odd}}^{\infty}\frac{\tanh\left\{\frac{\pi}{2\gamma}\left[m^2+\left(\frac{2\beta a}{\pi}\right)^2+\left(\frac{2Ha}{\pi}\right)^2\right]^{\frac{1}{2}}\right\}}{m^2\left[m^2+\left(\frac{2\beta a}{\pi}\right)^2+\left(\frac{2Ha}{\pi}\right)^2\right]\left(\frac{\pi}{2\gamma}\right)\left[m^2+\left(\frac{2\beta a}{\pi}\right)^2+\left(\frac{2Ha}{\pi}\right)^2\right]^{\frac{1}{2}}} \tag{20}$$

Uniform convergence of the above series is established in Appendix C.

It may also be shown that as β approaches infinity, $u/\bar{U}$ approaches 1, the condition of uniform entrance profile which was imposed earlier. Taking the limit of (15) as $\beta a \to \infty$ yields

$$\lim_{\beta a\to\infty} u/\bar{U}=\frac{\pi^2}{4}\ \frac{\sum_{m\ \text{odd}}^{\infty}\sum_{n\ \text{odd}}^{\infty}(-1)^{\frac{m+n}{2}-1}\left(\frac{1}{mn}\right)\cos\left(\frac{m\pi z}{2a}\right)\cos\left(\frac{n\pi y}{2b}\right)}{\sum_{m\ \text{odd}}^{\infty}\sum_{n\ \text{odd}}^{\infty}\frac{1}{m^2n^2}}$$

$$=\frac{\pi^2}{4}\left\{\frac{\pi^2/16}{\pi^4/64}\right\}=1$$

where the values of the infinite sums have been taken from Appendix C. Thus, it is seen that for x=0, βa should approach infinity to correspond to a uniform profile at the channel entrance. Since it has previously been stated that for β=0 the equation of motion reduces to that for fully developed flow, it is obvious that the use of equation (15), where β varies from infinite to zero, yields a smooth transition from a uniform entrance profile to a fully developed one. All that remains to be done is to find the relationship between β and x.

Variation of β-values with x

So far, an expression for the velocity at any value of $|y|<b$ or $|z|<a$ has been found. These velocities are functions of the parameter β which has not yet been determined. The relationship between β and the axial position will now be sought.

The two relationships between x and β which have already been pointed out are at the entrance,

$$x = 0,\ (u/\bar{U}) = 1 \quad \text{or} \quad \beta \to \infty \tag{21}$$

and for fully developed flow

$$x \to \infty, (u/\bar{U}) \to (u/\bar{U})_{fd} \text{ or } \beta = 0 \tag{22}$$

At the center line of the duct, the equation of motion (1) is localized to yield

$$u_o \frac{\partial u_o}{\partial x} = \frac{1}{\rho} \frac{\partial P}{\partial x} + \nu (\nabla^2 u)_o + \frac{\sigma B_o^2}{\rho} (K\bar{U} - u_o) \tag{23}$$

where

$$\nabla^2 = \frac{\partial^2}{\partial y^2} + \frac{\partial^2}{\partial z^2} \tag{24}$$

On multiplying by dydz and integrating across the cross section, the result is

$$\frac{\partial}{\partial x}\int_A \frac{u_o^2}{2}\,dA = -\frac{1}{e}\frac{\partial P}{\partial x}\int_A dydz + \nu\int_A (\nabla^2 u)_o\,dA$$

$$+ \frac{\sigma B_o^2}{e}\left(K\bar{U}\int_A dydz - \int_A U_o\,dA\right) \tag{25}$$

The Von Karman integral equation, which is derived in Appendix A, is

$$\frac{\partial}{\partial x}\int_A u^2 dA = -\frac{1}{e}\frac{\partial P}{\partial x}\int_A dydz + \nu\int_A (\nabla^2 u)\,dA$$

$$+ \frac{\sigma B_o^2}{e}\left(K\bar{U}\int_A dydz - \int_A u dA\right) \tag{26}$$

On subtracting (25) from (26), the result is

$$\frac{\partial}{\partial x}\int_A \left(u^2 - \frac{u_o^2}{2}\right)dA = \nu\int_A \left(\nabla^2 u - \left(\nabla^2 u\right)_o\right)dA - \frac{\sigma B_o^2}{e}\int_A (u - u_o)\,dA \tag{27}$$

It should be noted that all terms in equation (27) are now functions of β only, the y and z dependence having been eliminated by the integration procedure. Using

the following notation

$$I_1(\beta) = \int_A \left(u^2 - u_o^2/2\right) dA \tag{28}$$

and

$$I_2(\beta) = \left\{\int_A \left[\nu\left(\nabla^2 u - \left(\nabla^2 u\right)_o\right) - \frac{\sigma B_o^2}{e}(u-u_o)\right] dA\right\}^{-1} \tag{29}$$

equation (27) may be written

$$\frac{d}{dx}(I_1) = \frac{1}{I_2} \tag{30}$$

or

$$\int_o^x dx = \int_{\beta=\infty}^{\beta} I_2 \, dI_1 \tag{31}$$

or

$$x = \int_{\beta=\infty}^{\beta} I_2 \, dI_1 \tag{32}$$

Thus a direct relationship between x and β has been established. The procedure for evaluating (32) may be outlined as follows:

(1) Assign a series of β-values to equation (18).

(2) Calculate the integrands I_1 and I_2.

(3) Numerically integrate equation (32); i.e., calculate the area under the I_2-I_1 curve. This area represents the value of x corresponding to the β value at the end of the integration.

The β value also determines the ratio of the centerline velocity to the entrance

velocity. The relationship between x, $(u/\bar{U})_o$, and β is therefore determined.

Evaluation of I_1, I_2, and x

The evaluation of I_1 and I_2 from equations (28) and (29) involves expressing u as a function of β, y, and z by use of equations (18), (19), and (20), performing the indicated operations, and then integrating across the cross section.

Substitution of (18) into (28) and (29) yields

$$I_1(\beta) = \frac{\bar{U}^2}{F_2^2} \int_A F_1^2 dzdy - \frac{\bar{U}^2}{F_2^2}\left(F_1|_o\right)^2 (2ab) \tag{33}$$

and

$$I_2(\beta) = \left(\frac{\nu \bar{U}}{F_2}\right)^{-1} \left\{ \int_A \left[\nabla^2 F_1 - \left(\nabla^2 F_1\right)_o\right] dzdy \right.$$

$$\left. - \frac{\sigma B_o^2}{\eta} \int_A \left(F_1 - F_1|_o\right) dzdy \right\}^{-1} \tag{34}$$

where F_1 is given by (19), F_2 by (20), ∇^2 by (24), and $F_1|_o$ represents (19) evaluated at the duct centerline. F_2 may be removed from inside the integral since it does not depend on y or z. Since F_1 involves infinite series, the calculation of the integrals becomes somewhat involved and the details are given in Appendix D. Because of the uniform convergence of F_1, it is possible to perform the necessary differentiations and integrations.

The result of these operations is

$$I_1(\beta) = \left(\frac{a^2 \bar{U}^2}{F_2^2}\right)\left\{\frac{2}{\gamma C^4}\left(\frac{1}{\cosh^2(C)} - \frac{3\tanh(C)}{C}\right) + \frac{4}{\gamma C^4}\right.$$

$$- \frac{1536}{\pi^7} \sum_{m \text{ odd}}^{\infty} \frac{\tanh(B)}{m^2 A^5} + \frac{256}{6\pi\gamma} \sum_{m \text{ odd}}^{\infty} \frac{1}{m^2 A^4 \cosh^2(B)} \qquad (35)$$

$$\left. - \frac{2}{\gamma}\left(F_1|_o\right)^2\right\}$$

and

$$I_2(\beta) = \left(\frac{F_2}{\nu \bar{U}}\right)\left\{\frac{64}{\pi^3} \sum_{m \text{ odd}}^{\infty} \frac{\tanh(B)}{A}\left(\frac{1}{m^2} - \frac{1}{A^2}\right) + \frac{4}{C\gamma}\left(\tanh(C)\right.\right.$$

$$\left. - \frac{C}{\cosh(C)}\right) - \frac{16}{\pi\gamma} \sum_{m \text{ odd}}^{\infty} \frac{(-1)^{\frac{m-1}{2}}}{\cosh(B)}\left(\frac{1}{m} - \frac{m}{A^2}\right)$$

$$\left. - \frac{4H_a^2}{\gamma}\left(F_2 - F_1|_o\right)\right\}^{-1} \qquad (36)$$

where

$$C = \left[(\beta a)^2 + H_a^2\right]^{\frac{1}{2}} \qquad (37)$$

$$A = \left[\left(\frac{2\beta a}{\pi}\right)^2 + \left(\frac{2Ha}{\pi}\right)^2 + m^2\right]^{\frac{1}{2}} \qquad (38)$$

$$B = \frac{\pi}{2\gamma} A \qquad (39)$$

Two new non-dimensional functions are introduced by defining

$$I_1'(\beta) = \frac{I_1(\beta)}{a^2 \bar{U}^2} \tag{40}$$

and

$$I_2'(\beta) = \nu \bar{U} I_2(\beta) \tag{41}$$

Substituting these variables in (32) gives

$$x = \int_{\beta=\infty}^{\beta} \frac{I_2'(\beta)}{\nu \bar{U}} (a^2 \bar{U}^2)\, dI_1'(\beta) = \frac{a^2 \bar{U}}{\nu} \int_{\beta=\infty}^{\beta} I_2'(\beta)\, dI_1'(\beta) \tag{42}$$

or

$$x' = \frac{x/a}{\bar{U}a/\nu} = \frac{x/a}{Re_a} = \int_{\beta=\infty}^{\beta} I_2'(\beta)\, dI_1'(\beta) \tag{43}$$

where x' is a non-dimensional axial distance. Thus, equation (43) gives the relationship between x' and β.

Numerical Results

Functional relationships between the velocity, axial position and the parameter β have been determined in equations (18) and (43). It is now possible to calculate the velocity profile at any given position down the channel. Because of the nature of equations (18) and (43), it is necessary to carry out these calculations on a digital computer. The equations were programmed for the Burroughs 5500 digital computer at the Rich Electronic Computer Center.

The first step in the calculations involved assigning values to the Hartmann number and to the aspect ratio. With these parameters assigned, thirty-five values of βa were read by the computer. The parameter βa was used instead of just β because the equations all contained the former parameter. The values of βa used ranged from 20 to 0.1 in unevenly spaced increments. The spacing was chosen to attempt to minimize the error in calculating x'. The values of z and y were also read by the computer. The centerline position was always used as the initial point for the program. This facilitated the calculation of I_1' and I_2' and thus x'.

Knowing the Hartmann number, aspect ratio, the parameter βa, and the cross-sectional position in the channel, the non-dimensional velocity at the chosen position could be determined immediately from equations (18), (19), and (20). For the centerline position, the next step was to calculate the values of I_1' and I_2' corresponding to this particular value of βa. It was now necessary to calculate the area under the $I_1' - I_2'$ curve. The area was evaluated numerically by using the trapezoidal rule for the area between two successive βa values and adding this incremental area to that previously accumulated. The result was the value of x' corresponding to the given βa. Since the relationship between x' and βa is unique, it was necessary to calculate the $x' - \beta a$ relationship only once for a given set of conditions. Velocities at points other than on the centerline could now be found for all values of βa and hence x'.

One hundred terms were carried in the summation of all series. Because of the rapid convergence of the series, the error involved in neglecting the higher

terms is small. The terms in some of the series, in fact, get so small that they exceed the limits of the computer. Special provision was made to truncate these series before the limit was exceeded.

The use of the trapezoidal rule to calculate the area is justified mainly by the ease of its use in this situation without much loss in accuracy. The plot of I_1' vs. I_2' is quite regular and there are no abrupt changes. Near the points of maximum curvature, the βa values are chosen more closely together to improve accuracy.

The complete program is given in Appendix E.

CHAPTER III

AN EXPERIMENTAL STUDY OF MHD CHANNEL FLOW

In order to effectively evaluate the analytical results which were obtained, it is necessary to design and conduct an experiment which matches the conditions and assumptions of the analytical model as closely as possible. Such an experiment was performed as part of this work.

It is recalled from Chapter II that the assumptions were made that the fluid was incompressible, that it had constant physical properties and that the Hall parameter and magnetic Reynolds number were small. A number of fluids satisfy these requirements. Thus, other criteria may be used to select a working fluid. These criteria would include cost, ease of use, and actual values of physical properties. After consideration of these factors, it was decided to use an aqueous salt solution. Potassium chloride was chosen on the basis of its relatively high electrical conductivity at normal concentrations (1 to 3 moles/liter). The electrical conductivity is important because it determines to a great degree the range of Hartmann numbers which may be investigated. A potassium chloride solution satisfies the conditions of incompressibility and constant physical properties quite well. For the range of conditions of interest in this experiment, the Hall parameter and the magnetic Reynolds number are on the order of 10^{-6} or less which satisfies the condition on their size. The advantages of a potassium chloride solution from a cost and ease of use standpoint are numerous and quite apparent. High temperature

problems are eliminated, which is a considerable saving in time and cost; instrumentation problems are somewhat simplified; and property values are more readily available and more easily determinable.

Description of Equipment

For ease of operation and economy, a closed loop system was utilized. A diagram of the flow arrangement is presented in Figure 2. As seen in this figure, the major components of the system are the control section, the test section, the magnet and the instrumentation.

Control System

The tubing, connectors, and adapters for the entire flow system were made of polyvinyl chloride. Two types of tubing were used. Rigid tubing was used for most short connections while flexible tubing was used for the longer ones. The flexible tubing was used for both connections to the test section to eliminate the transmission of mechanical vibration from the pumps to the test section. The nominal inside diameter of the tubing was $\frac{1}{2}$". The tubing was fastened securely to the adapters and connectors by stainless steel hose clamps. No leakage problem was encountered.

A stand, to which the pumps, orifices, and control valves were attached, was constructed of 3/4" plywood. The dimensions were 43" high by 30" wide by 12" deep. The manometers for the orifices were also fastened here. In addition, the electrical controls for the pumps were located conveniently on the stand. This stand is shown in Figure 3.

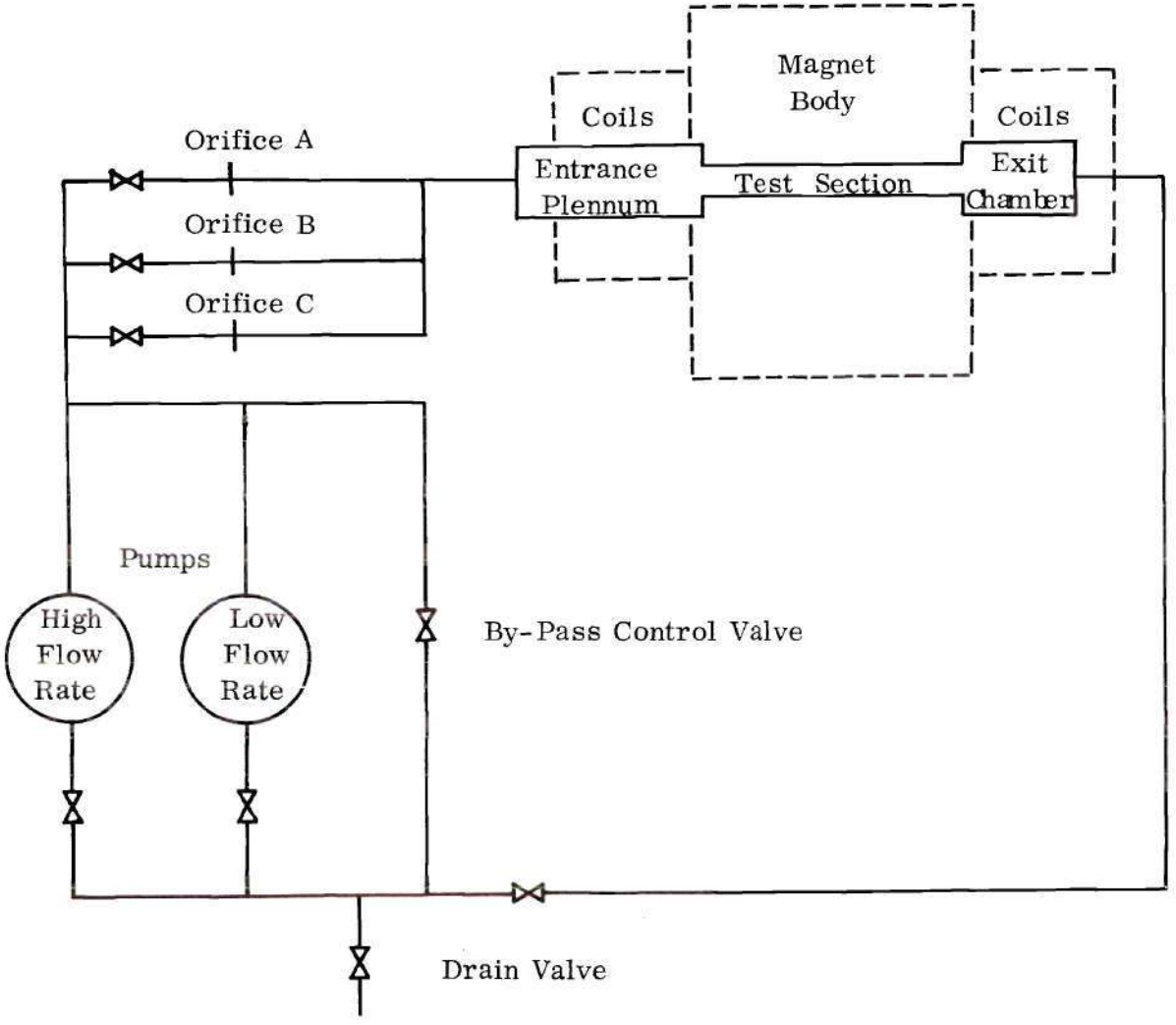

Figure 2. Schematic of Flow Loop.

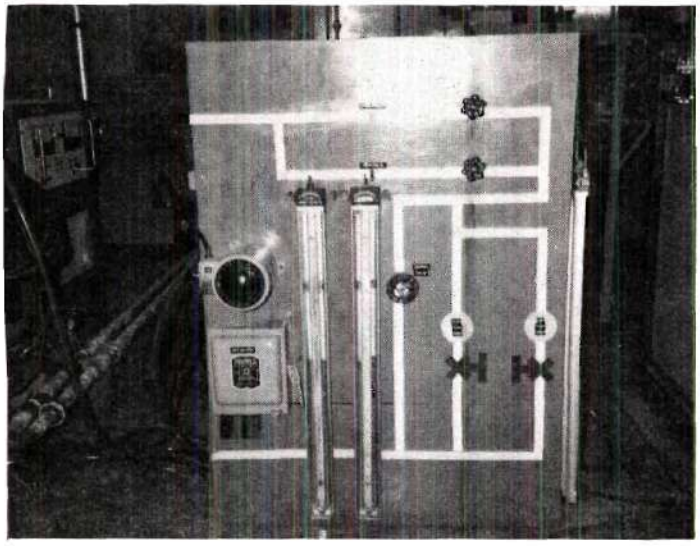

Figure 3. Control Stand.

The valves used were standard $\frac{1}{2}$" brass gate valves. A total of eight were used as shown in Figure 2. The drain in the connection consisted of a standard hose and a valve. This arrangement allowed the system to be filled, drained, or flushed with tap water very easily.

Because of the large range of flow rates which were required to conduct this experiment, it was necessary to utilize two centrifugal pumps, one for low flow rates and another for higher ones. The low flow rate one was a Sears single stage centrifugal pump. It was driven by a small electric motor connected through a belt drive. The speed of the motor was controlled by a powerstat. The high flow rate pump was a Worthington Monobloc pump driven by a 3/4 horsepower motor. Only on-off control was provided for this pump through a SQUARE-D 30-amp fused switch. Control of the flow rate was made possible by the by-pass loop shown in Figure 2. Through adjustment of the by-pass valve, the pressure drop through the by-pass loop could be changed. This influenced the amount of fluid which passed through the test section, and control of the test section flow rate was accomplished.

Test Section

The test section consisted of three distinct parts which were joined together. These parts were the entrance plennum, the test channel, and the exit plennum. All components were fabricated from plexiglass. The test section is shown in Figure 4.

The entrance plennum was essentially a rectangular box with interior dimensions of 5" high by 2" wide by 11" long. The sides, top and bottom were

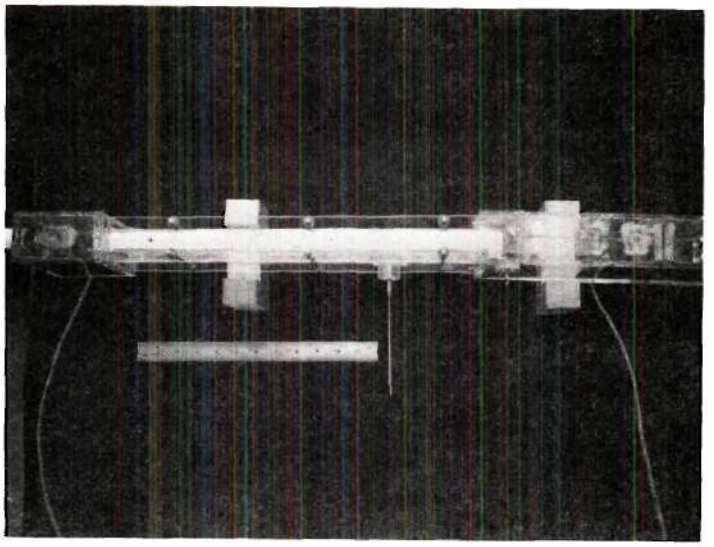

Plan View

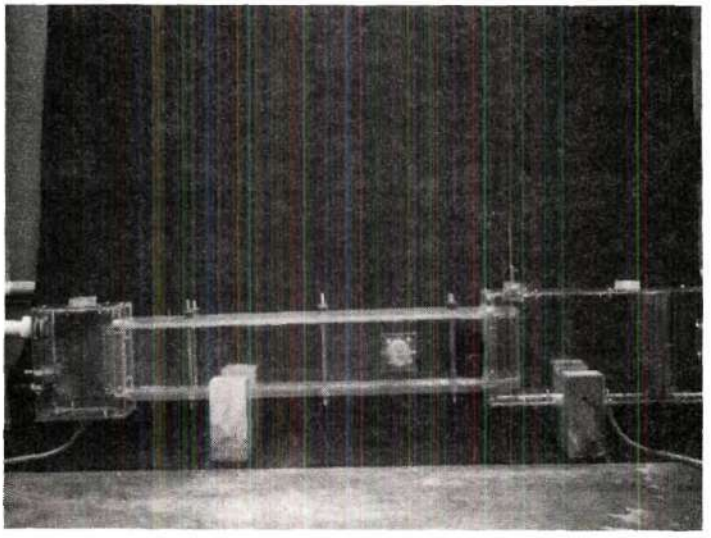

Elevation View

Figure 4. Test Section.

made from 1/8" thick plexiglass which was machined to the proper dimensions on a vertical milling machine. The ends were made from 3/8" plexiglass. The plennum was held together by a number of No. 2-56 brass screws. Brass screws were used to avoid the forces which would be exerted on ferrous screws by the magnetic field. Epoxy cement was used also to help hold the plennum together as well as to provide sealing against leaks. A drain, which consisted of a $\frac{1}{4}$" hole into which a $\frac{1}{4}$" OD polyvinyl chloride tube was inserted and glued into place, was provided in the bottom of the plennum. A clamp was used to close the tube when desired. Another $\frac{1}{4}$" hole was located in the top to allow air to escape during filling of the test section. An adapter which had pipe threads was glued around this hole to permit sealing after the section was filled.

Several other features were incorporated in the entrance plennum. The flow entered from the control section through one end plate. Connection to the control section was made by means of a flexible tube and an adapter. The adapter had $\frac{1}{2}$" pipe threads on one end and was screwed into the properly threaded hole in the center of the end plate. A baffle plate was located over this hole one inch from the end plate to divert the flow to all parts of the plennum. Two inches downstream of the baffle were two 100-mesh non-magnetic stainless steel screens. These screens served as a filter to prevent any large particles from passing through the test channel. Provision was made for insertion of a probe through the top of the entrance plennum at the channel entrance. A screw-type arrangement allowed movement of the probe across the channel. Details of the probe mechanism are given in Figure 5.

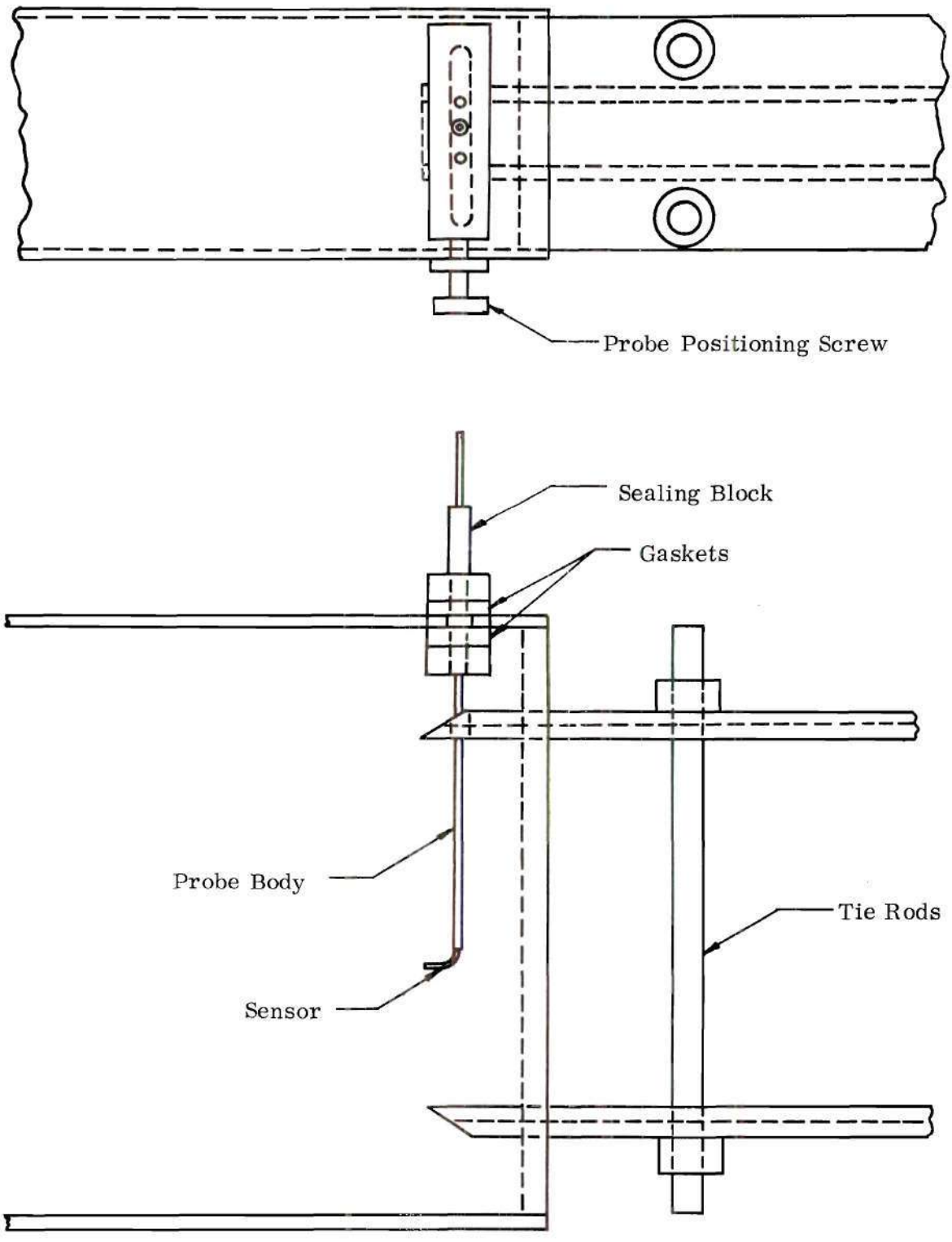

Figure 5. Details of Entrance Probe Insertion.

The exit chamber was similar to the entrance plennum in construction. The interior dimensions were 5" high by 2" wide by 4" long. A $\frac{1}{4}$" tube inserted in the bottom served as a drain. A $\frac{1}{4}$" hole in the top with a threaded adapter glued around it served two purposes. First, it allowed air to be removed from the system. Secondly, a thermocouple well was inserted through this opening during operation to provide the possibility of monitoring temperature. Return of the fluid to the control section was through a connection in the end plate of the chamber.

The test channel was fabricated from four distinct pieces. The sides were machined from 1/8" thick plexiglass to a height of $3\frac{1}{4}$" and a length of 20". The inlet side edges were cut on an angle to provide a sharp edge. The top and bottom were fabricated from 3/8" thick plexiglass. In order to insure proper and uniform channel width, two grooves 1/8" wide by 1/8" deep were milled in the top and bottom pieces. The side pieces fitted snugly into these grooves. Six tie rods extended through the top and bottom to hold the entire assembly together. Epoxy was placed in the grooves also for strength and for sealing. Two test channels were built. One had interior dimensions of $\frac{1}{2}$" x 3" or a 1 to 6 aspect ratio. The other had dimensions of 3/4" x 3" or a 1 to 4 aspect ratio.

To provide a conducting surface along the top and bottom of the channel, aluminum foil was attached to the plexiglass with epoxy cement. Electrical connection to the electrodes was possible through a brass screw which was in contact with the aluminum.

Provision was made for the insertion of probes at two points in the channel.

The first insertion point was at the entrance of the channel. The details of this section of the channel and the mechanism for moving the probe have already been given in Figure 5. The second point at which a probe was inserted was located 5 3/4" from the channel entrance. This probe is inserted through the side wall. Movement of the probe across the narrow channel dimension at the centerline was accomplished through attachment of the probe to a micrometer head. Details of this arrangement are given in Figure 6. The use of the connecting rod between the probe and the micrometer was necessitated by the space restraints imposed by the magnet. Sealing around the probe was accomplished using an O-ring seal built into the probe mounting block.

The entire test section was supported by a stand which consisted of a board 2 3/4" wide by 40" long mounted horizontally on two 2 x 4's 31½" high. One support was located on each side of the magnet with the horizontal board extending through the magnet slightly below the pole faces. The test stand was held firmly in place against the magnet coils by rubber spacers. Holes in the horizontal board allowed the drain tubes of the entrance and exit chamber to hang freely.

Magnet

The magnetic field used in this experiment was provided by a large electromagnet built by Pacific Electric Motor Company. The magnet weighed 9,000 pounds and had dimensions 59" high by 30" wide by 15" deep. The pole faces were 15" long by 3½" high. A hole 1" in diameter was located through the center of the left pole face to provide access for instrumentation. The air gap could be varied in increments of ¼" from ½" to 4½" by adding spacers.

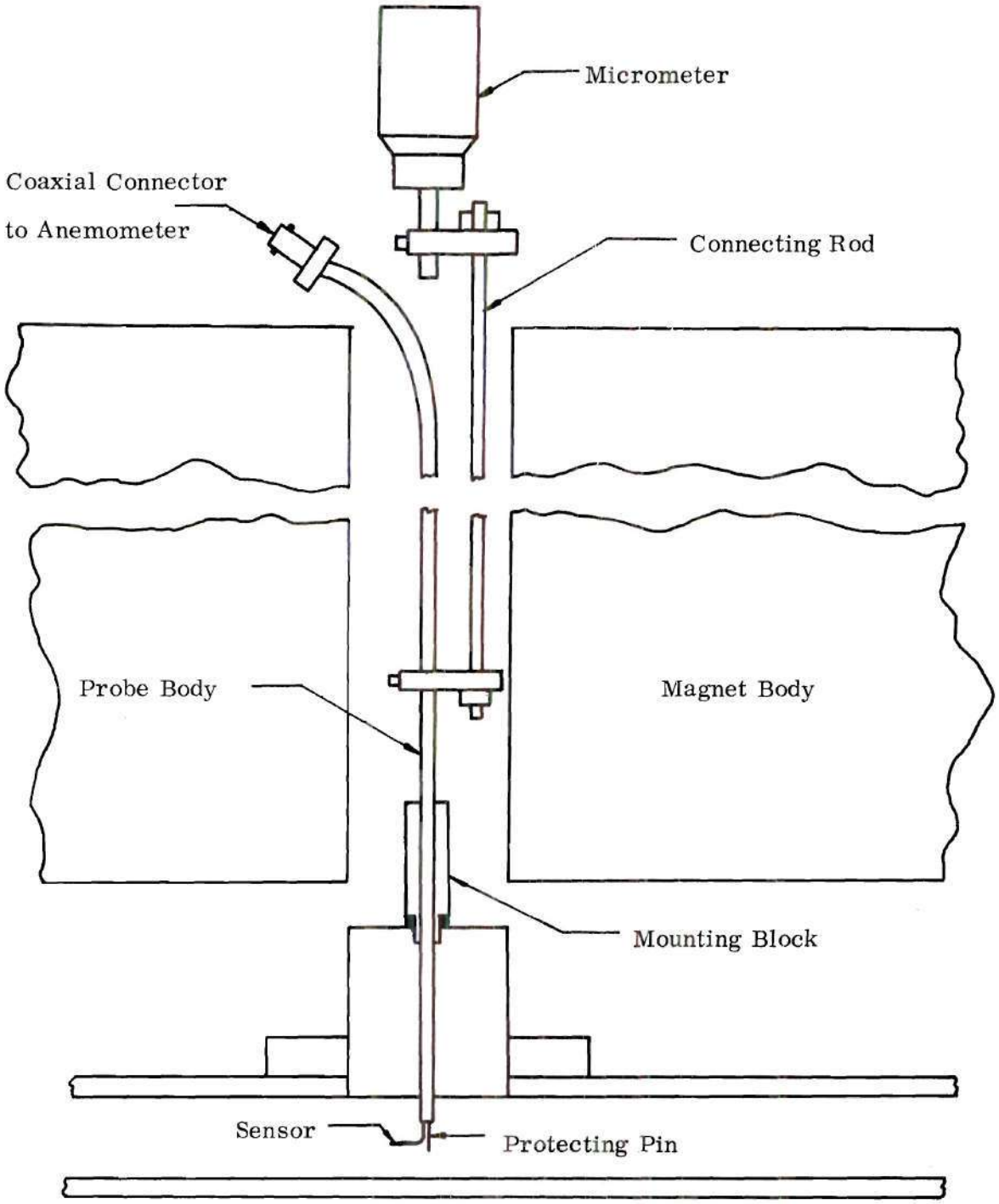

Figure 6. Details of Test Section Probe Insertion.

The magnet had two coils, each containing 200 turns. The coil conductor was 0.467" square copper with a 0.275" hole bore through the center for cooling water. The yokes of the magnet were mounted on a "V" groove track to insure proper realignment after movement of the yokes. The magnet was opened and closed using a hydraulic ram mounted to the bottom of the yokes. The magnet is shown in Figure 7.

Power for the magnet was supplied by a Miller Model SR-1500-C1 Direct Current Power Unit. This unit could supply up to 1500 amps DC. It was connected to provide 160 volts open circuit and operated from a 220-volt, 3 phase line. The electrical connection to the magnet was made using No. 4/0 welding cable.

Cooling water for the magnet was taken from a 2" city water line which had a nominal pressure of 90 psig. The flow rate was approximately six gallons per minute per coil. The magnet utilized a manifold arrangement on each coil with five equal length flow paths to reduce the flow resistance through the coil. Each coil was protected by a Texas Instruments Klixon temperature switch in the discharge and a Hays Shur-Flo flow indicator. These instruments were connected to warning lights which were lighted if the flow rate dropped below six gpm or the discharge water temperature rose above 160^{o}F.

Instrumentation

In order to measure parameters of interest such as velocity, temperature and current, it was necessary to have proper instrumentation. This instrumentation consisted of orifices, an anemometer, a thermocouple, and a shunt.

Three orifices were utilized to provide flow rate measurement over the

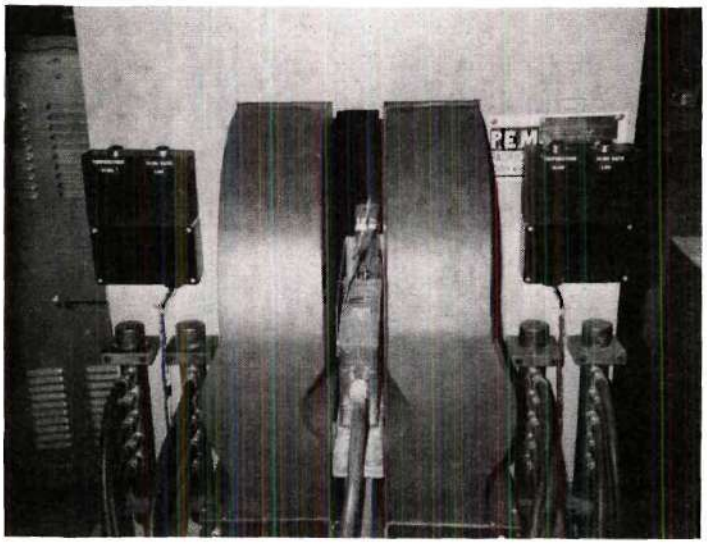

Figure 7. Electromagnet with Test Section in Place.

large range of flow rates encountered in this work. Stainless steel flanges were silver-soldered to standard $\frac{1}{2}$" galvanized pipe. These sections of pipe were five inches long in accord with standards. The orifice plate was also of stainless steel. The flanged pipe, orifice plate, and sealing gaskets were held securely in place with four equally spaced bolts. Three different sized openings in the orifice plates were used: 3/32", 3/16", and 9/32". The pressure taps were located $1\frac{1}{4}$" upstream and $1\frac{1}{4}$" downstream. The connections from the pressure taps to the manometers were made using flared fittings and $\frac{1}{4}$" copper tubing. The manometers were 24" clean-out types and contained mercury.

For velocity measurements in the test channel, a Thermo-Systems, Inc., Model 1050 anemometer system was used. The principle on which this system works involves the relationship between the heat transfer from a small heated resistance element and the velocity of the medium surrounding it. The resistance element is one leg of a bridge circuit. Since the resistance is a strong function of temperature, and the heat transfer is a function of velocity, a change in fluid velocity will cause a change in the temperature of the sensor and hence an unbalance of the bridge circuit. By utilizing a feedback system which maintains the element at a constant temperature, a correlation between velocity and bridge voltage is obtained. The temperature of the wire is controlled by the values of the other resistances in the bridge circuit. For convenient operation, this model anemometer was equipped with a variable decade arrangement which permitted easy adjustment of the probe temperature.

The sensing elements were quartz-coated platinum wires 0.002" in diameter

by 0.040" long mounted on gold-plated stainless steel supports. The body of the probe was also of stainless steel. The probe which was used at the channel entry had the sensor parallel to the probe shank and facing upstream (TSI Model 1271-20W-6). The other probe had the sensor directed upstream perpendicular to the shank (TSI Model 1277-20W-6). The probes had a split-pin type electrical connector and were connected to the anemometer module by an adapter and a 15' long coaxial cable.

To get improved readability of the bridge voltage, this system was equipped with a signal conditioner. This enabled the operator to subtract a certain number of volts from the bridge voltage and use a smaller scale on the monitor output. Thus bridge voltages could be read to $\pm$ 0.010 volts.

The fluid temperature was measured with a copper-constantan thermocouple. The reference junction was submerged in an ice bath. The voltage output was read using a Leeds and Northrup Model 8686 Millivolt Potentiometer.

In order to measure the current through the magnet, a 100mv, 500 amp shunt was used. The voltage drop across this shunt was monitored on a Hewlett-Packard Model 7100 B Strip Chart Recorder.

Calibration of Instrumentation

To use the instrumentation accurately, it was necessary to compare each piece with a suitable known value. Such calibration procedures were carried out for the orifices, the anemometer, the magnet, and the thermocouple.

Orifices

The calibration of the orifices required the determination of the flow rate as a function of the pressure drop. The orifice was connected to a water line by a hose and the flow rate adjusted by a valve. The discharge was collected for a period of time which was measured by a stopwatch. This effluent was weighed and the flow rate calculated. The pressure drop across the orifice during the test time was recorded. This procedure was used for all three orifices. The test period was always of sufficient duration to minimize the errors inherent in starting and stopping the watch. The amount of effluent was such that the accuracy in reading the scales was good ($\pm$ 1%). The results of the calibration are given in Figure 8.

To calibrate the anemometer, it was necessary to obtain a reliable velocity standard. After an attempt to use a flow-through calibrator proved unacceptable, it was decided to utilize the relationship between linear and angular velocity which exists for rotating objects. This relationship is

$$V = r\omega \tag{44}$$

where V is linear velocity in feet/second, r is radius in feet, and ω is angular velocity in radians/second. A calibration device which permitted the angular velocity to be determined was constructed. This device, shown in Figure 9, consisted of an arm which rotated above the fluid in a two-foot diameter tank. The probe was mounted on an arm at either 9 or $4\frac{1}{2}$ inches depending on the desired velocity range to be produced. The arm was turned by a motor whose speed was

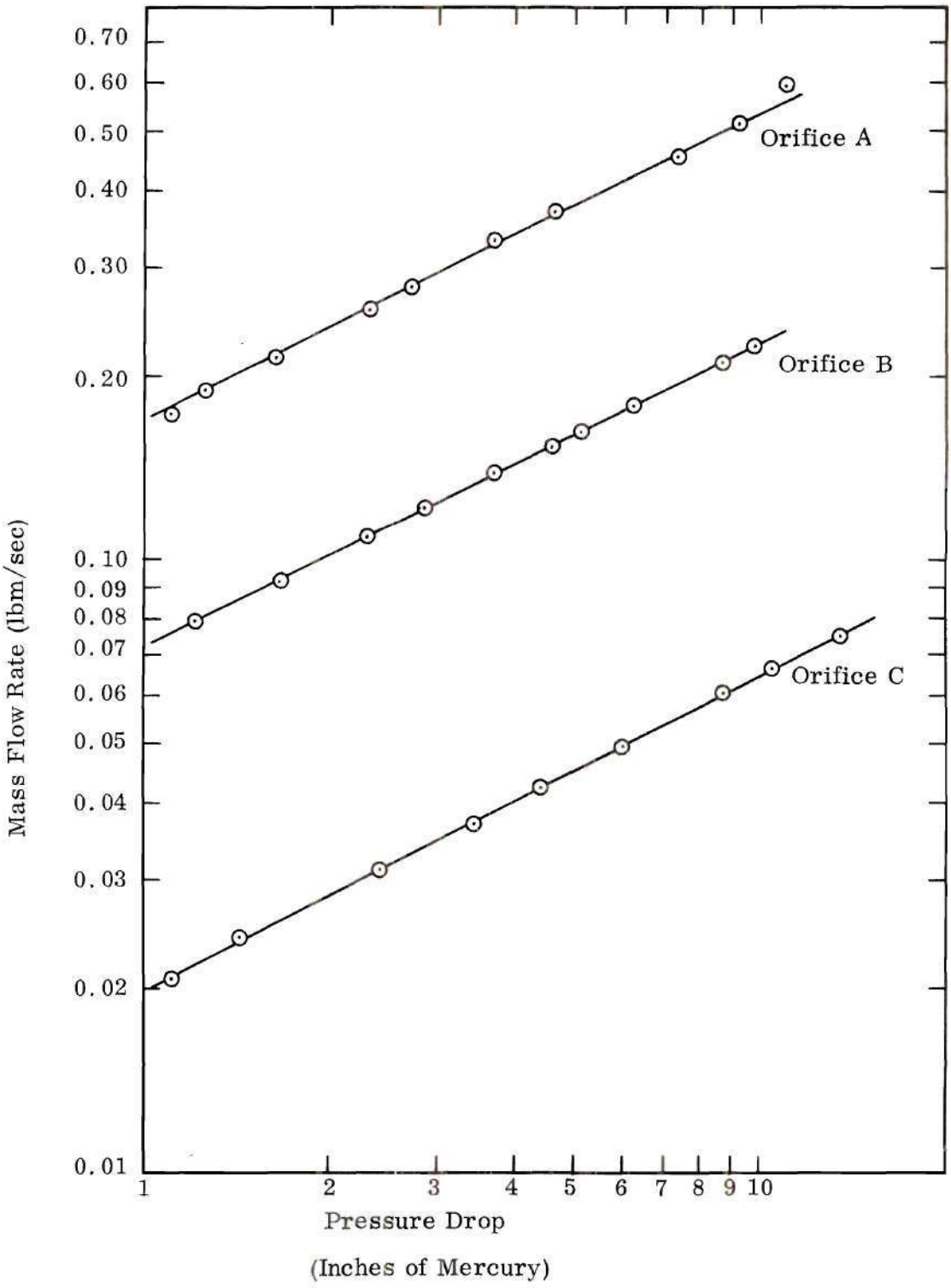

Figure 8. Orifice Calibration Curves.

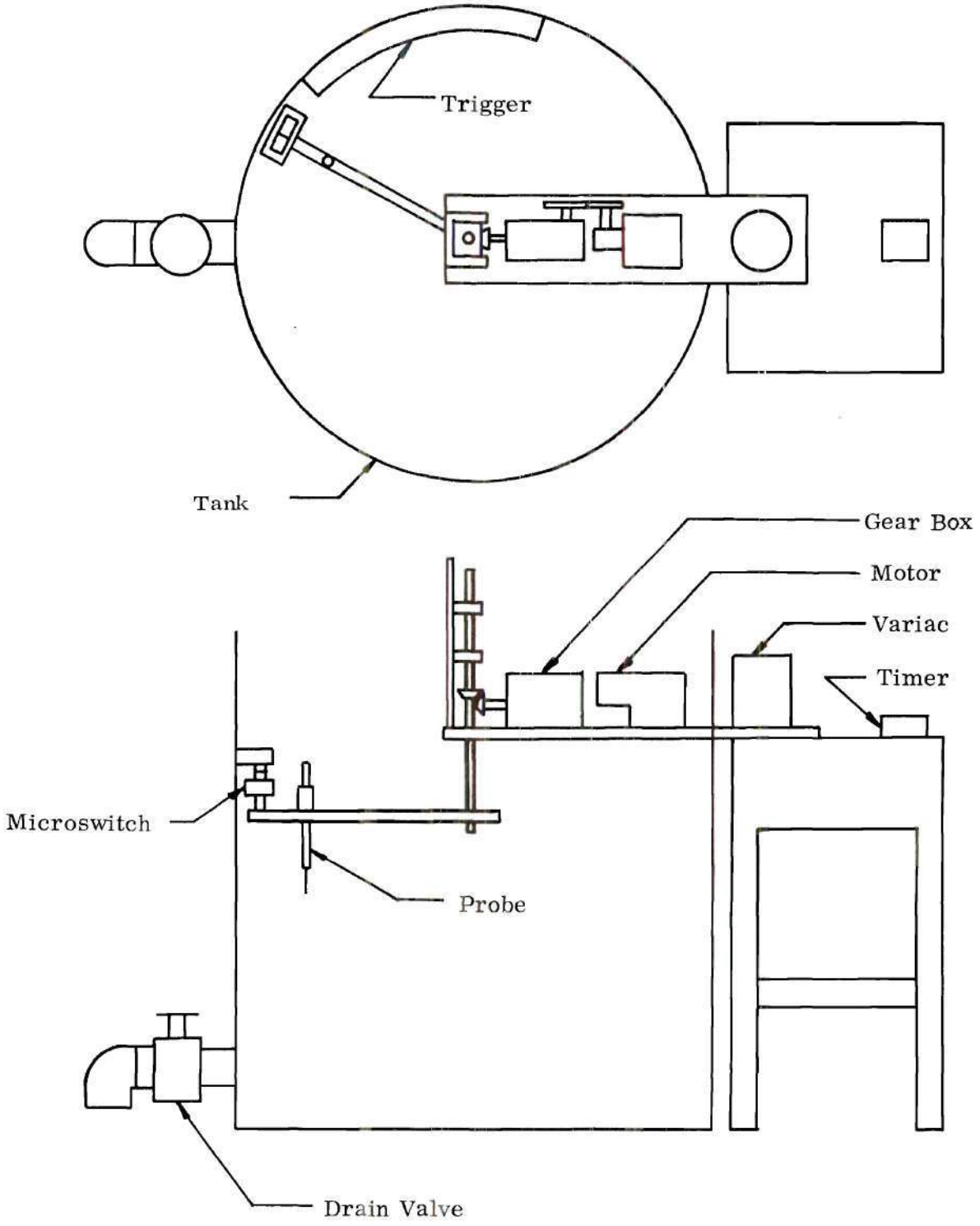

Figure 9. Hot-Film Anemometer Calibration Device.

controlled by a Variac. Further reduction in the angular velocity of the arm was accomplished through gearing. A gear box with input-output ratio of 100 to 1 was used. Additional gears were used to produce the lowest velocities of interest. A microswitch was mounted on the arm. This microswitch was connected to a Porto-Clinic Instruments electronic timer. The microswitch was triggered by contact with a piece of plexiglass which was fastened to the sides of the tank. The piece of plexiglass used was either 5.25 or 13.25 inches across, depending on the speed of the arm. Two lengths were necessary to reduce the percentage error involved in starting and stopping the timer. The time to traverse the triggering piece was always greater than 2.00 seconds. It was estimated that the timer had an accuracy of $\pm$ 0.02 seconds so that the time was always known to within $\pm$ 1%.

To calibrate a probe, the tank was filled with fluid. Sufficient time was allowed for any currents in the fluid from the filling process to die out. The fluid temperature was measured with a thermocouple and recorded. The resistance of the probe was then measured using the resistance measuring circuit of the anemometer. A quantity called the overheat ratio was selected. This quantity is the ratio of the resistance of the probe at the operating temperature to that at the environmental temperature. Several factors influence the selection of the overheat ratio. One is sensitivity. Greater sensitivity is achieved for the higher overheat ratios. However, for use in water and aqueous solutions, a limit on the operating temperature exists. For temperatures near the boiling point, problems are encountered because of the tendency to form bubbles around the probe. Thus it is necessary

to use a lower operating temperature. For an overheat ratio of 1.1, the probe temperature is approximately 140°F and the sensitivity is quite good for the velocity range of interest in this experiment. Therefore, an overheat ratio of 1.1 was used throughout this experiment. The resistance corresponding to this overheat ratio (i.e., 1.1 times the resistance at the environmental temperature) was set on the resistance decades. The probe was now ready for calibration.

To obtain a calibration point, the anemometer was turned to the "run" position. The corresponding bridge voltage was noted. This bridge voltage corresponded to a velocity of zero. Next, the arm was set in motion by activating the motor. Time was allowed for the arm to reach a steady velocity. After this condition was attained, the bridge voltage during the timing portion of the rotation was recorded as was the time to traverse the known distance. Thus, a correlation between bridge voltage and velocity was found. This procedure was repeated many times over the entire velocity range from 0 to approximately 0.6 feet/second. The reproducibility of the data was checked thoroughly by calibrating over the velocity range several different times. Some runs were made starting at slow speeds and increasing the velocity while others began at high speeds and then decreased. It was found that for greatest accuracy, the density should also be included in the calibration. Thus, curves of ($e\nu$) vs. bridge voltage were plotted. The calibration curves for the probes used are shown in Figures 10 and 11. From these curves, it is seen that the correlation is quite good. It is estimated that the error is 3 per cent.

The magnetic field was measured using a Hall-effect gaussmeter. This

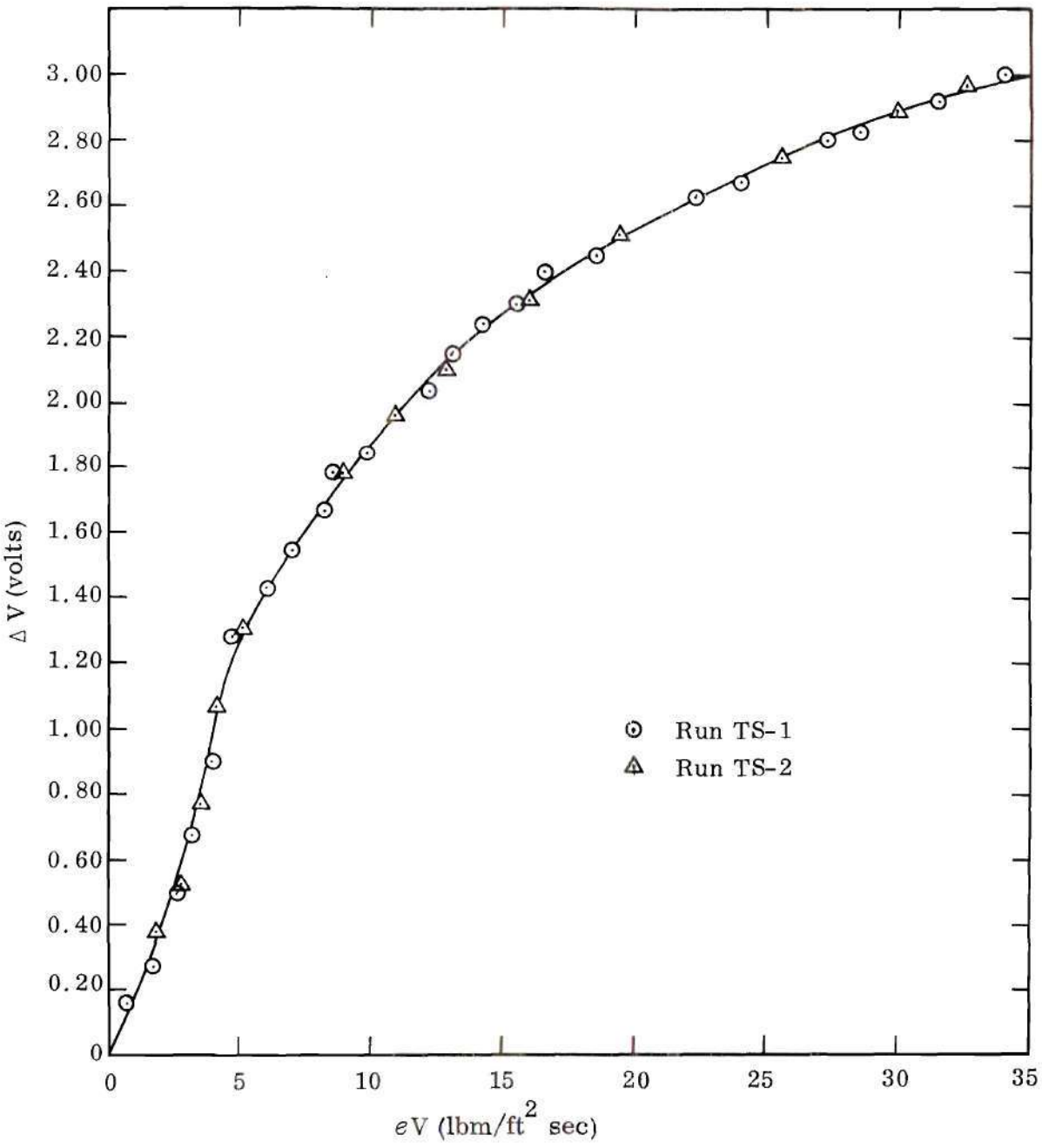

Figure 10. Calibration Curve for Test Section Probe.

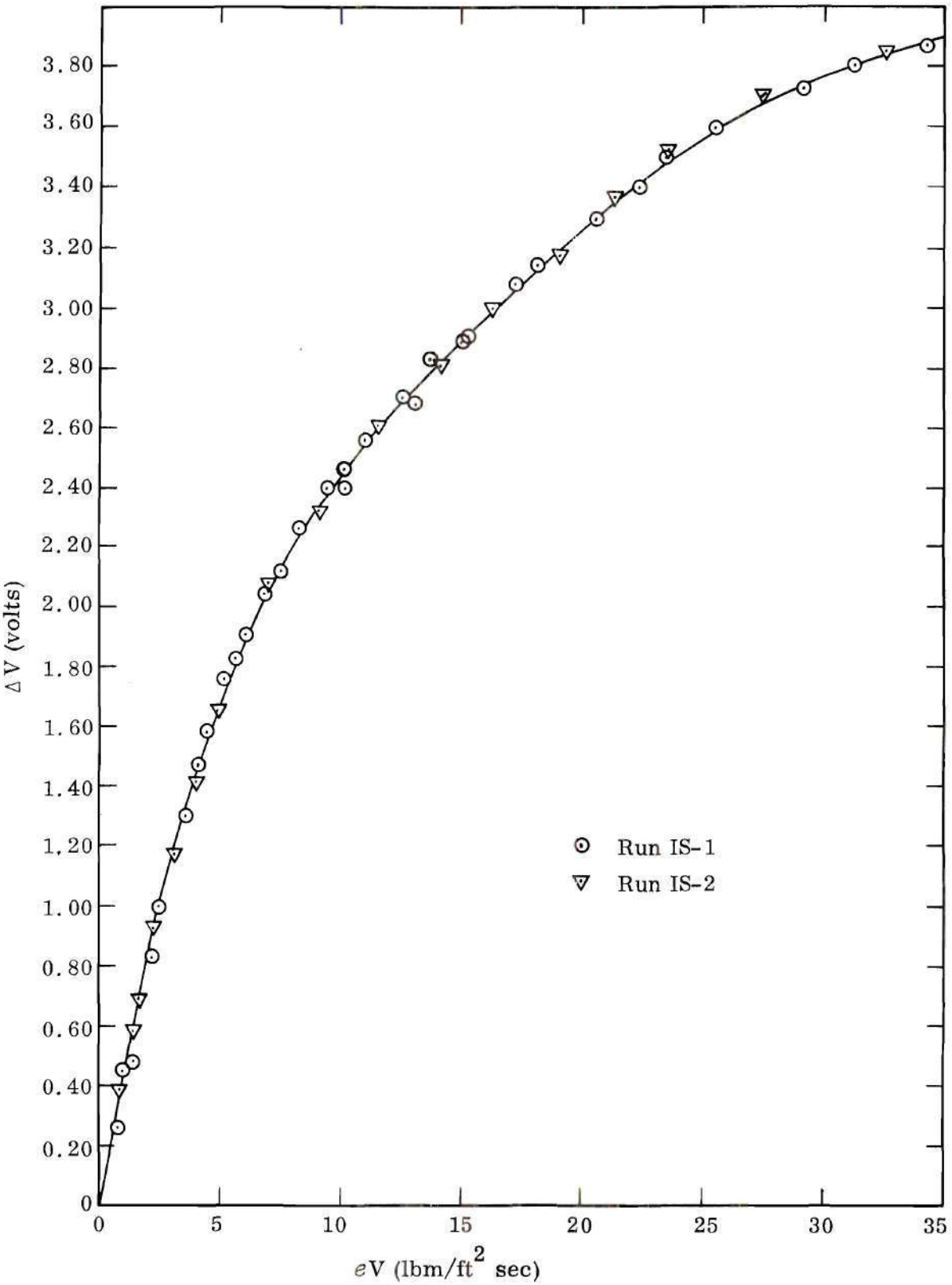

Figure 11. Calibration Curve for Entrance Plennum Probe.

device utilizes a thin rectangular wafer of semiconductor material with four leads attached. A control current is allowed to flow in one direction and the resulting voltage in the perpendicular direction due to the deflection of the electrons by the Lorentz force is measured. This Hall voltage is directly proportional to the flux density. This gaussmeter had an accuracy of 4% for the probe used. Calibration was made by using the built-in calibration feature of the unit.

All tests were conducted with a magnet air gap of three inches. Two types of tests were run. The first involved a measurement at many positions in the air gap to determine the field uniformity. For these tests, a magnet current was selected and maintained. The field was then measured at many points. Typical results of these tests are shown in Figures 12 and 13. From these results, it is seen that a field that is uniform to within $\pm$ 5% exists in the volume located between 2 and 13 inches from the start of the pole faces, and extending from $1\frac{1}{4}$" above to $1\frac{1}{4}$" below and from $1\frac{1}{4}$" to the right and to 3/4" to the left of the centerline. The large drop in the field strength near the left pole face is a result of the 1" diameter hole for instrumentation located there.

The other test was a calibration test of magnetic field strength versus current through the coils. For this test, the probe was located at the centerline of the air gap 5 inches from the end of the pole face. The magnet current was varied and the corresponding magnetic field strength recorded. This curve, shown in Figure 14, was considered to represent the calibration for the magnet. It was used to determine the magnetic field for the measured magnet current during any test run.

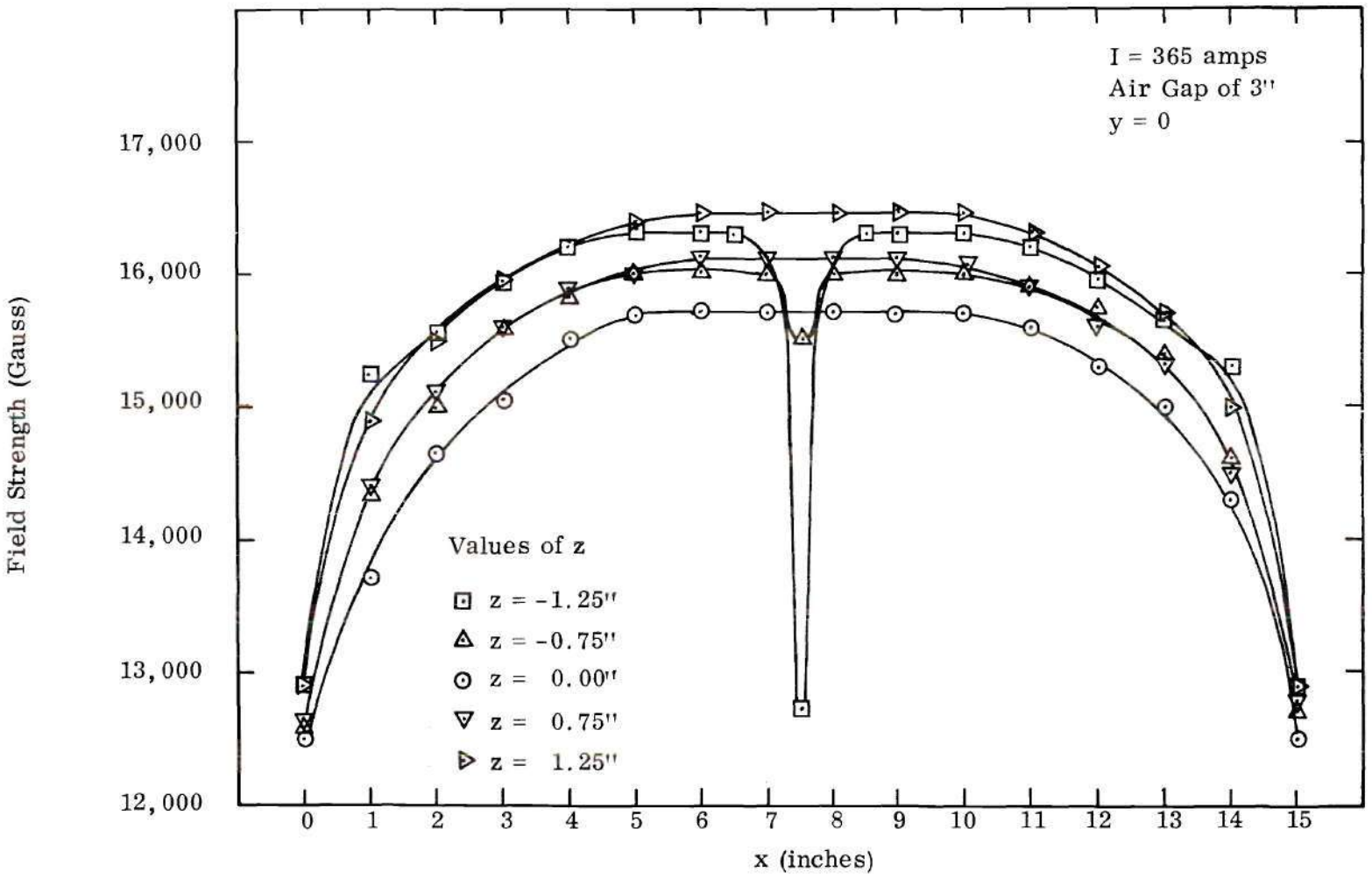

Figure 12. Field Strength Variation with Distance Along the Pole Face for Several Positions Across the Air Gap.

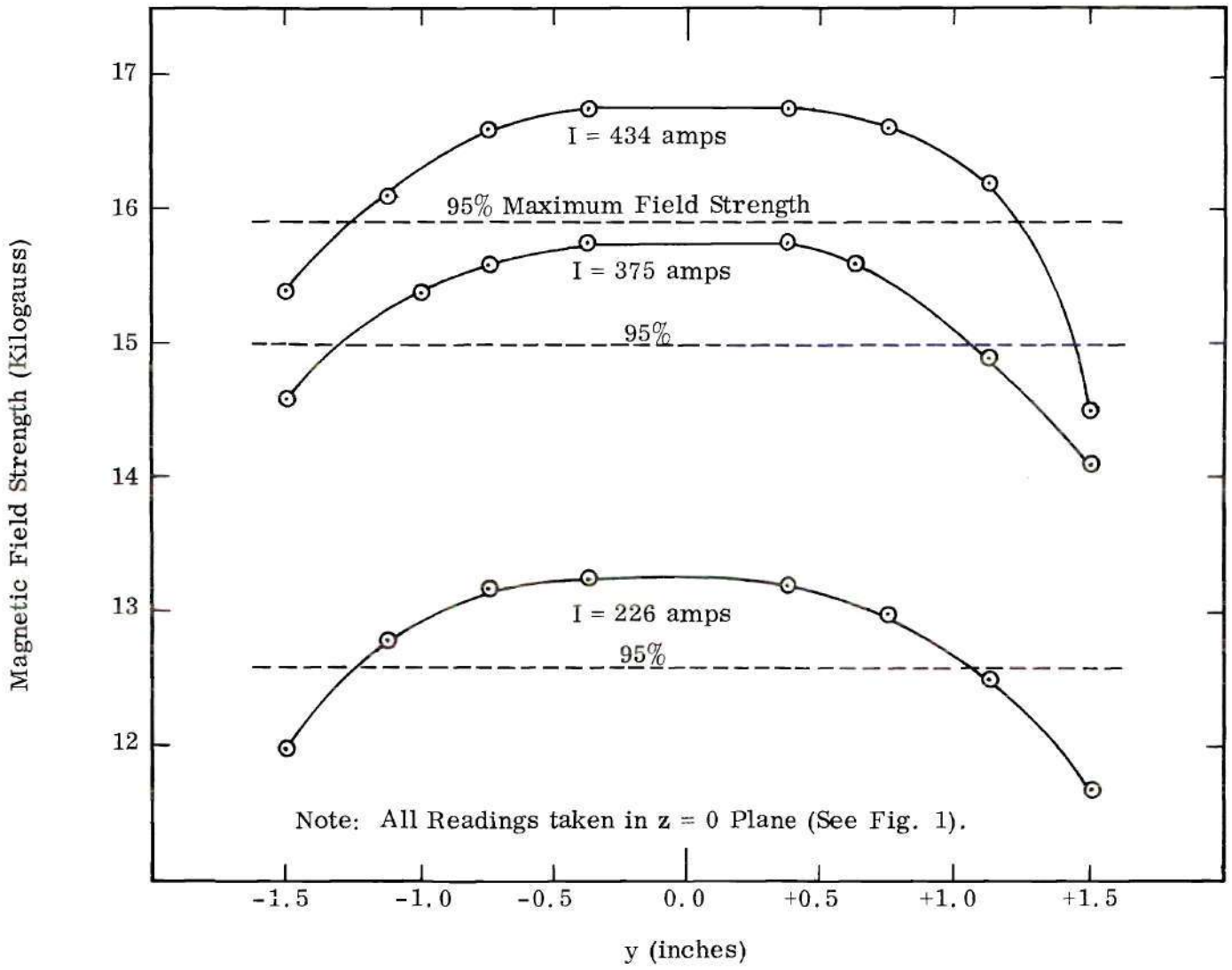

Figure 13. Variation of Field Strength with Height in Air Gap.

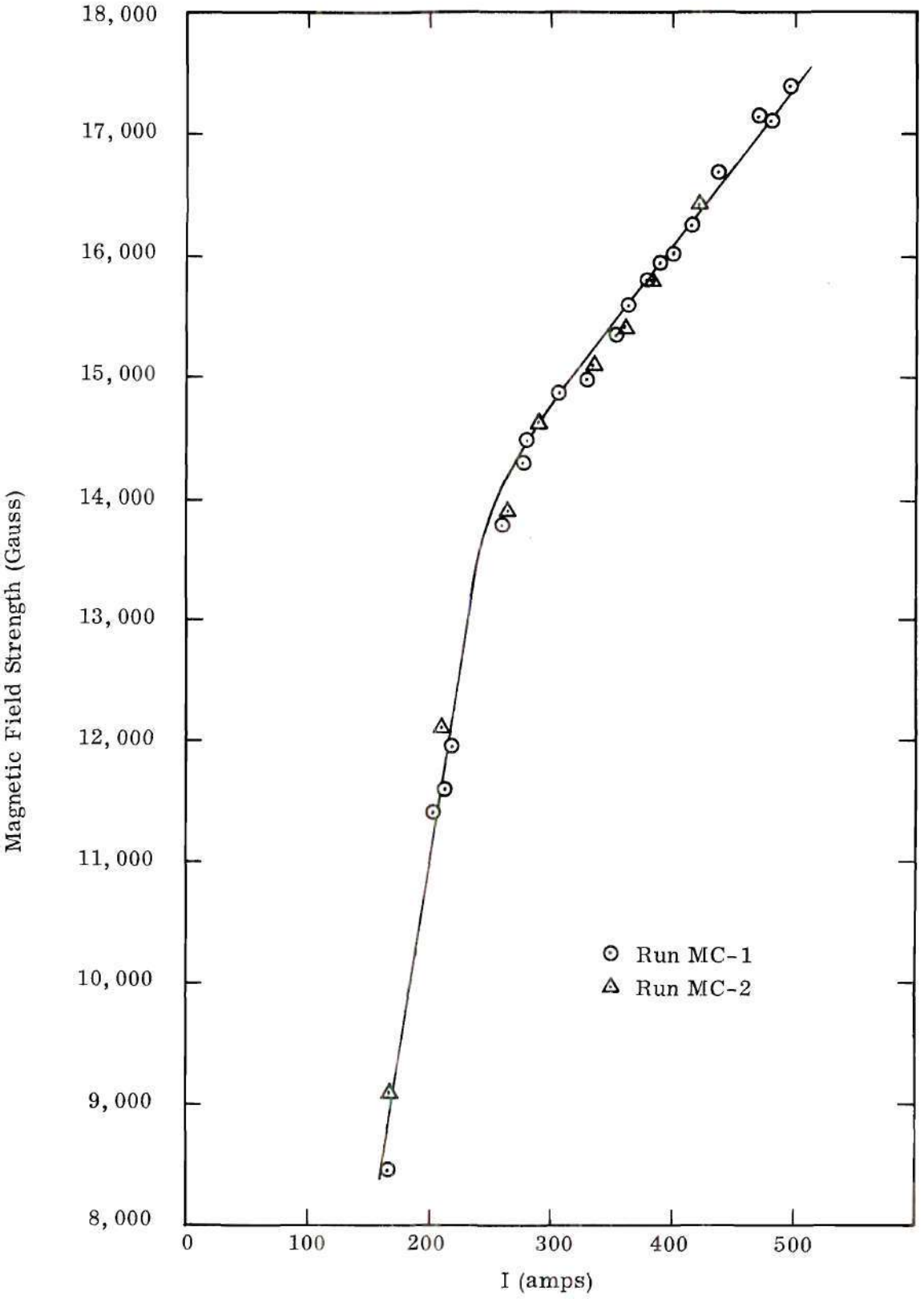

Figure 14. Calibration Curve for Electromagnet Giving Current-Field Strength Relationship.

Calibration of the copper-constantan thermocouple was against a standard thermocouple. The two thermocouples were placed in a container. A small beaker was also placed in the container. The junctions were suspended in this beaker to assure that the temperature of the environment was the same. The water temperature was adjusted by addition of hot water. The results of the calibration are given in Figure 15. The calibration was conducted over only the temperature range to be encountered.

Evaluation of Properties

For those tests run with water, the determination of the physical properties of density and viscosity was simply a matter of using accepted, tabulated values for the temperature measured. For the other tests, however, it was necessary to somehow determine these properties as well as the electrical conductivity.

Density

The density of the aqueous potassium chloride solution was found by weighing a measured volume of the solution. A 100 ml graduated cylinder was weighed on a Christian Becker beam balance. This beam balance gave the weight in grams with an error of $\pm$ .0001 gram. The cylinder was then filled with solution and weighed. The net weight of the solution in grams divided by the volume in cubic centimeters (milliliters) gave the density of the solution with an error of less than 0.5 per cent. Knowing the density, it was now possible to find the specific gravity and from tables (49) the molar concentration of solute (KCl). The variation of density with molar concentration is given in Figure 16.

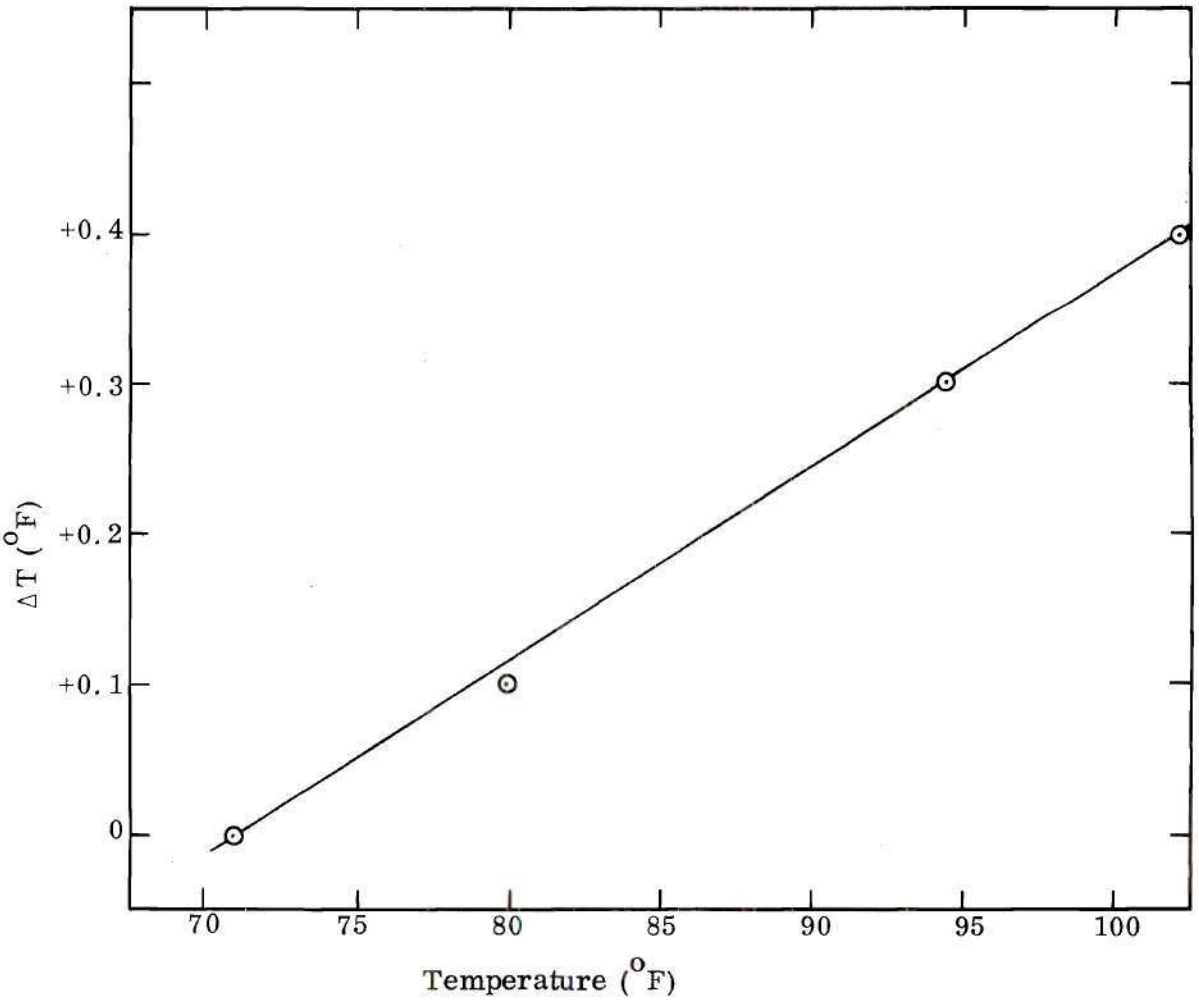

Figure 15. Thermocouple Calibration Curve.

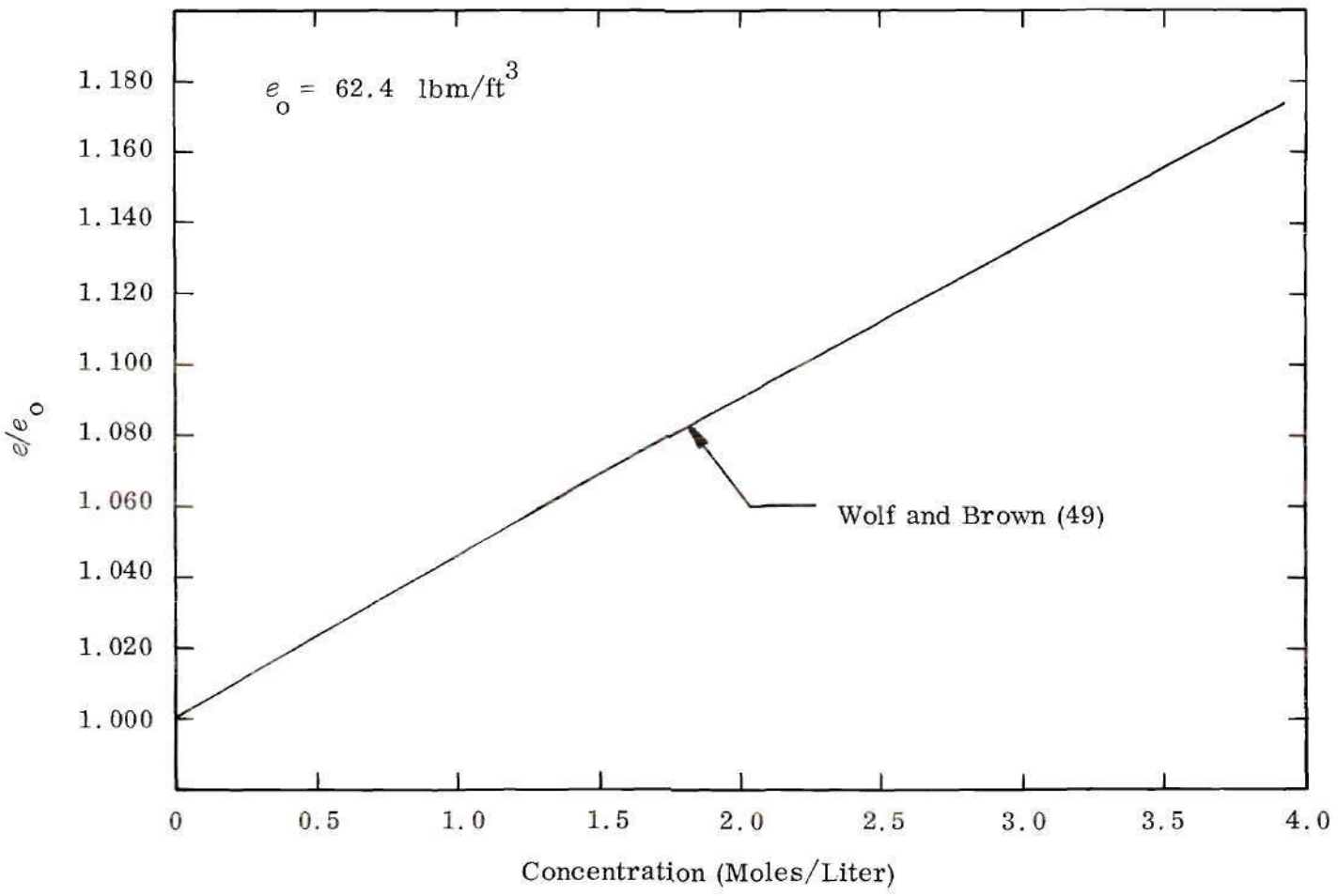

Figure 16. Density vs. Concentration.

Viscosity

A viscometer that would give accurate results in the range of viscosities of interest was not immediately available. Thus it was necessary to use tabulated viscosity data for potassium chloride solutions (50). The variation of viscosity with concentration is shown in Figure 17, where η_o is the viscosity of pure water. It should be noted that the maximum increase in viscosity is approximately 7.5 per cent. It is felt that the error involved in determining the viscosity from this method is small.

Electrical Conductivity

The electrical conductivity is strongly dependent on the concentration as shown in Figure 18 which is taken from data given by Robinson and Stokes (51). Attempts to measure the electrical conductivity using a "conductivity cell" located in the exit section were not very successful. The values were not reproducible with any degree of accuracy. Consequently, the tabulated values of conductivity for the measured concentration were used in the calculation of the Hartmann number. It was estimated that the error in the electrical conductivity was less than 4 per cent. The experimental determination of the electrical conductivity would have required very sensitive equipment which was not readily available.

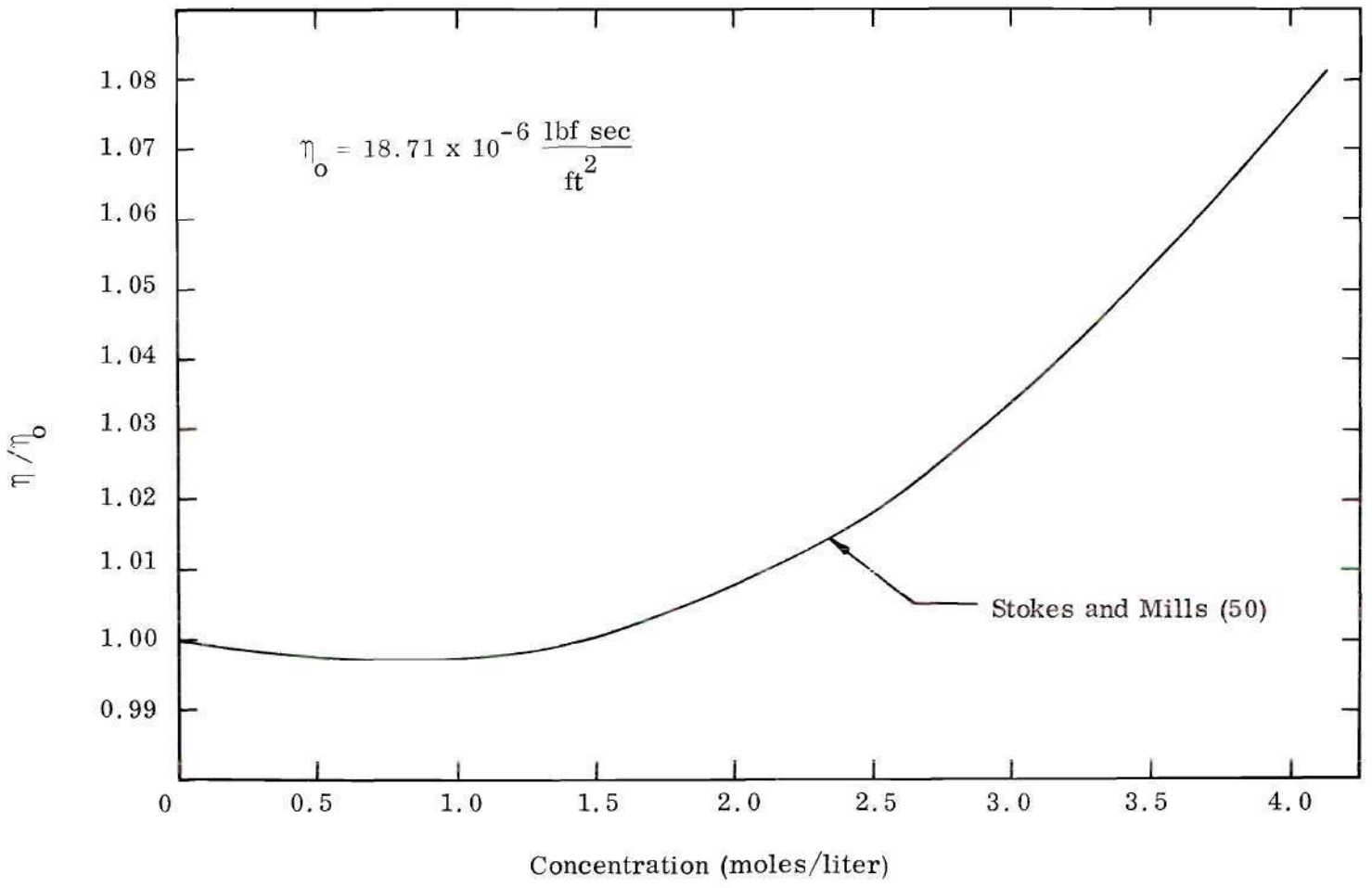

Figure 17. Viscosity vs. Concentration.

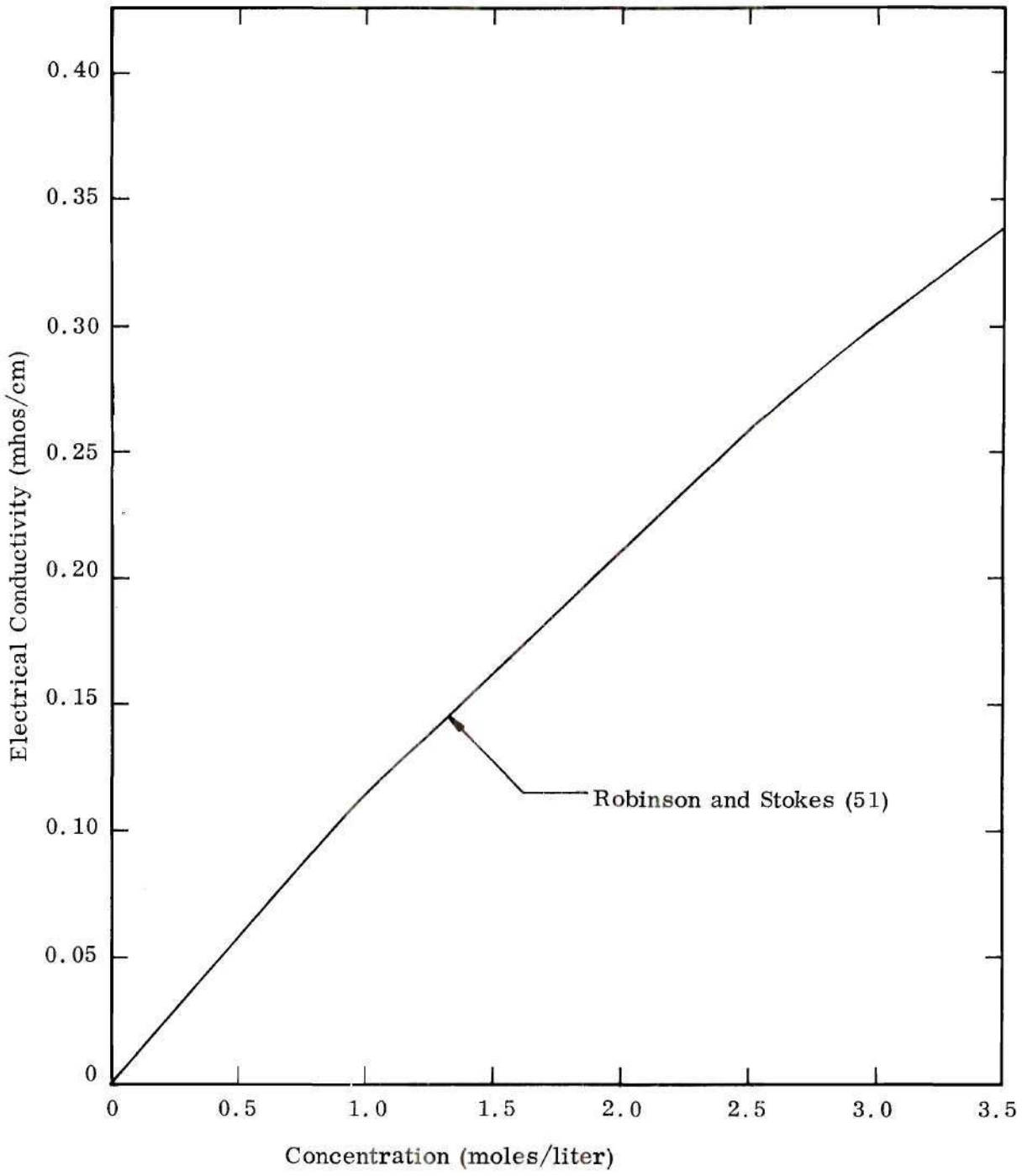

Figure 18. Electrical Conductivity vs. Concentration.

CHAPTER IV

TEST PROCEDURE AND RESULTS

Using the equipment which was described in Chapter III, it was possible to investigate the development of the velocity profile in channels with aspect ratios of 4 to 1 and 6 to 1. The Hartmann number ranged from 0 to 2.0 for the 6-to-1 channel and from 0 to 2.9 for the other. It was not possible to investigate higher Hartmann numbers using this equipment because of limitations imposed by the properties of the working fluid and because of current limitations to the magnet. The maximum electrical conductivity which could be attained for the potassium chloride solution was 0.375 mhos/cm. This value occurs at a concentration of 4.0 moles/liter which is very near saturation of the solution. The maximum field attainable in the magnet is limited by the current which may pass safely through the coils. This limit is approximately 500 amps. Although these restrictions permitted only a narrow range of Hartmann numbers to be investigated, fortunately the velocity development was a strong enough function of the Hartmann number to disclose the importance of this parameter.

Test Procedure

To begin any test, it was necessary to fill the system with fluid. First, however, the system was flushed with tap water to remove any sedimentary particles that might have accumulated between runs. A quantity of test fluid

(approximately 2 gallons) was then prepared in a large stainless steel bucket. The bucket was placed on a stand and connected to the control and test sections by a hose. All valves in the control section were opened and the fluid flowed into the system. Air escaped through the vents in the top of the entrance and exit chambers. When the system was completely filled and all entrapped air had been removed, the system was sealed and testing began.

A preliminary test was made for every Hartmann number to determine the uniformity of the velocity profile at the channel entrance. The hot film probe located at the channel entrance was used for this test. A flow rate was set by controlling the pump motor speed and the by-pass control valve. The velocity profile was then measured over the entrance. It was found that in all cases the profile was uniform to within 3%. Such flow development typically occurred at x' values less than 0.001, so that the error involved in assuming the profile to be uniform is small.

Two types of tests were run. The first involved a measurement of the centerline velocity development as a function of the non-dimensional axial distance x'. For these tests, the probe in the test channel was positioned at the centerline of the channel using the micrometer attached to it. A flow rate was set and sufficient time allowed for the system to reach steady conditions. The velocity at the probe was then recorded as was the manometer reading. From this information, it was possible to determine the non-dimensional velocity at the centerline and the non-dimensional axial position. For tests at Hartmann numbers other than zero, the magnet current was monitored and the density of fluid measured. These

quantities permitted the Hartmann number to be calculated. In all tests, the fluid temperature was monitored.

In the other tests, a flow rate was set using the proper controls. After the system had reached a steady state, velocity readings were made at the appropriate points across the channel. The manometer reading, the magnet current and density were recorded also. Again the micrometer was used to position the probe. The probe was always moved in the same direction to eliminate uncertainty in position. First, it was moved toward the wall until the protecting pin on the probe stopped it. This pin extended 0.005" beyond the probe so that the exact position of the probe was known. Positions were calculated which corresponded to non-dimensional values of z/a of +0.90 to -0.60 in steps of 0.10. The probe was never moved closer to the right wall than indicated above to prevent any chance of damaging the probe. It was found that the flow was symmetrical so that the loss of these points was not critical. Sufficient time was allowed for any disturbance introduced by moving the probe to die out before a reading was taken. All data were taken only at the y=0 position (See Figure 1) because of physical limitations on the insertion of instrumentation.

After a test had been completed, the test and control sections were drained. In those cases where a KCl solution had been used, these sections were flushed with tap water several times to prevent salt accumulations.

To check for reproducibility, all tests were repeated. Flow conditions were as close to the same for each test as possible. For each set of flow parameters, tests were run in both the short and open circuit conditions.

Discussion of Test Results

Velocity profiles have been obtained for various portions of the entrance region for Hartmann numbers of 0, 1.2, 1.6 and 2.0 for the 6-to-1 channel and for Hartmann numbers of 0, 1.2, 2.0 and 2.9 for the 4-to-1 channel. These profiles are shown in Figures 19 through 26. The corresponding theoretical profiles are shown also. The experimental results agree quite well with the analytically predicted values. The data are also shown to be reproducible as profiles from different runs agree quite well. The scatter in the data falls within the range of the experimental error in almost all cases. In those cases where the disagreement is largest, the experimental values measured approached the limits of resolution of the instrumentation.

As shown on the figures, profiles were measured over the entire range of values of x' which could be obtained. Attempts to measure profiles at values of x' above or below those indicated were not successful due to the limitations of the instrumentation and the flow system. It was not possible to obtain values of x' large enough to obtain a fully developed flow situation at the probe station. To have done so would have required extremely small space-average velocities (typically less than 0.020 feet/second) that could not be obtained with this flow system. The use of the anemometer below this velocity becomes more difficult and results more subject to error. Although a fully developed profile was not measured, from the figures it was observed that the profiles changed in such a way that the attainment of the predicted fully developed profile seemed likely.

The measured profiles demonstrated the influence of the Hartmann number

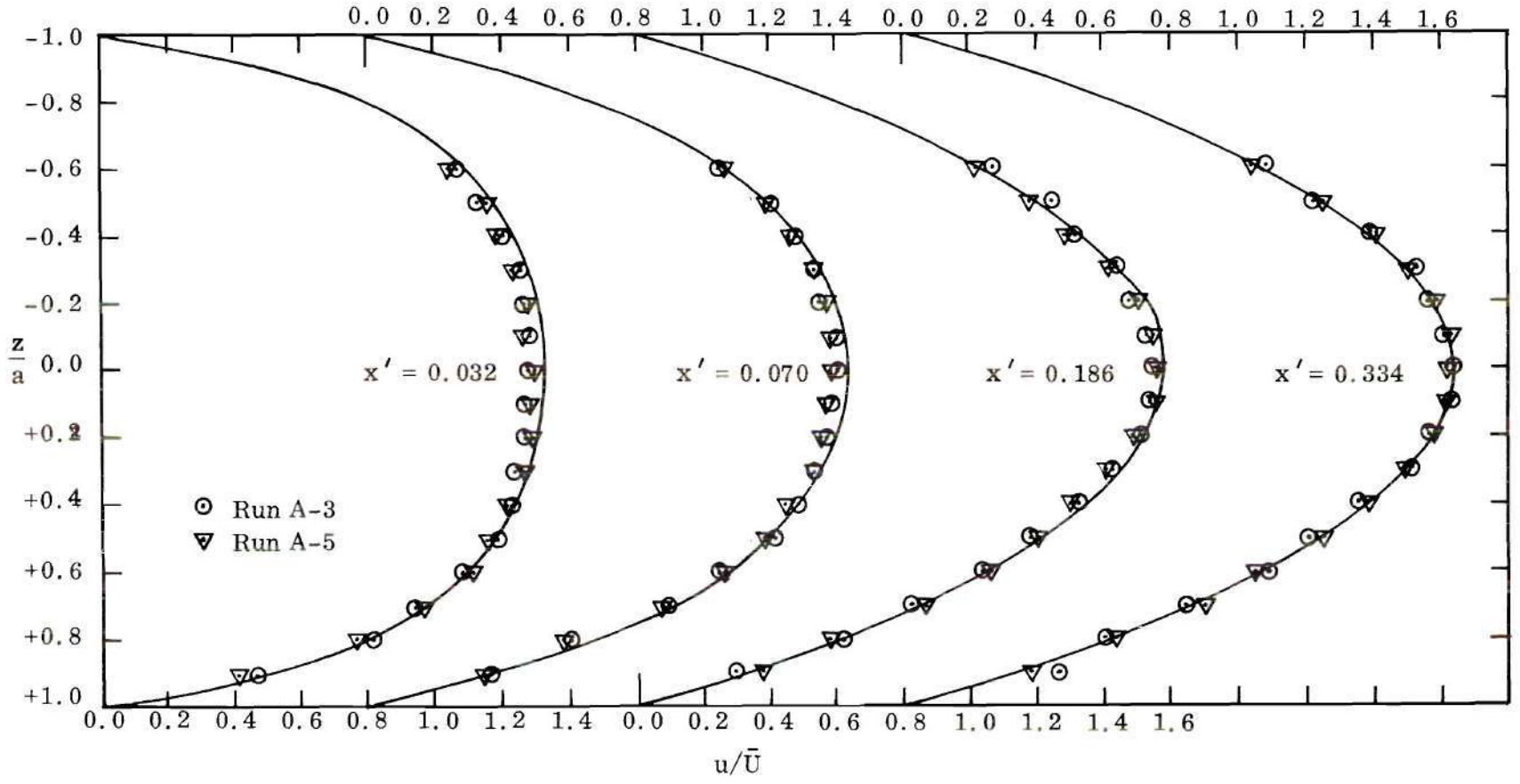

Figure 19. Velocity Profiles for Ha = 0 in 6-to-1 Channel.

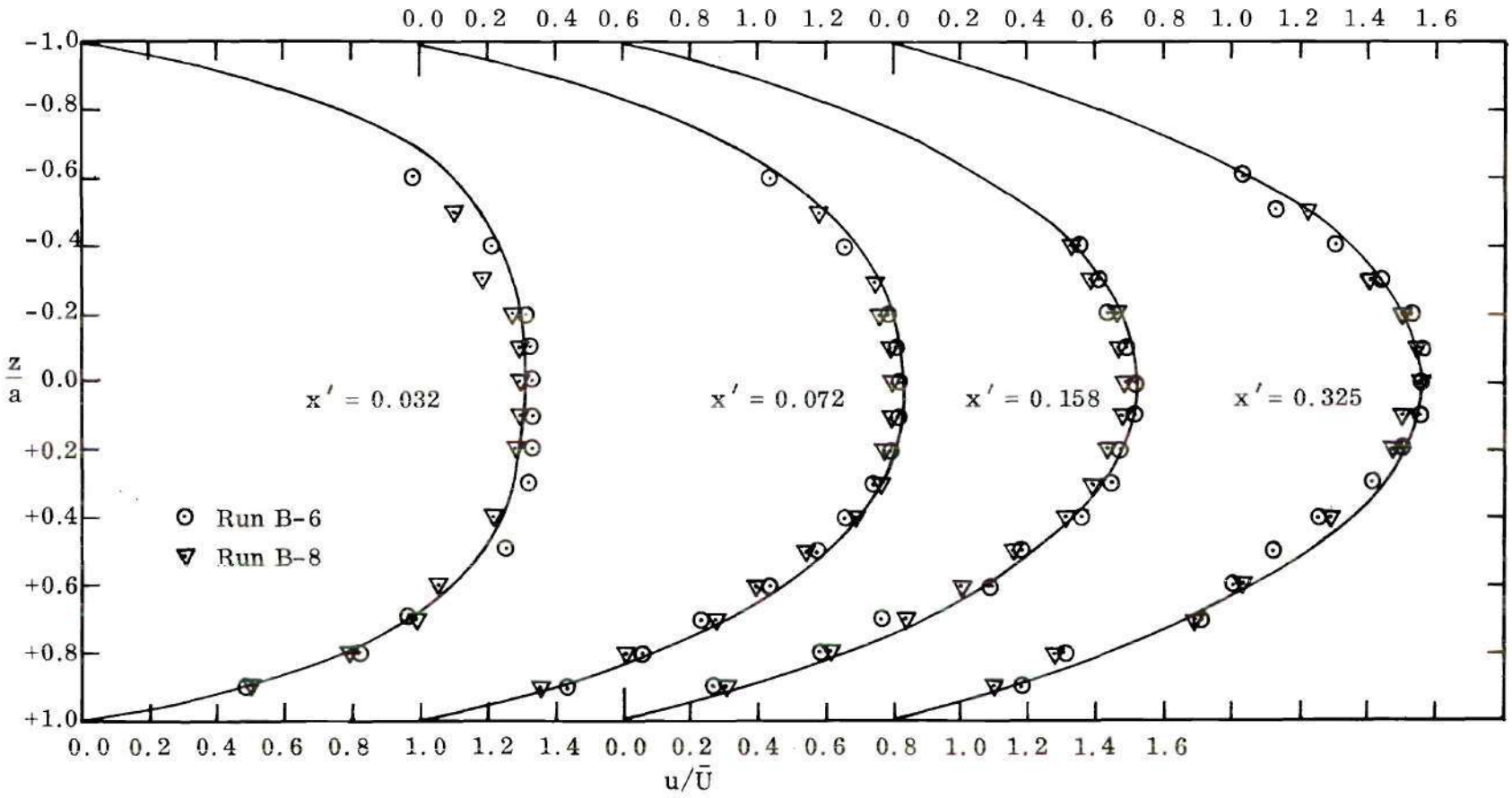

Figure 20. Velocity Profiles for Ha = 1.2 in 6-to-1 Channel.

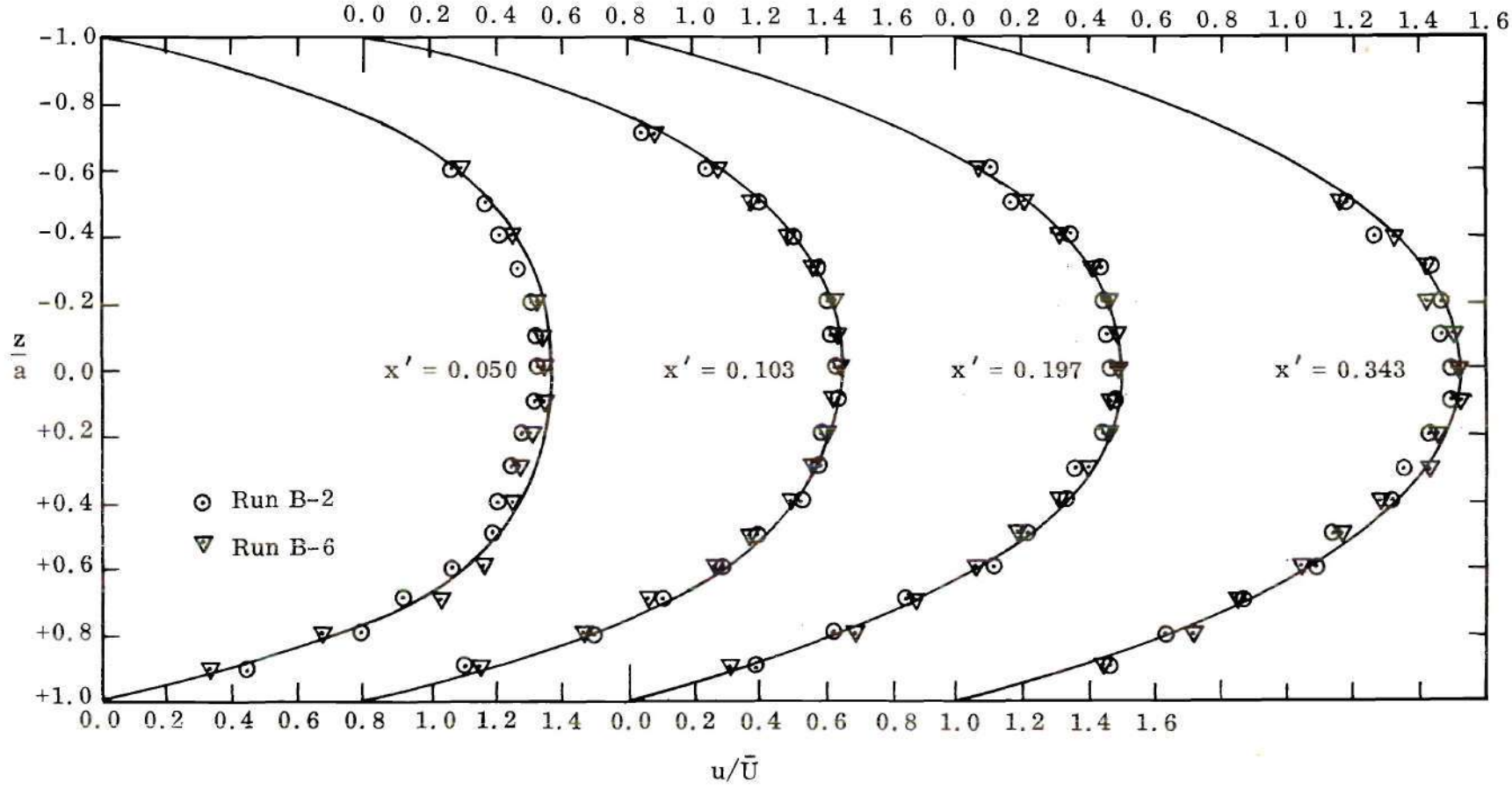

Figure 21. Velocity Profiles for Ha = 1.6 in 6-to-1 Channel.

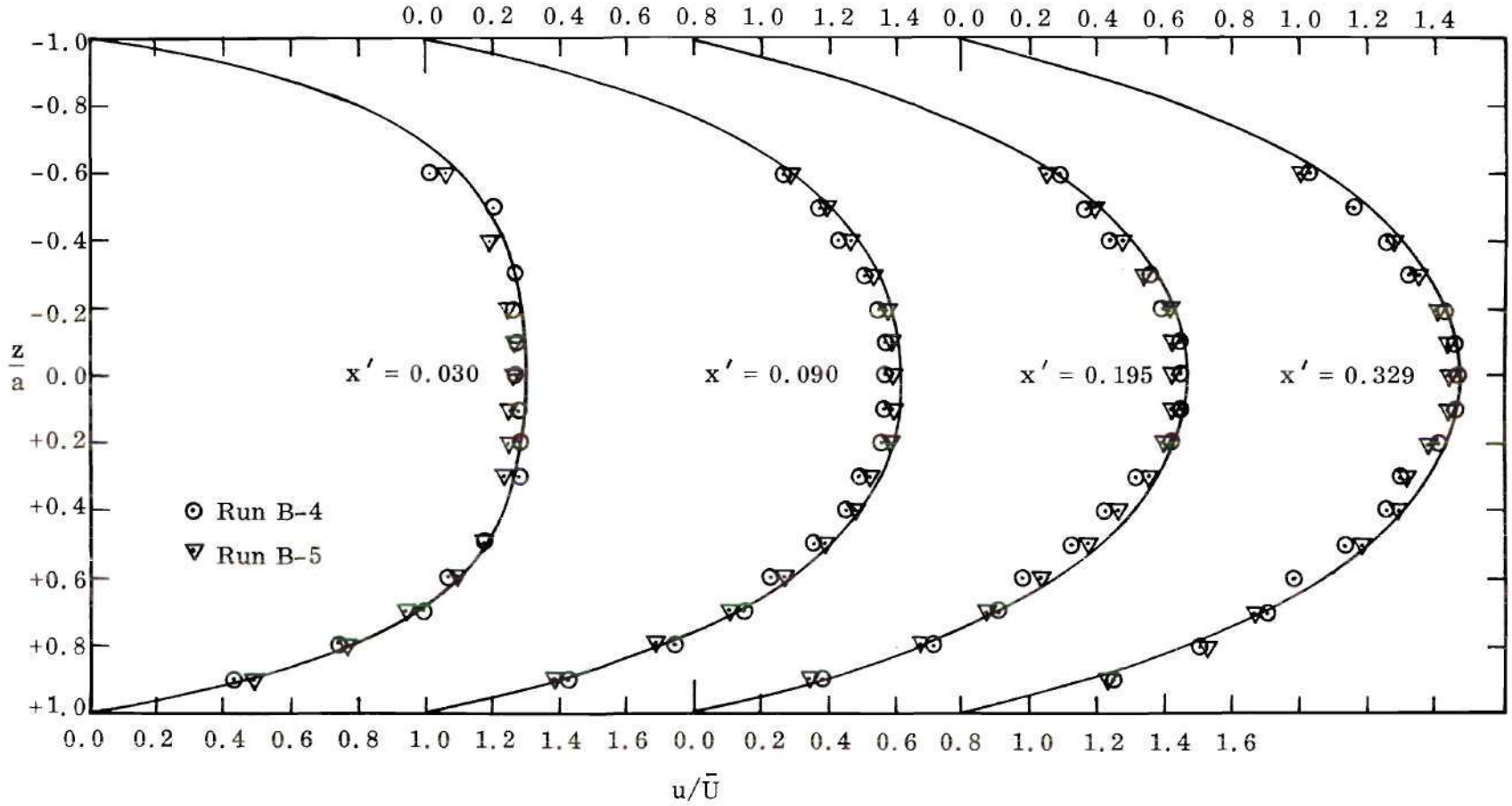

Figure 22. Velocity Profiles for Ha = 2.0 in 6-to-1 Channel.

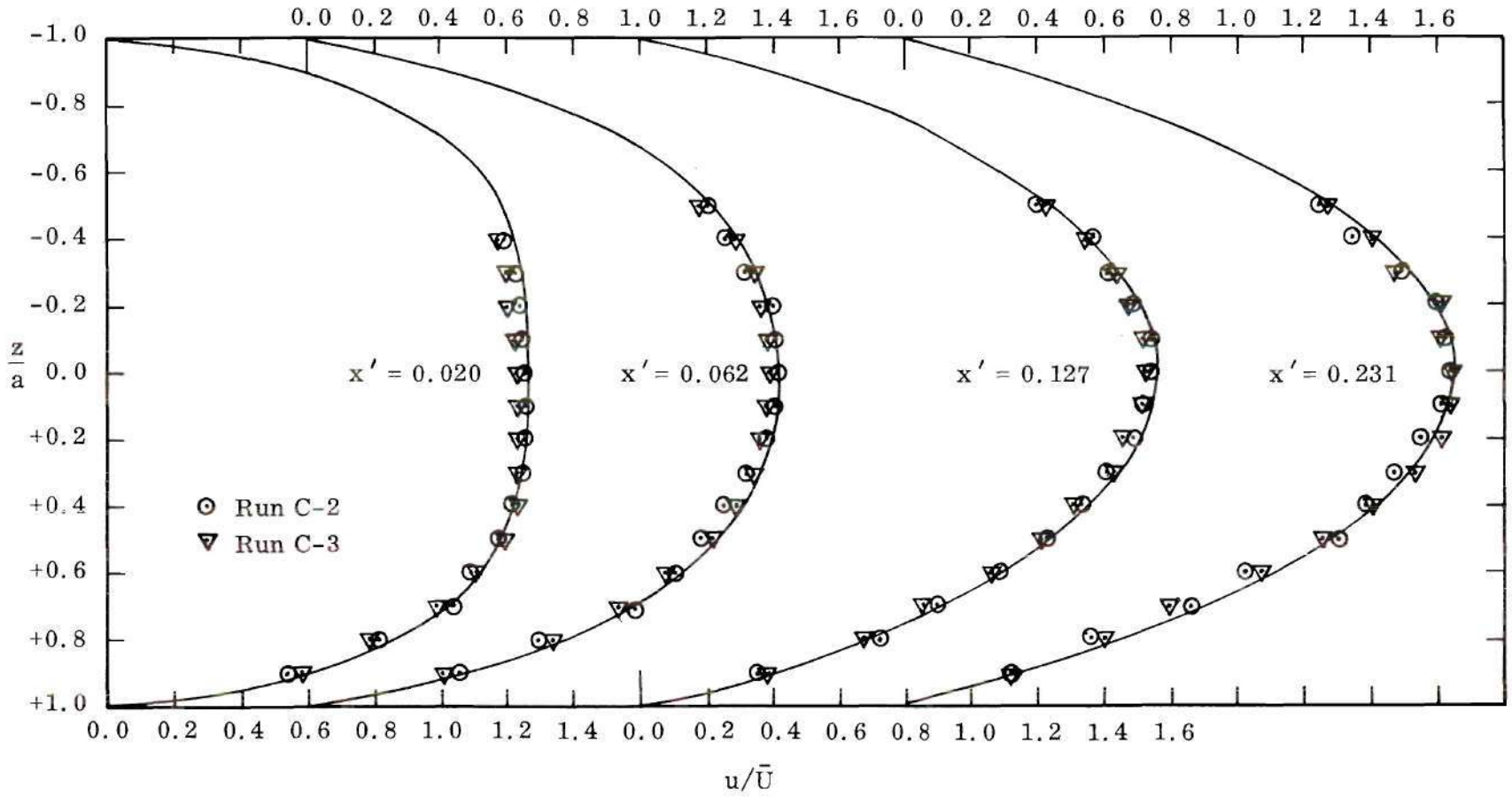

Figure 23. Velocity Profiles for Ha = 0 in 4-to-1 Channel.

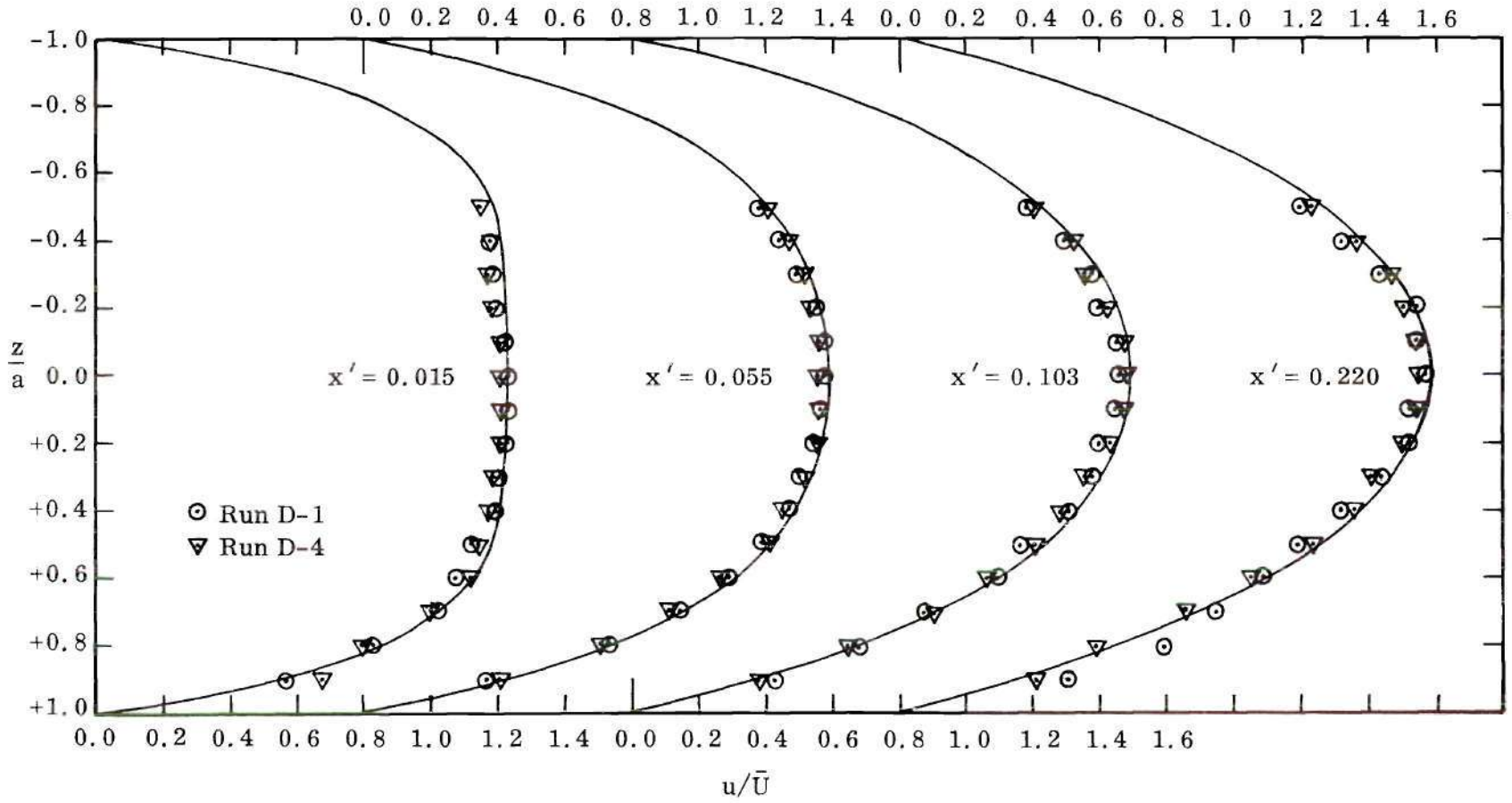

Figure 24. Velocity Profiles for Ha = 1.2 in 4-to-1 Channel.

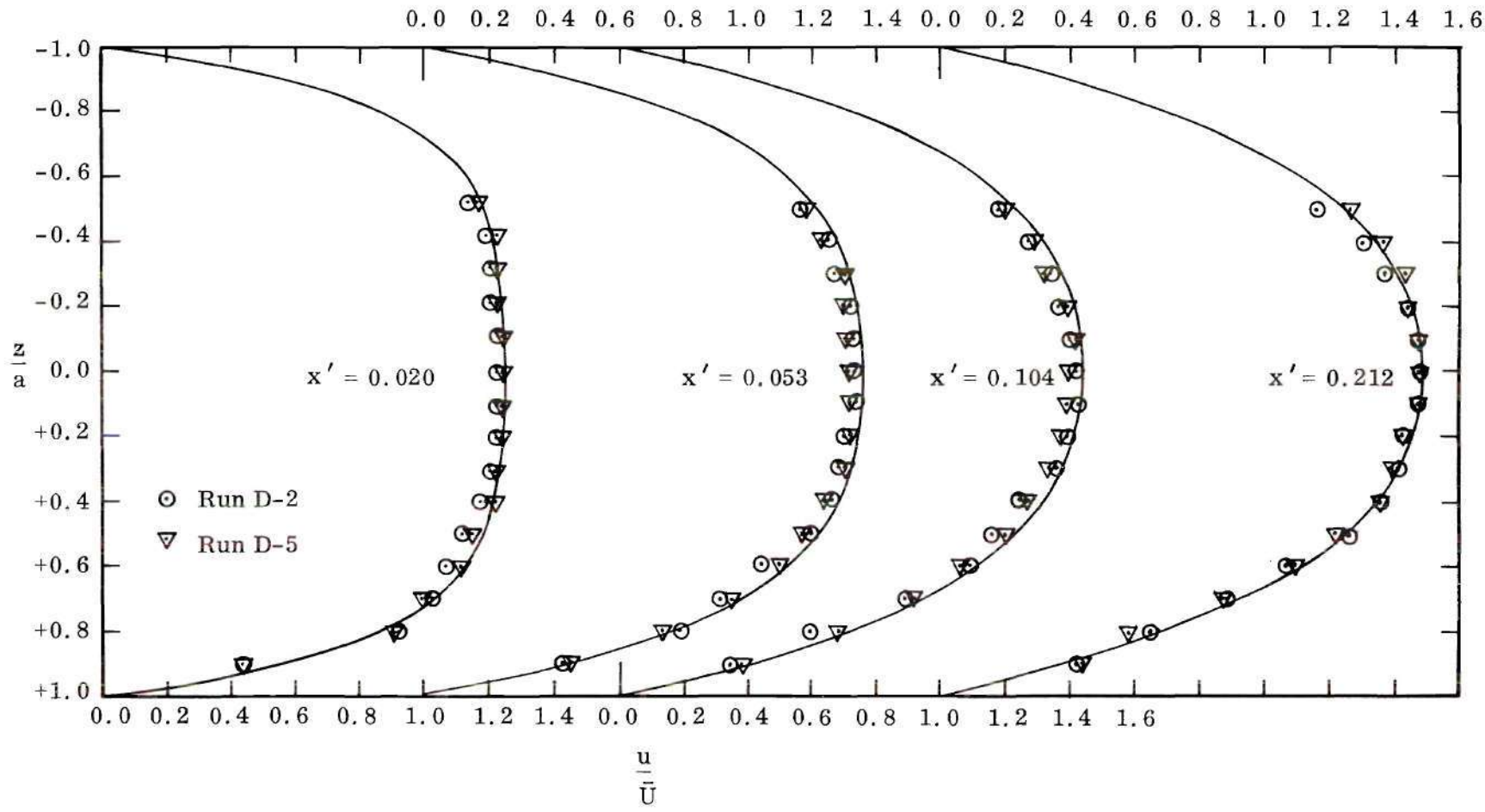

Figure 25. Velocity Profiles for Ha = 2.0 in 4-to-1 Channel.

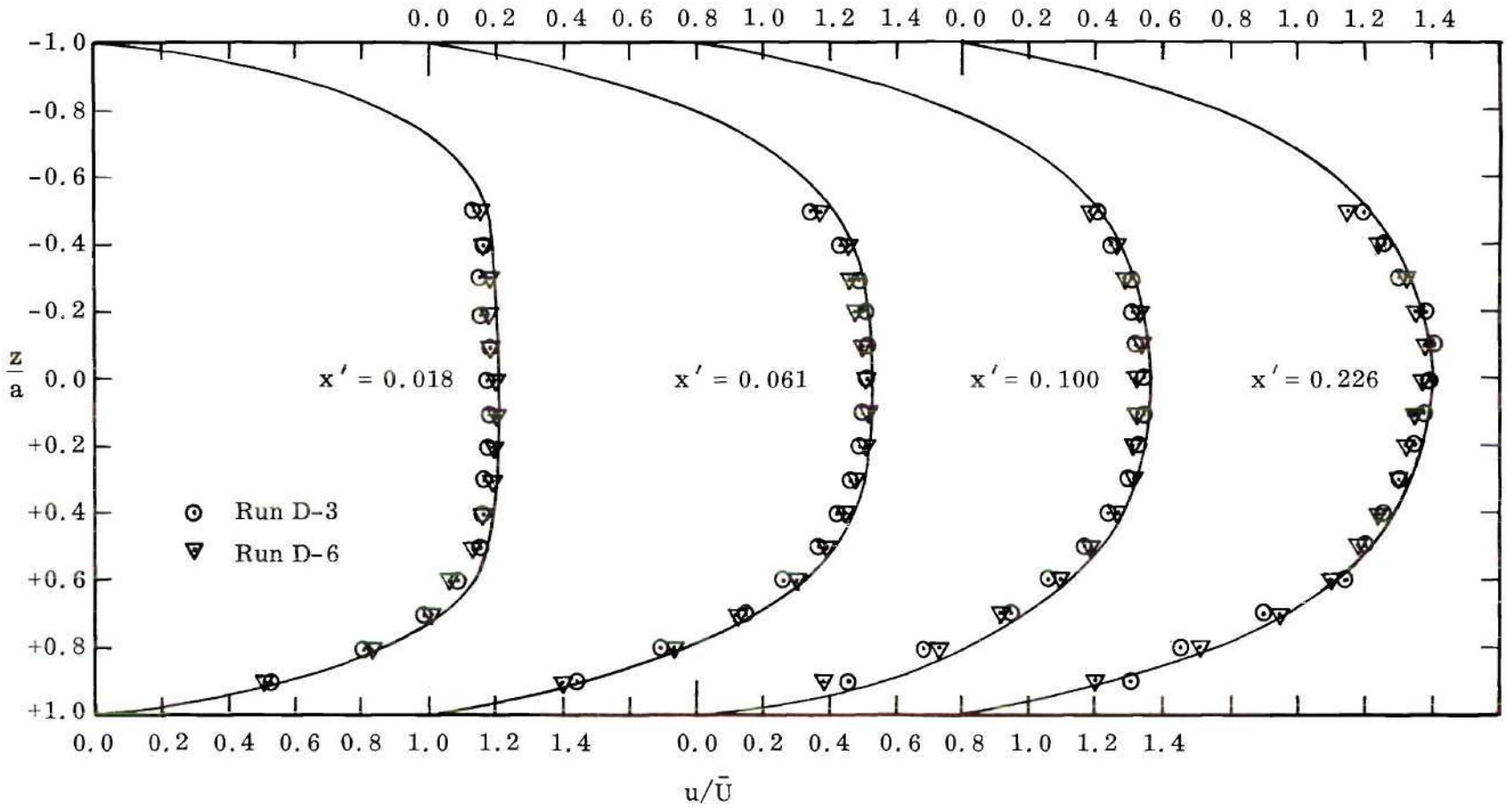

Figure 26. Velocity Profiles for Ha = 2.9 in 4-to-1 Channel.

quite clearly. For an x' value of approximately 0.225 the maximum non-dimensional velocity was reduced from 1.62 for Ha=0 to 1.40 for Ha=2.9 in the 4-to-1 channel. The reduction in the 6-to-1 channel was from 1.62 at Ha=0 to 1.46 at Ha=2.0 for x'=0.330. The "flattening" of the profile with increasing Hartmann number was also observed. The decrease in the velocity near the centerline was accompanied by an increase closer to the boundaries. This flattening of the profile resulted from the Lorentz force and was more pronounced for the larger Hartmann numbers, as shown by the results obtained.

The results of tests to obtain entrance length data are shown in Figures 27 through 34. These figures show the non-dimensional centerline velocity as a function of x'. The theoretical curve is also shown. An examination of the data reveals that the analytical model predicted a more rapid development of the velocity profile than was found experimentally for all cases. The difference in values was consistently less than 5%. This result was not totally unexpected. Other investigators have obtained similar results. Sparrow, et. al. (43), in their investigation of non-MHD flow in 2-to-1 and 5-to-1 channels, found that the centerline velocities predicted by Han (19) were approximately 5% higher than their experimental results. Similarly, the results of Goldstein and Kreid (44) for non-MHD flow in a square channel exhibited the same tendencies. The experimental data of Sparrow, Lin, and Lundgren (20) for a circular tube show the identical qualitative results when compared to Langhaar's (18) analytically predicted values which were obtained using the linearization technique. Thus, it would appear that this method tends to predict a more rapid development of the velocity field than

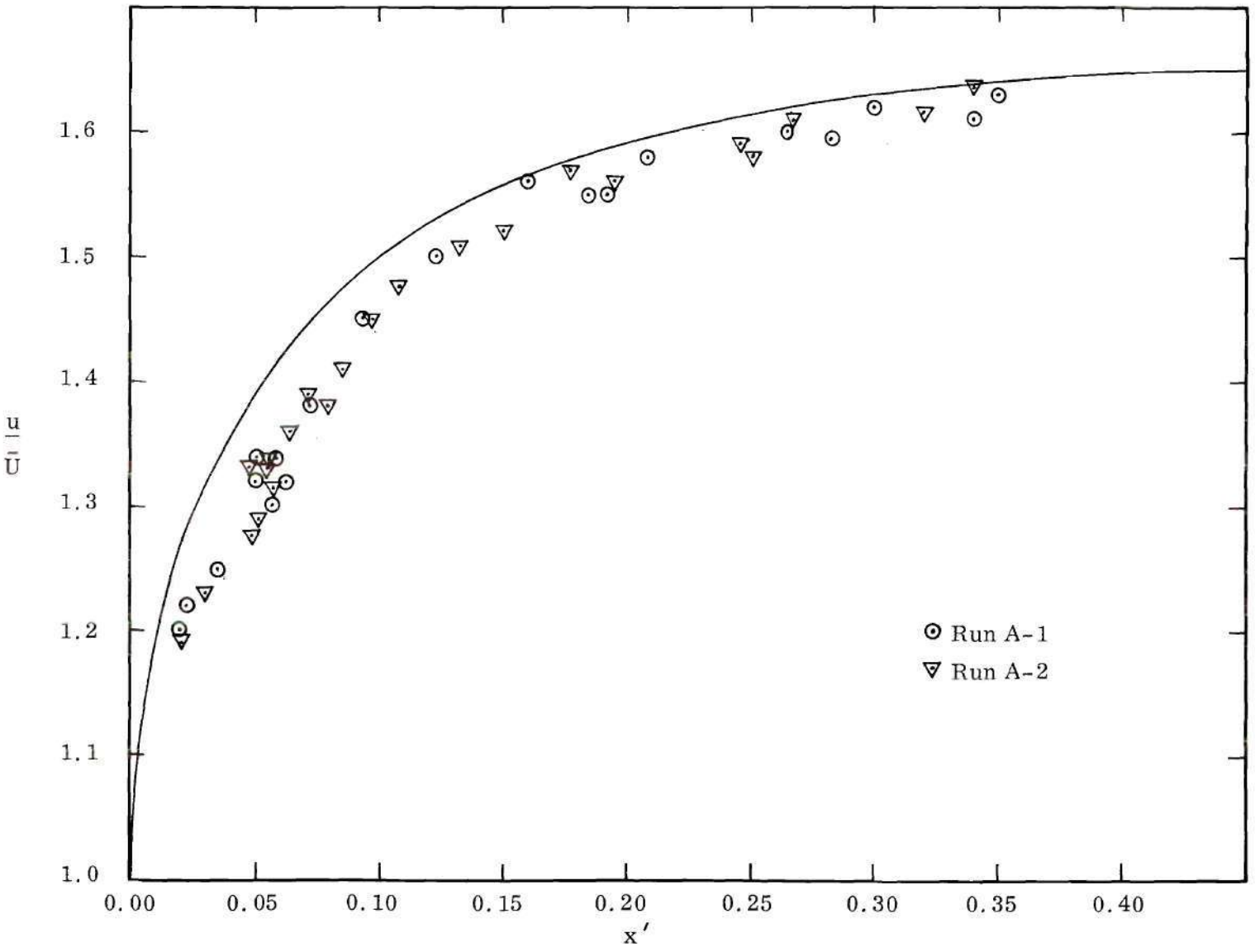

Figure 27. Centerline Velocity vs. Axial Position for Ha = 0, $\gamma = 1/6$.

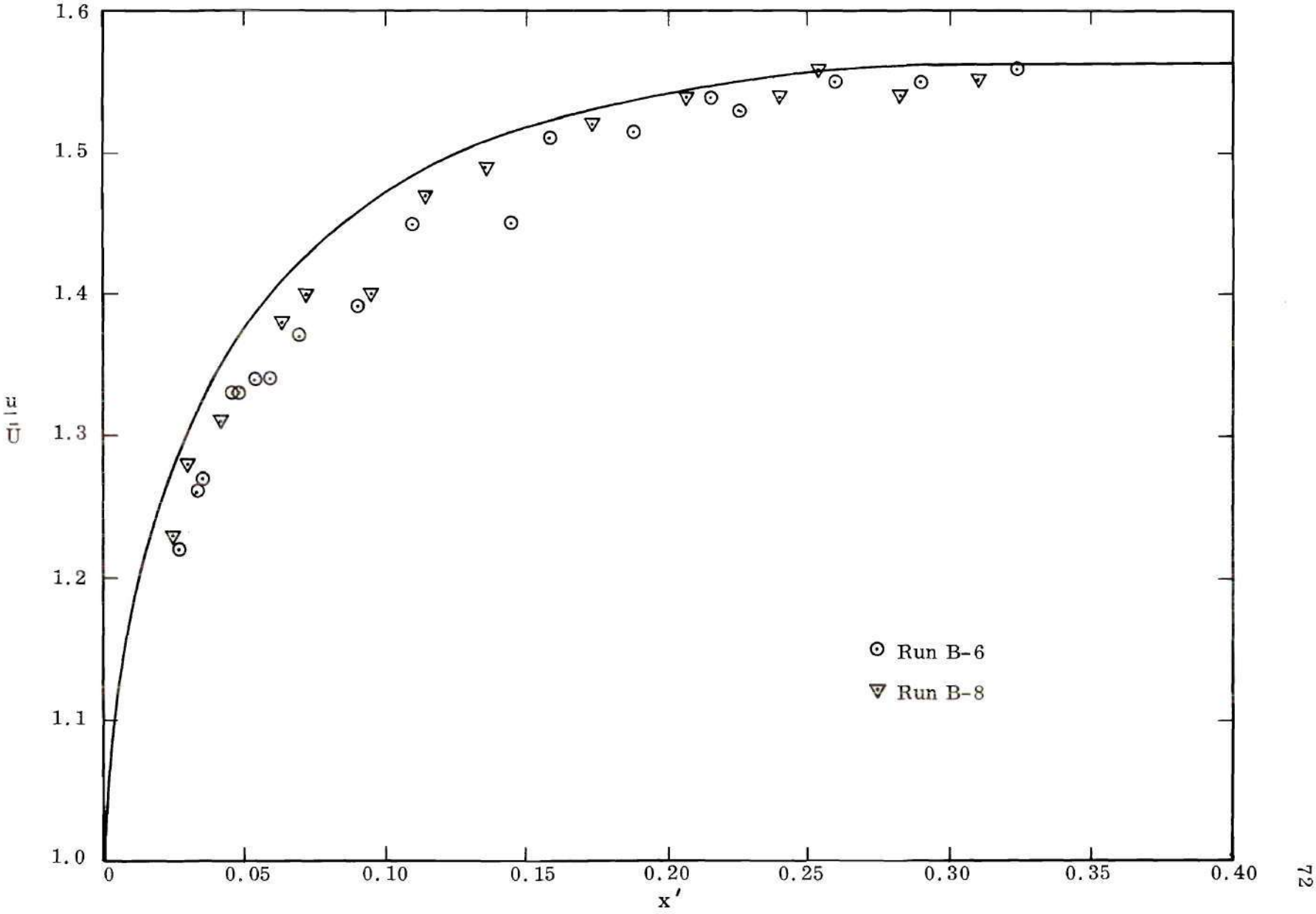

Figure 28. Centerline Velocity vs. Axial Position for Ha = 1.2, $\gamma = 1/6$.

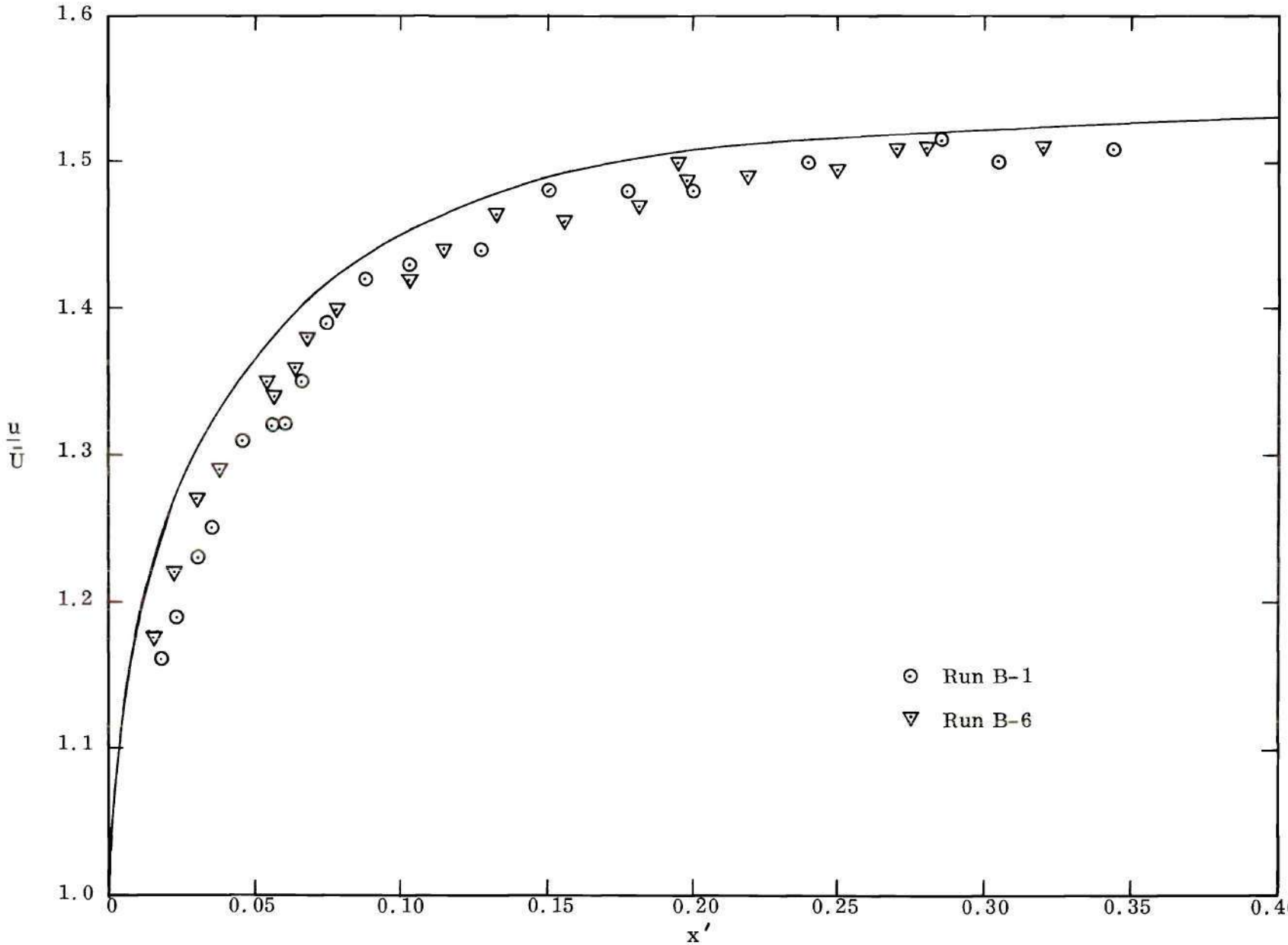

Figure 29. Centerline Velocity vs. Axial Position for Ha = 1.6, $\gamma = 1/6$.

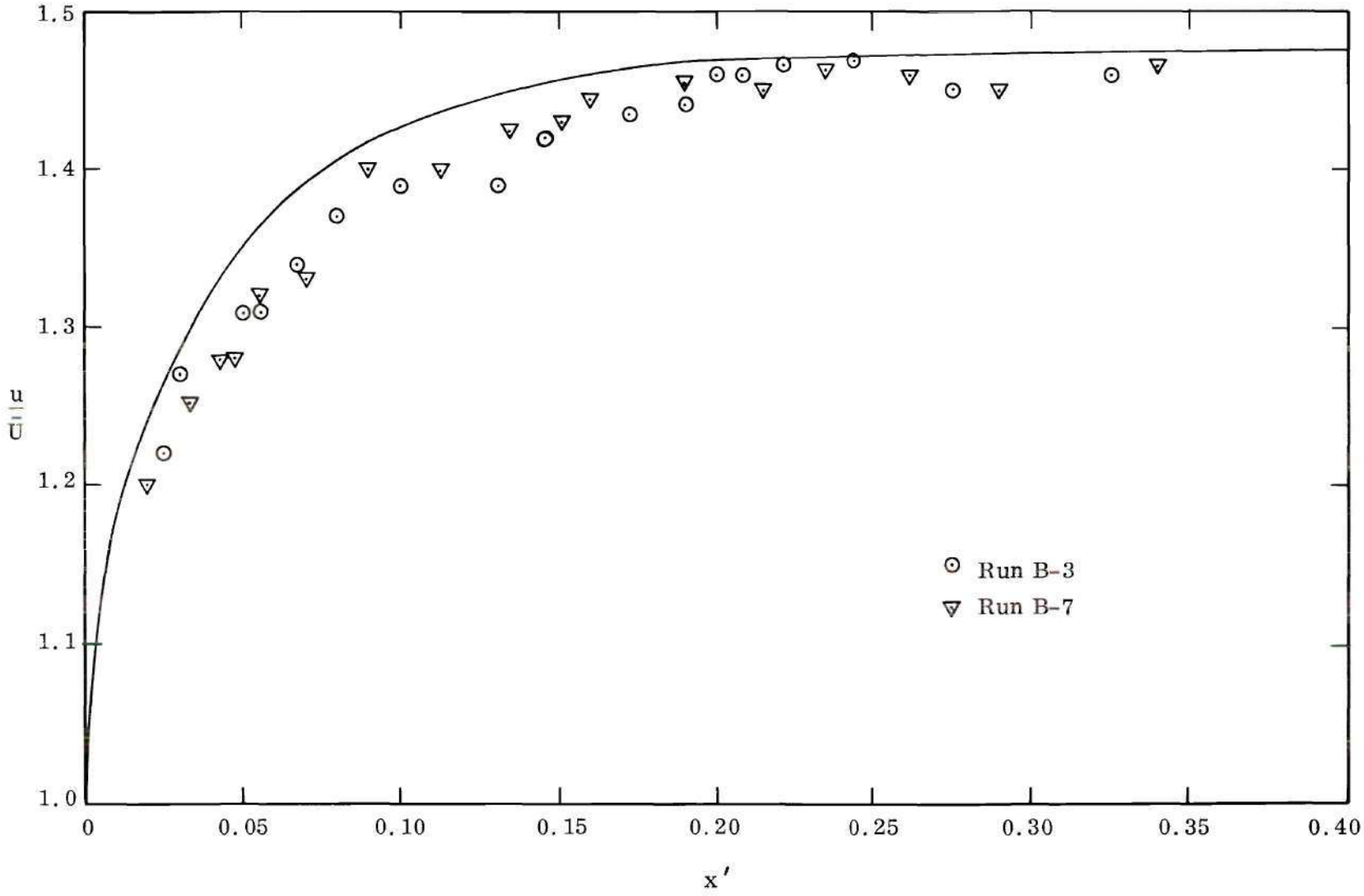

Figure 30. Centerline Velocity vs. Axial Position for Ha = 2.0, $\gamma = 1/6$.

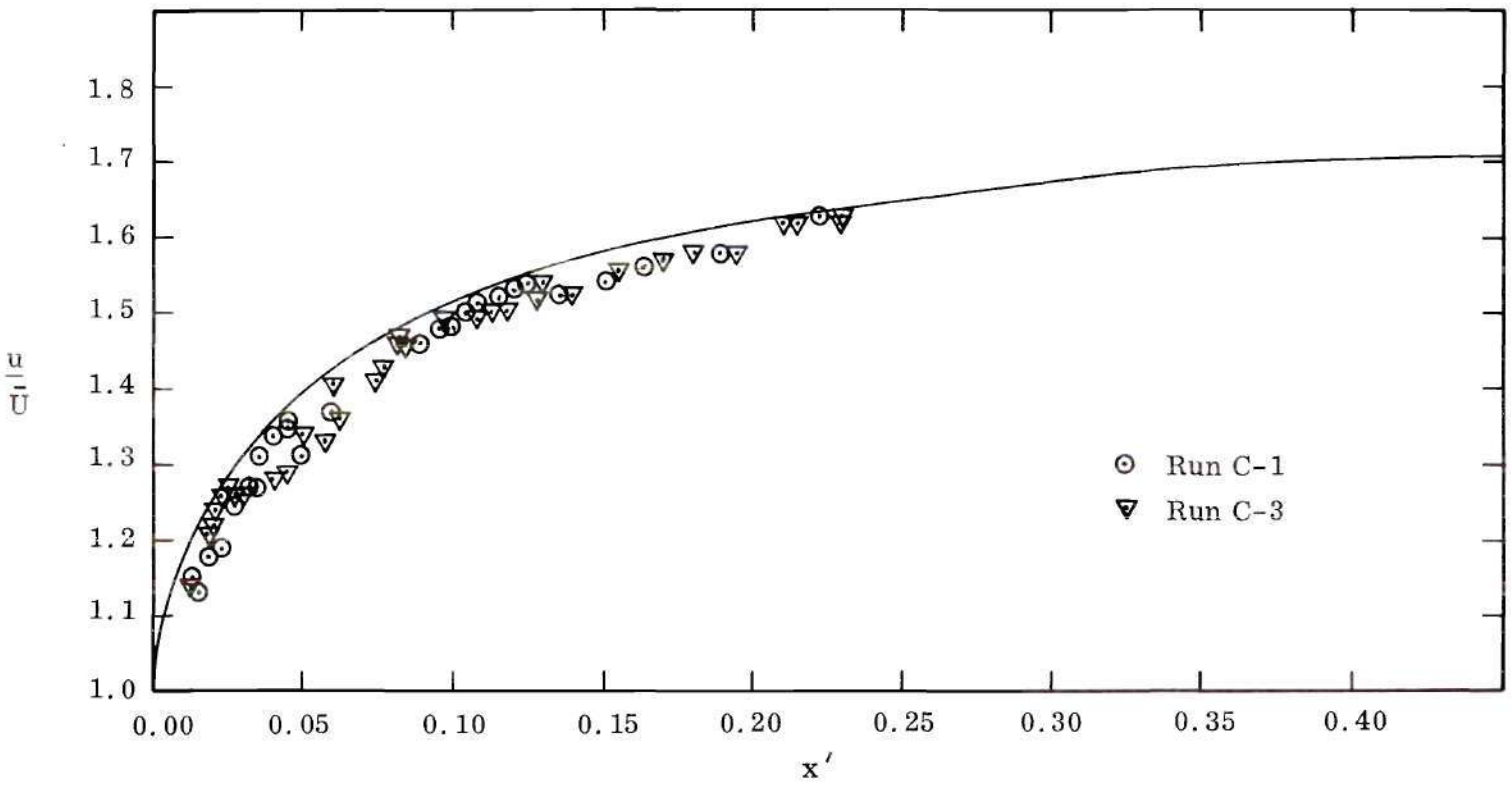

Figure 31. Centerline Velocity vs. Axial Position for Ha = 0, $\gamma = 1/4$.

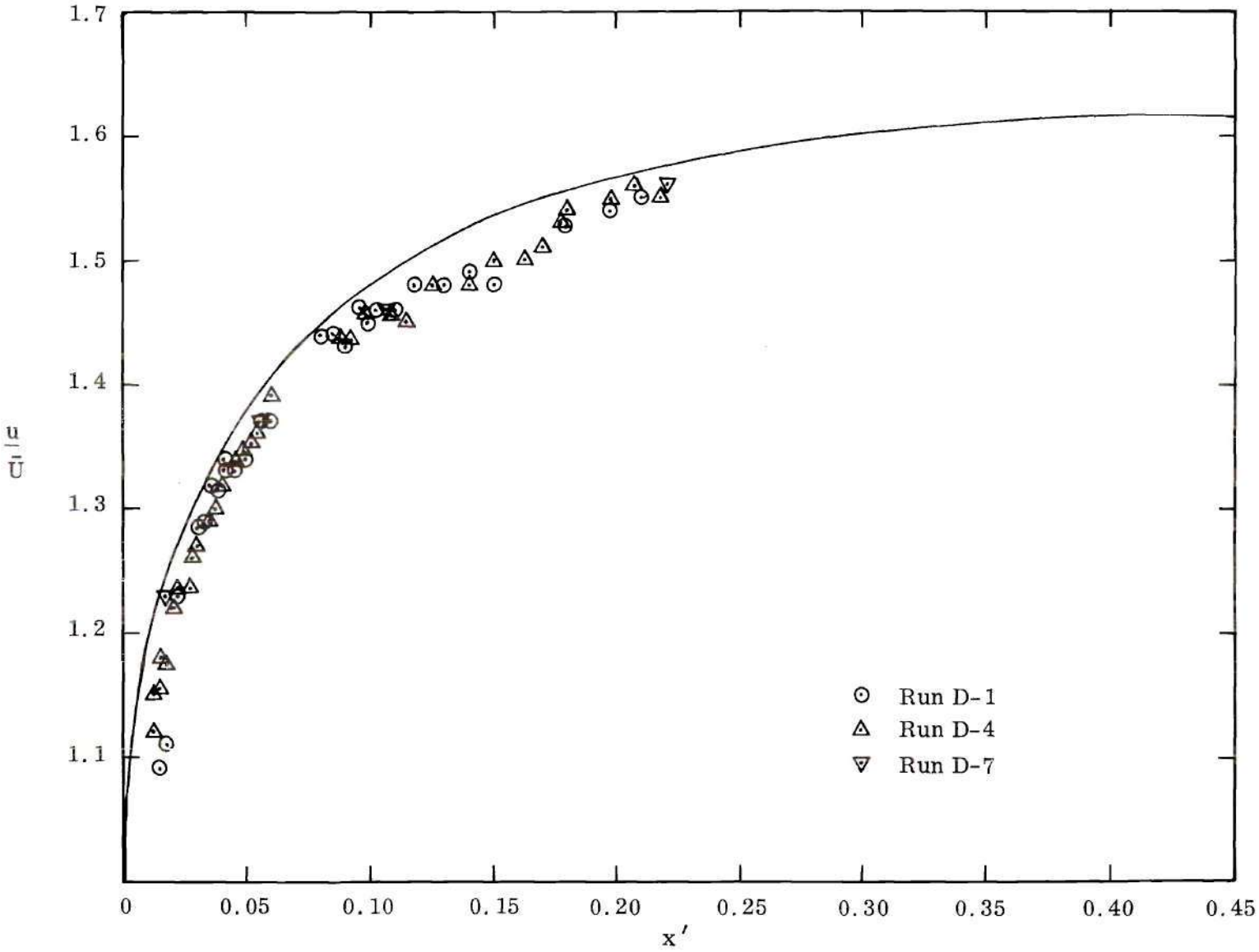

Figure 32. Centerline Velocity vs. Axial Position for Ha = 1.2, γ= 1/4.

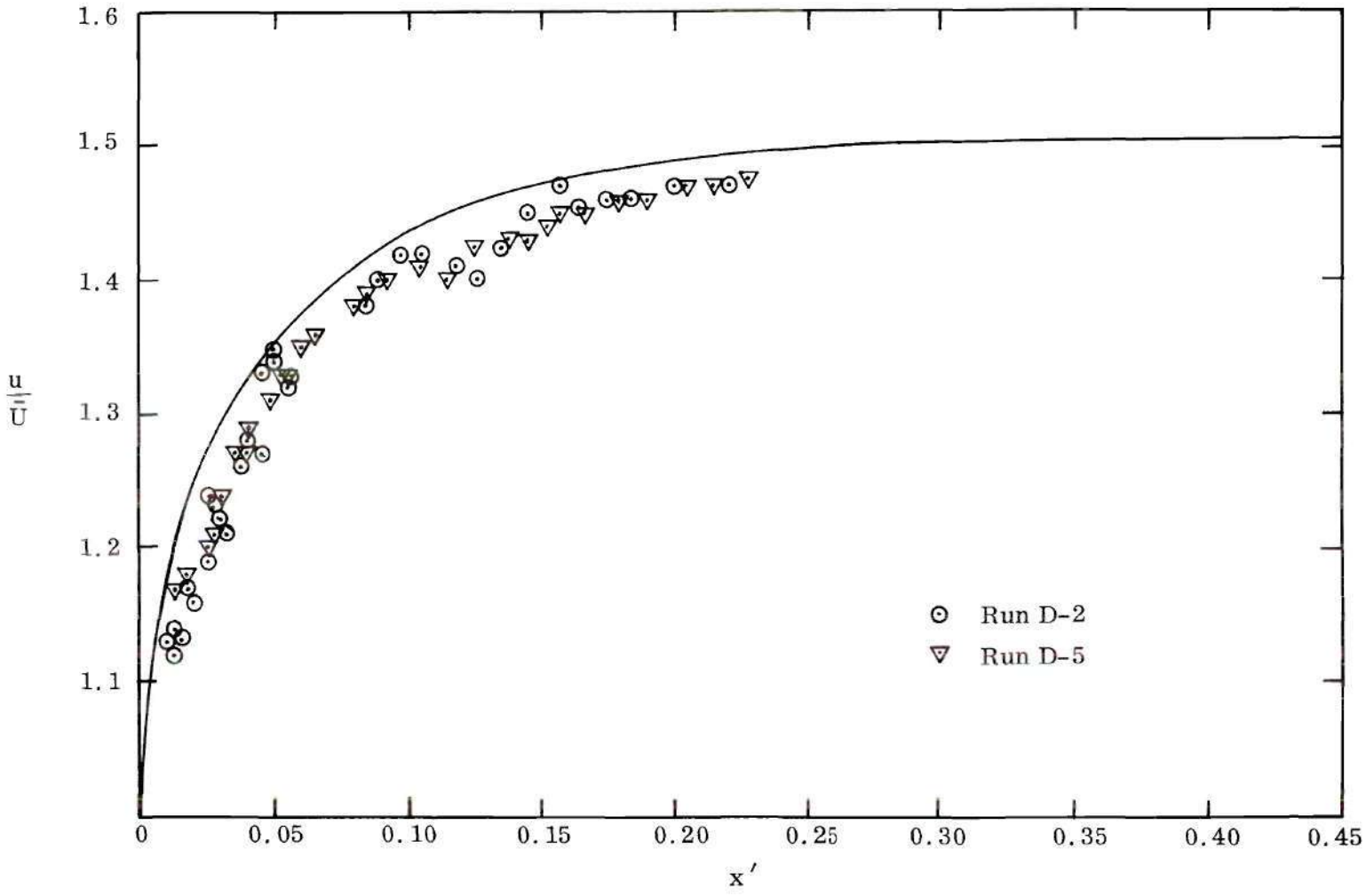

Figure 33. Centerline Velocity vs. Axial Position for Ha = 2.0, $\gamma = 1/4$.

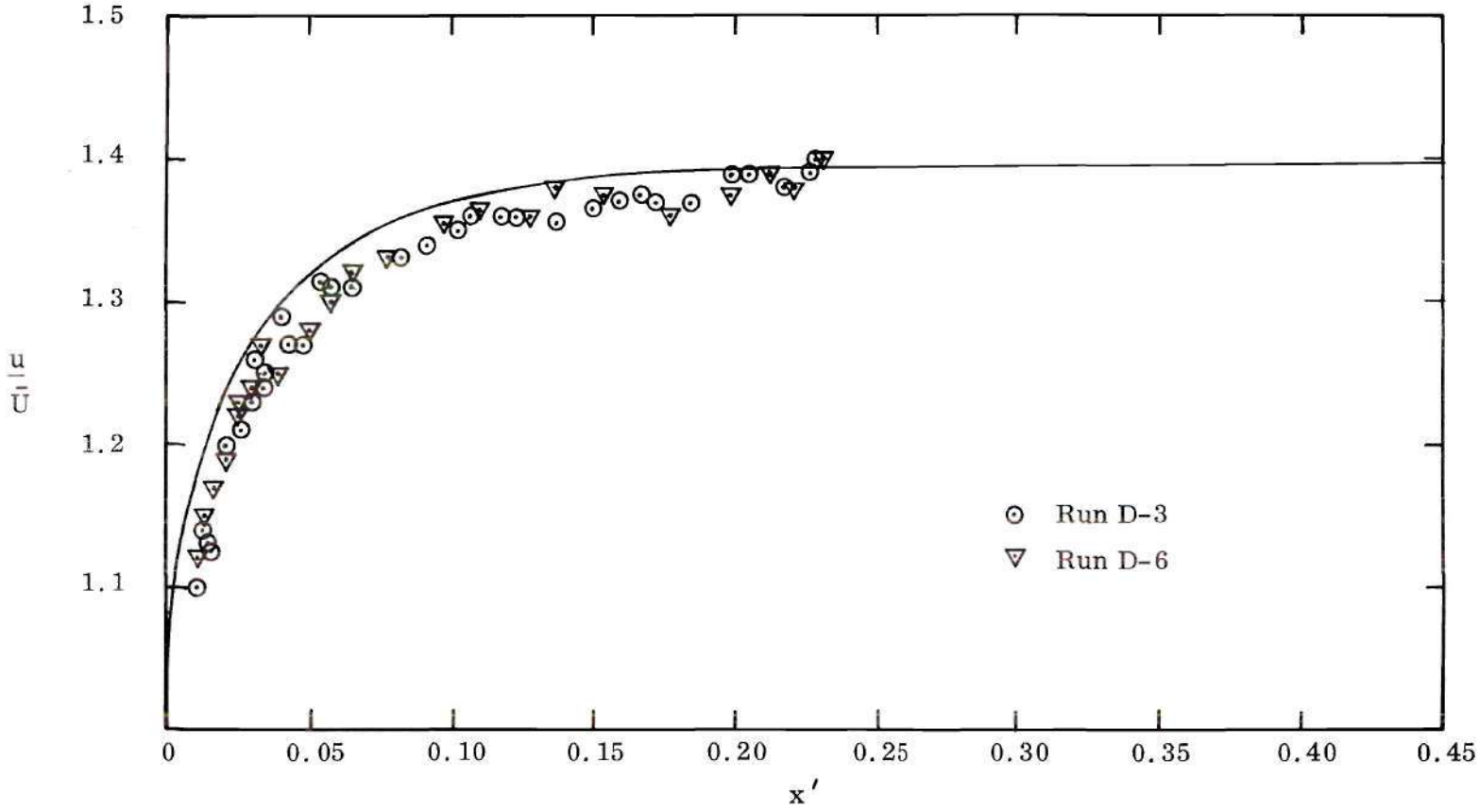

Figure 34. Centerline Velocity vs. Axial Position for Ha = 2.9, $\gamma = 1/4$.

occurs in reality for seemingly all conditions. However, the deviation is not excessive and the utilization of the method for predicting entrance region conditions would appear to be justifiable.

As stated previously, the maximum value of x' which could be attained was limited by the minimum flow rate which it was practical to maintain. Thus it was not possible in most cases to obtain the fully developed state at the probe. In these cases, the data tended toward the analytical fully developed values. In the 6-to-1 aspect ratio channel, for Hartmann numbers of 1.6 and 2.0 and in the 4-to-1 channel for Ha=2.9, the experimental values began to change very slowly with increasing x' for the larger values of this parameter, indicating the approach to the fully developed condition. The magnitudes of the analytical and experimental velocities agreed quite closely in this region also. The favorable results obtained in these cases lend credence to the earlier hypothesis that the fully developed state was being approached.

The centerline data point out the effect of the aspect ratio on the flow development very graphically. A comparison of results for the two channels at the same Hartmann number shows that the development in the 6-to-1 channel was somewhat faster than in the 4-to-1. As the Hartmann number increased, however, this difference in the entrance length became smaller.

The centerline data also show that the fully-developed centerline velocity attained was a function of the channel aspect ratio for a given Hartmann number. For Ha=0, this velocity approached 1.77 for the 4-to-1 channel but only 1.67 for the 6-to-1 channel. These values are considerably higher than the fully-developed

centerline velocity magnitude of 1.50 for the two-dimensional parallel plate channel. The centerline velocity for full-developed flow approached 1.51, 1.47, and 1.42 for the 4-to-1, 6-to-1, and parallel plate channels, respectively, when the Hartmann number was 2.0. A higher centerline velocity was experienced in the two finite width channels as expected because of the influence of the side walls. The boundary layer formation on these walls retards a portion of the flow necessitating a larger velocity in the center portion of the channel to maintain the same average flow rate. As the width-to-height ratio decreases, so does the effect of the side walls, resulting in smaller centerline velocities as shown by the data.

The results of these tests show the Hartmann effect clearly also. The decrease in the centerline velocity at a given value of x' for increasing Hartmann number reflects the "flattening" of the profile caused by the Lorentz force. Comparison of centerline velocities reveals the decrease in the entrance length associated with the increase in Hartmann number. Since the profile assumed a flatter shape for larger values of the Hartmann number, the adjustment from the initial uniform profile to the fully-developed one required a shorter distance and the entrance length was reduced accordingly.

No appreciable difference in non-dimensional centerline velocities between the short and open circuit conditions were noted. This also was in accord with the analytical model. The effect of the electric field was to change the pressure drop in the channel which was necessary to maintain a given flow rate. Only very slight adjustment of the flow rate was necessary when changing from one field condition to another. This was expected since the pressure drop in the channel was small

compared to that in the other parts of the system. Since no pressure measurements were taken, it was not possible to reach any conclusions concerning the effect of the electric field on the pressure drop in the channel.

CHAPTER V

CONCLUSIONS AND RECOMMENDATIONS

The experimental results obtained in the course of this work tended to support the results predicted analytically using the approximate model described in Chapter II. Although the model predicted values which were consistently 2 to 5% high, it is felt that this discrepancy is not sufficiently large to invalidate the results. Nor was the disagreement large enough to warrant major revision in the model which would increase the complexity and, consequently, the difficulty in obtaining a solution.

As predicted, the velocity profile in the entrance region and the entrance length itself are functions of both the Hartmann number and the aspect ratio of the channel. An increase in Hartmann number decreases the entrance length and flattens the velocity profile at all cross sections in the channel. The entrance length and the centerline velocity are increased as the aspect ratio approaches 1. The electric field has no effect on the non-dimensional velocity profile or its development.

Since it was possible to investigate only a small range of Hartmann numbers in this work, future investigators might consider increasing the value of the Hartmann number in an experiment of this type. To do so will require either a much stronger electromagnet or a working fluid with a much higher electrical conductivity than a potassium chloride solution.

Another parameter which needs to be increased from the values obtainable in this work is x'. This would involve increasing the distance of the probe from the inlet or decreasing the channel width. These parameters are subject to several physical constraints. Perhaps a better method of increasing x' would be to decrease the flow rate through the channel. To do so and still be able to measure the velocity will be difficult. The use of a laser velocimeter could possibly overcome these difficulties. Difficulties in setting up the optical system in the confined space of the electromagnet might eliminate this method of velocity measurement.

Further investigations might include the effect of entrance velocity profile, the Hall parameter, or variable electrical conductivity on the entrance region.

APPENDICES

APPENDIX A

DERIVATIONS RELEVANT TO THE ANALYTICAL STUDY

Electric Field in the Channel

For the geometry and flow conditions being investigated here, it is possible to show that the electric field inside the channel is constant. In the electrodes, the electric field is by necessity everywhere zero. From Maxwell's equation

$$\nabla \times \bar{E} = 0 \tag{A-1}$$

the electrostatic boundary condition for problems involving the interface of two dielectrics is

$$E_{t_1} = E_{t_2} \tag{A-2}$$

where the subscripts indicate the tangential field in materials 1 and 2, respectively (52). Since the tangential field is zero in the electrodes, it will be zero in the fluid as well. Thus

$$E_x = 0 \tag{A-3}$$

and

$$E_z = 0 \tag{A-4}$$

Using these equations in conjunction with the Maxwell relation above yields.

$$\frac{\partial E_y}{\partial x} = \frac{\partial E_x}{\partial y} = 0 \qquad \text{(A-5)}$$

$$\frac{\partial E_y}{\partial z} = \frac{\partial E_z}{\partial y} = 0 \qquad \text{(A-6)}$$

From the Maxwell relation

$$\nabla \cdot \bar{E} = 0 \qquad \text{(A-7)}$$

it follows that

$$\frac{\partial E_x}{\partial x} + \frac{\partial E_y}{\partial y} + \frac{\partial E_z}{\partial z} = 0 \qquad \text{(A-8)}$$

or

$$\frac{\partial E_y}{\partial y} = 0 \qquad \text{(A-9)}$$

Since it has been shown that E_y is not a function of any spatial variables, it follows that E_y is a constant across the channel. Use of this fact has been made in the analysis given in Chapter II.

Von Kármán Integral Equation

The continuity equation for an incompressible fluid is given by

$$\frac{\partial u}{\partial x} + \frac{\partial v}{\partial y} + \frac{\partial w}{\partial z} = 0 \qquad \text{(A-10)}$$

Using the relationships

$$u \frac{\partial u}{\partial x} = \frac{\partial u^2}{\partial x} - u \frac{\partial u}{\partial x} \tag{A-11}$$

$$v \frac{\partial u}{\partial y} = \frac{\partial (uv)}{\partial y} - u \frac{\partial v}{\partial y} \tag{A-12}$$

and

$$w \frac{\partial u}{\partial z} = \frac{\partial (uw)}{\partial z} - u \frac{\partial w}{\partial z} \tag{A-13}$$

the left-hand side of equation (1) may be written

$$u \frac{\partial u}{\partial x} + v \frac{\partial u}{\partial y} + w \frac{\partial u}{\partial x} = \frac{\partial u^2}{\partial x} - u \frac{\partial u}{\partial x} + \frac{\partial (uv)}{\partial y} - u \frac{\partial v}{\partial y} + \frac{\partial (uw)}{\partial z} - u \frac{\partial w}{\partial z} \tag{A-14}$$

But from equation (A-10) above, the three terms which are subtracted are equal to zero. Thus,

$$u \frac{\partial u}{\partial x} + v \frac{\partial u}{\partial y} + w \frac{\partial u}{\partial z} = \frac{\partial u^2}{\partial x} + \frac{\partial (uv)}{\partial y} + \frac{\partial (uw)}{\partial z} \tag{A-15}$$

To obtain the Von Ka'rman integral equation, equation (1) with the left-hand side represented by equation (A-15) is integrated across the cross-section. Now

$$\int_{-a}^{a} \int_{-b}^{b} \frac{\partial (uv)}{2y} \, dydz = \int_{-a}^{a} (uv) \Big|_{-b}^{b} \, dz = 0 \tag{A-16}$$

since the velocities u and v must vanish at the surface. Similarly,

$$\int_{-b}^{b} \int_{-a}^{a} \frac{\partial (uw)}{\partial z} \, dzdy = \int_{-b}^{b} (uw) \Big|_{-a}^{a} \, dy = 0 \tag{A-17}$$

Therefore, the integration of equation (1) yields

$$\frac{\partial}{\partial x}\int_A u^2 dA = -\frac{1}{\rho}\frac{\partial P}{\partial x}\int_A dA + \nu\int_A (\nabla^2 u)\, dA$$

$$+ \frac{\sigma B_o^2}{\rho}\left(K\bar{U}\int_A dA - \int_A u\, dA\right) \qquad \text{(A-18)}$$

which is equation (26).

APPENDIX B

REDUCTION OF DOUBLY INFINITE SERIES

From equation (15), the non-dimensional velocity field is given by

$$\frac{u}{\bar{U}} = \frac{\frac{\pi^2}{4} \sum_{m\ \text{odd}}^{\infty} \sum_{n\ \text{odd}}^{\infty} \frac{(-1)^{\frac{m+n}{2}-1} \cos\left(\frac{m\pi z}{2a}\right) \cos\left(\frac{n\pi y}{2b}\right)}{mn\left[\left(\frac{2\beta a}{\pi}\right)^2 + m^2 + \gamma^2 n^2 + \left(\frac{2Ha}{\pi}\right)^2\right]}}{\sum_{m\ \text{odd}}^{\infty} \sum_{n\ \text{odd}}^{\infty} \frac{1}{m^2 n^2\left[\left(\frac{2\beta a}{\pi}\right)^2 + m^2 + \gamma^2 n^2 + \left(\frac{2Ha}{\pi}\right)^2\right]}} \tag{15}$$

Defining new terms, which are independent of m and n, by

$$D = \left[\left(\frac{2\beta a}{\pi}\right)^2 + \left(\frac{2Ha}{\pi}\right)^2\right]^{\frac{1}{2}} \tag{B-1}$$

$$y' = \pi y/2b \tag{B-2}$$

$$z' = \pi z/2a \tag{B-3}$$

and introducing E_1 and E_2, equation (15) may be written

$$\frac{u}{\bar{U}} = \frac{E_1}{E_2} \tag{B-4}$$

where E_1 is the numerator and E_2 is the denominator of the right-hand side of equation (15).

Attention is first directed toward reducing E_1. E_1 may also be written

$$E_1 = \frac{\pi^2}{4}\left[\sum_{n\ \text{odd}}^{\infty} \frac{(-1)^{\frac{n-1}{2}}\cos(ny')\cos(z')}{n(D^2+1+\gamma^2 n^2)}\right.$$

$$-\sum_{n\ \text{odd}}^{\infty} \frac{(-1)^{\frac{n-1}{2}}\cos(ny')\cos(3z')}{3n(D^2+9+\gamma^2 n^2)} + \sum_{n\ \text{odd}}^{\infty} \frac{(-1)^{\frac{n-1}{2}}\cos(ny')\cos(5z')}{5n(D^2+25+\gamma^2 n^2)}$$

$$\left. - \ldots\ldots\ldots\right] \qquad \text{(B-5)}$$

where it has been expanded for the values of m. Expanding the terms in the denominators of each series in equation (B-5) leads to the result

$$E_1 = \frac{\pi^2}{4}\left[\sum_{n\ \text{odd}}^{\infty} \frac{(-1)^{\frac{n-1}{2}}\cos(ny')\cos(z')}{1(D^2+1)} \cdot \left(\frac{1}{n} - \frac{\gamma^2 n}{D^2+1+\gamma^2 n^2}\right)\right.$$

$$-\sum_{n\ \text{odd}}^{\infty} \frac{(-1)^{\frac{n-1}{2}}\cos(ny')\cos(3z')}{3(D^2+9)} \cdot \left(\frac{1}{n} - \frac{\gamma^2 n}{D^2+9+\gamma^2 n^2}\right)$$

$$\left. + \ldots\ldots\ldots\right] \qquad \text{(B-6)}$$

Collecting similar terms and rewriting them in series forms yields

$$E_1 = \frac{\pi^2}{4}\left[\sum_{n\ \text{odd}}^{\infty} \frac{(-1)^{\frac{n-1}{2}}\cos(ny')}{n} \sum_{m\ \text{odd}}^{\infty} \frac{(-1)^{\frac{m-1}{2}}\cos(mz')}{m(D^2+m^2)}\right.$$

$$\left. - \sum_{n\ \text{odd}}^{\infty} (-1)^{\frac{n-1}{2}} \gamma^2 n \cos(ny') \sum_{m\ \text{odd}}^{\infty} \frac{(-1)^{\frac{m-1}{2}}\cos(mz')}{m(D^2+m^2)(D^2+m^2+\gamma^2 n^2)}\right] \qquad \text{(B-7)}$$

In its present form (B-7) is still not very useful. Further reduction is possible by operating on the series involving m. Let

$$S_1 = \sum_{m\ \text{odd}}^{\infty} \frac{(-1)^{\frac{m-1}{2}}\cos(mz')}{m(D^2+m^2)} = \sum_{m\ \text{odd}}^{\infty} \frac{(-1)^{\frac{m-1}{2}}\cos(mz')}{D^2}\cdot\left(\frac{1}{m} - \frac{m}{D^2+m^2}\right) \qquad \text{(B-8)}$$

where the same technique has been used as was used in deriving (B-6). S_1 may also be written

$$S_1 = \sum_{m\ \text{odd}}^{\infty} \frac{(-1)^{\frac{m-1}{2}}\cos(mz')}{D^2 m} - \sum_{m\ \text{odd}}^{\infty} \frac{(-1)^{\frac{m-1}{2}} m\cos(mz')}{D^2(D^2+m^2)} \qquad \text{(B-9)}$$

Now

$$\sum_{m\ \text{odd}}^{\infty} \frac{(-1)^{\frac{m-1}{2}} \cos(mz')}{D^2 m} = \frac{\pi}{4D^2} \tag{C-5}$$

as shown in Appendix C.

It is also shown in Appendix C, that

$$\cosh(C_1 z/a) = \sum_{m\ \text{odd}}^{\infty} \frac{(-1)^{\frac{m-1}{2}} 4m\pi \cosh(C_1) \cos(mz')}{m^2\pi^2 + 4C_1^2} \tag{C-12}$$

where C_1 is some non-dimensional constant that does not involve the index of summation m. If

$$C_1 = \frac{\pi D}{2} \tag{B-10}$$

then

$$\sum_{m\ \text{odd}}^{\infty} \frac{(-1)^{\frac{m-1}{2}} m \cos(mz')}{D^2(m^2 + D^2)} = \frac{\pi \cosh(Dz')}{4D^2 \cosh\left(\frac{\pi D}{2}\right)} \tag{B-11}$$

Thus substituting (C-5) and (B-11) into (B-9), S_1 may be expressed

$$S_1 = \frac{\pi}{4D^2} \left[1 - \frac{\cosh(Dz')}{\cosh\left(\frac{\pi D}{2}\right)} \right] \tag{B-12}$$

The second part of equation (B-7) may also be reduced by rewriting it as

$$S_2 = \frac{\pi}{4} \sum_{m\ \text{odd}}^{\infty} \left[\frac{(-1)^{\frac{m-1}{2}} \cos(mz')}{m(D^2 + m^2)} \cdot \sum_{n\ \text{odd}}^{\infty} \frac{(-1)^{\frac{n-1}{2}} \cos(ny')(4n\pi)}{\pi^2 \left(\frac{D^2 + m^2}{\gamma^2}\right) + n^2\pi^2} \right] \tag{B-13}$$

By introducing

$$B = \frac{\pi}{2\gamma} (D^2 + m^2)^{\frac{1}{2}} \tag{B-14}$$

multiplying numerator and denominator by cosh (B), and utilizing equation (C-12), equation (B-13) may be written

$$S_2 = \frac{\pi}{4} \sum_{m\ \text{odd}}^{\infty} \frac{(-1)^{\frac{m-1}{2}} \cos(mz') \cosh\left(\frac{By}{b}\right)}{m(D^2 + m^2) \cosh(B)} \tag{B-15}$$

Substituting (C-5), (B-12), and (B-15) into (B-7) yields

$$E_1 = \frac{\pi^3}{16} \left\{ \frac{\pi}{4D^2} \left[1 - \frac{\cosh(Dz')}{\cosh\left(\frac{\pi D}{2}\right)} \right] - \sum_{m\ \text{odd}}^{\infty} \frac{(-1)^{\frac{m-1}{2}} \cos(mz') \cosh\left(\frac{By}{b}\right)}{m(D^2 + m^2) \cosh(B)} \right\} \tag{B-16}$$

The method of evaluation of E_2 is similar to that for E_1. It is first rewritten, factored, and the new sums evaluated. Rewriting and factoring yields

$$E_2 = \sum_{m\ \text{odd}}^{\infty} \left[\frac{1}{m^2} \sum_{n\ \text{odd}}^{\infty} \frac{1}{n^2 (m^2 + \gamma^2 n^2 + D^2}} \right]$$

$$= \sum_{m\ \text{odd}}^{\infty} \left[\frac{1}{m^2} \sum_{n\ \text{odd}}^{\infty} \left(\frac{1}{m^2 + D^2} \right) \left(\frac{1}{n^2} - \frac{\gamma^2}{m^2 + \gamma^2 n^2 + D^2} \right) \right] \qquad \text{(B-17)}$$

Regrouping

$$E_2 = \sum_{m\ \text{odd}}^{\infty} \left[\frac{1}{m^2} \left(\frac{1}{m^2 + D^2} \right) \cdot \sum_{n\ \text{odd}}^{\infty} \frac{1}{n^2} \right] - \sum_{m\ \text{odd}}^{\infty} \left[\frac{1}{m^2} \left(\frac{1}{m^2 + D^2} \right) \right.$$

$$\left. \cdot \sum_{n\ \text{odd}}^{\infty} \frac{\gamma^2}{m^2 + \gamma^2 n^2 + D} \right] \qquad \text{(B-18)}$$

Now from (C-14)

$$\sum_{n\ \text{odd}}^{\infty} \frac{1}{n^2} = \frac{\pi^2}{8} \qquad \text{(C-14)}$$

Also, the first term in (B-18) may be factored to give

$$S_3 = \frac{\pi^2}{8 D^2} \left(\frac{\pi^2}{8} - \pi^2 \sum_{m\ \text{odd}}^{\infty} \frac{1}{m^2 \pi^2 + D^2 \pi^2} \right) \qquad \text{(B-19)}$$

Now

$$\sum_{m\ \text{odd}}^{\infty} \frac{1}{m^2\pi^2 + 4C_1^2} = \frac{\tanh(C_1)}{8C_1} \tag{C-16}$$

where C_1 is an arbitrary constant that does not involve m. If $C_1 = \pi D/2$, then the sum in (B-19) may be replaced and

$$S_3 = \frac{\pi^2}{8D^2}\left(\frac{\pi^2}{8} - \frac{\pi^2}{8}\,\frac{\tanh(\pi D/2)}{\left(\frac{\pi D}{2}\right)}\right) \tag{B-20}$$

Rewriting the sum involving n in the last part of (B-18) and again using (C-16) with $C_1 = (\pi/2\gamma)(m^2 + D^2)^{\frac{1}{2}}$ yields

$$\sum_{n\ \text{odd}}^{\infty} \frac{\gamma^2}{\gamma^2 n^2 + m^2 + D^2} = \sum_{n\ \text{odd}}^{\infty} \frac{1}{n^2 + \frac{m^2 + D^2}{\gamma^2}} = \sum_{n\ \text{odd}}^{\infty} \frac{\pi^2}{n^2\pi^2 + \pi^2\left(\frac{m^2 + D^2}{\gamma^2}\right)}$$

$$= \frac{\pi^2 \tanh\left[\frac{\pi}{2\gamma}(m^2 + D^2)^{\frac{1}{2}}\right]}{8\left(\frac{\pi}{2\gamma}\right)(m^2 + D^2)^{\frac{1}{2}}} \tag{B-21}$$

Substituting (B-20) and (B-21) into (B-18) gives

$$E_2 = \frac{\pi^4}{(64D^2)}\left(1 - \frac{\tanh\left(\frac{\pi}{2}D\right)}{\pi D/2}\right) - \sum_{m\ \text{odd}}^{\infty} \frac{\pi^2 \tanh\left[\frac{\pi}{2\gamma}(m^2 + D^2)^{\frac{1}{2}}\right]}{8(\pi/2\gamma)\, m^2 (m^2 + D^2)(m^2 + D^2)^{\frac{1}{2}}} \tag{B-22}$$

Define

$$F_1 = E_1 \left(\frac{256}{\pi^6}\right) \tag{B-23}$$

and

$$F_2 = - \frac{256}{\pi^6} E_2 \tag{B-24}$$

Since

$$\frac{u}{\bar{U}} = \frac{E_1}{E_2} \tag{B-4}$$

then

$$\frac{u}{\bar{U}} = \frac{F_1}{F_2} \tag{B-25}$$

which is equation (18) and

$$F_1 = \left(\frac{1}{(\beta a)^2 + Ha^2}\right)\left(\frac{\cosh\{[(\beta a)^2 + Ha^2]^{\frac{1}{2}} z/a\}}{\cosh\{[(\beta a)^2 + Ha^2]^{\frac{1}{2}}\}} - 1\right)$$

$$+ \frac{16}{\pi^3} \sum_{m \text{ odd}}^{\infty} \frac{(-1)^{\frac{m-1}{2}} \cos(mz') \cosh\{[D^2 + m^2]^{\frac{1}{2}} y'/\gamma\}}{m(D^2 + m^2) \cosh\{\frac{\pi}{2\gamma}[D^2 + m^2]^{\frac{1}{2}}\}} \tag{B-26}$$

and

$$F_2 = \left(\frac{1}{(\beta a)^2 + Ha^2}\right)\left(\frac{\tanh\{[(\beta a)^2 + Ha^2]^{\frac{1}{2}}\}}{[(\beta a)^2 + Ha^2]^{\frac{1}{2}}} - 1\right)$$

$$+ \frac{32}{\pi^4} \sum_{m \text{ odd}}^{\infty} \frac{\tanh\{\frac{\pi}{2\gamma}[m^2 + D^2]^{\frac{1}{2}}\}}{m^2(m^2 + D^2)(\pi/2\gamma)(m^2 + D^2)^{\frac{1}{2}}} \tag{B-27}$$

which are equations (19) and (20) of Chapter II.

Comparison of equations (B-26) and (B-27) for Ha=0 with equation (18) of reference (19) reveals that the equations are identical which was to be expected.

It is also of interest to derive the velocity profile for the parallel plate channel from equation (17). The parallel plate channel corresponds to $\gamma=0$ or $b\to\infty$. Inspection of (B-26) and (B-27) reveals that the terms involving γ are contained in the summation. Taking the limit as $\gamma \to 0$ in (B-26) yields

$$\lim_{\gamma \to 0} \frac{\cosh\left[\frac{\pi}{2\gamma}\left(D^2 + m^2\right)^{\frac{1}{2}} \frac{y}{b}\right]}{\cosh\left[\frac{\pi}{2\gamma}\left(D^2 + m^2\right)^{\frac{1}{2}}\right]}$$

$$= \lim_{\gamma \to 0} \frac{\cosh\left[\frac{\pi}{2}\left(D^2 + m^2\right)^{\frac{1}{2}} \frac{y}{a}\right]}{\cosh\left[\frac{\pi}{2\gamma}\left(D^2 + m^2\right)^{\frac{1}{2}}\right]} = 0 \qquad \text{(B-28)}$$

since a remains finite and non-zero and cosh(s) becomes large for large s, where s is a dummy variable. In (B-27), taking the limit as $\gamma \to 0$ yields

$$\lim_{\gamma \to 0} \gamma \tanh\left[\frac{\pi}{2\gamma}\left(m^2 + D^2\right)^{\frac{1}{2}}\right] = \lim_{\gamma \to 0} \gamma \frac{1 - \exp\left(\frac{-\pi(m^2+D^2)^{\frac{1}{2}}}{\gamma}\right)}{1 + \exp\left(\frac{-\pi(m^2+D^2)^{\frac{1}{2}}}{\gamma}\right)}$$

$$= 0 \qquad \text{(B-29)}$$

Thus (16) reduces to

$$\frac{u}{\bar{U}} = \frac{F_1}{F_2} = \frac{\cosh\{[(\beta a)^2 + Ha^2]^{\frac{1}{2}} z/a\} - \cosh\{[(\beta a)^2 + Ha^2]^{\frac{1}{2}}\}}{\frac{\sinh\{[(\beta a)^2 + Ha^2]^{\frac{1}{2}}\}}{[(\beta a)^2 + Ha^2]^{\frac{1}{2}}} - \cosh\{[(\beta a)^2 + Ha^2]^{\frac{1}{2}}\}} \qquad \text{(B-30)}$$

For fully developed flow, $\beta = 0$, so that

$$\left(\frac{u}{\bar{U}}\right)_{fd} = \frac{\cosh[Ha(z/a)] - \cosh(Ha)}{\frac{\sinh(Ha)}{Ha} - \cosh(Ha)} = \frac{Ha[\cosh(Ha) - \cosh(Ha(z/a))]}{Ha\cosh(Ha) - \sinh(Ha)} \qquad \text{(B-31)}$$

which is the Hartmann profile for fully developed flow through a parallel plate channel as given in Reference (52).

It may also be shown that (B-30) reduces to fully-developed parabolic profile for Ha=0. Rewriting (B-30) with Ha=0 and letting $\beta \to 0$ (fully-developed criterion) yields

$$\left(\frac{u}{\bar{U}}\right)_{fd} = \lim_{\beta \to 0} \frac{\beta a[\cosh(\beta z) - \cosh(\beta a)]}{\sinh(\beta a) - \beta a \cosh(\beta a)} \qquad \text{(B-32)}$$

Now this limit cannot be determined as written since it reduces to the indeterminate form 0/0. However, both numerator and denominator are differentiable, so that the hypotheses of l'Hospital's Rule are met (53). When these operations are carried out and the limit taken, again the limit assumes the form 0/0, making

it necessary to apply 1'Hospital's Rule once more. This operation still yields an indeterminate form. Another application of 1'Hospital's Rule is needed and yields, after combination of terms,

$$\left(\frac{u}{\bar{U}}\right)_{fd} = \lim_{\beta \to 0} \frac{\beta a(z^3 \sinh(\beta z) - a^3 \sinh(\beta a) + 3a(z^2 \cosh(\beta z) - a^2 \cosh(\beta a))}{-\beta a^4 \sinh(\beta a) - 2a^3 \cosh(\beta a)} \quad \text{(B-33)}$$

Finally the limit may be taken and the result is

$$\left(\frac{u}{\bar{U}}\right)_{fd} = \frac{3a(z^2 - a^2)}{-2a^3} = \frac{3}{2}(1 - z^2/a^2) \quad \text{(B-34)}$$

which is the parabolic profile for fully developed flow between parallel plates as given in Reference (54). Thus at the limiting values, the solution for the velocity profile agrees with that found by other methods.

APPENDIX C

EVALUATION AND CONVERGENCE OF SERIES

In the reduction of the doubly infinite series of equation (15), as given in Appendix B, use has been made of several relationships involving the evaluation of particular series. It is the purpose of this appendix to justify these relationships.

The first expression of interest is the expansion of the constant 1 in a Fourier cosine series; i.e.,

$$1 = \sum_{m \text{ odd}}^{\infty} C_m \cos\left(\frac{m\pi z}{2a}\right) \qquad -a < z, < a \tag{C-1}$$

where the C_m are to be determined and the summation is taken over odd values only. To evaluate the constants C_m, both sides are multiplied by $\cos(\pi r\, z/2a)$ where r is an arbitrary odd integer. Integration of both sides from -a to +a yields

$$\int_{-a}^{a} \cos\left(\frac{r\pi z}{2a}\right) dz = \sum_{m \text{ odd}}^{\infty} C_m \int_{-a}^{a} \cos\left(\frac{r\pi z}{2a}\right) \cos\left(\frac{m\pi z}{2a}\right) dz \tag{C-2}$$

Now from the orthogonality of $\cos(m\pi z/2a)$ on the interval (-a, a) it follows that

$$\int_{-a}^{a} \cos\left(\frac{r\pi z}{2a}\right) \cos\left(\frac{m\pi z}{2a}\right) dz = \begin{cases} 0 & m \neq r \\ a & m = r \end{cases} \tag{C-3}$$

Thus

$$C_r = \frac{2}{r\pi}\left(2 \sin\left(\frac{r\pi}{2}\right)\right) = \frac{4}{r\pi}\left(-1\right)^{\frac{r-1}{2}} \tag{C-4}$$

and

$$1 = \sum_{m \text{ odd}}^{\infty} \frac{4\left(-1\right)^{\frac{m-1}{2}}}{m\pi} \cos\left(\frac{m\pi z}{2a}\right) \qquad -a < z < a \tag{C-5}$$

Since m and z can be considered dummy variables in (C-5), this relationship may also be written

$$1 = \sum_{n \text{ odd}}^{\infty} \frac{4\left(-1\right)^{\frac{n-1}{2}}}{n\pi} \cos\left(\frac{n\pi y}{2b}\right) \qquad -b < y < b \tag{C-6}$$

Also, it is obvious that if the constant 1 is expanded by a doubly infinite series, the procedure outlined above leads to the result

$$1 = \frac{16}{\pi^2} \sum_{m \text{ odd}}^{\infty} \sum_{n \text{ odd}}^{\infty} \frac{\left(-1\right)^{\frac{m+n}{2}-1}}{mn} \cos\left(\frac{m\pi z}{2a}\right) \cos\left(\frac{n\pi y}{2b}\right) \tag{C-7}$$

for

$$-a < z < a \quad \text{and} \quad -b < y < b$$

which is equation (8).

It is also desired to expand the hyperbolic cosine function (cosh) in a Fourier series. Using $C_1\, y/b$ as the argument of the hyperbolic cosine, where C_1 is an arbitrary constant, the Fourier series is

$$\cosh(C_1\, y/b) = \sum_{n\ \text{odd}}^{\infty} C_n \cos\left(\frac{n\pi y}{2b}\right) \qquad -b < y < b \tag{C-8}$$

On taking advantage of the orthogonality of $\cos\left(\frac{n\pi y}{2b}\right)$ on the interval (-b, b) by multiplying both sides by $\cos\left(\frac{r\pi y}{2b}\right)$ and integrating from -b to b, C_n may be expressed as

$$C_n = \frac{1}{b}\int_{-b}^{b} \cos\left(\frac{n\pi y}{2b}\right) \cosh(C_1\, y/b)\, dy \tag{C-9}$$

Evaluation of the integral on the right hand side is accomplished by integrating by parts successively. This results in the integral to be evaluated appearing as a term on both sides of the equation and it is then only a matter of solving for the value of the integral. In this case, the result is

$$\int_{-b}^{b} \cos\left(\frac{n\pi y}{2b}\right) \cosh(C_1\, y/b)\, dy = \frac{4bn\pi \cosh(C_1)\left(-1\right)^{\frac{n-1}{2}}}{r^2\pi^2 + 4C_1^2} \tag{C-10}$$

Thus

$$C_n = \frac{4n\pi\left(-1\right)^{\frac{n-1}{2}} \cosh(C_1)}{n^2\pi^2 + 4C_1^2} \tag{C-11}$$

and

$$\cosh(C_1\, y/b) = \sum_{n\ \text{odd}}^{\infty} \frac{\left(-1\right)^{\frac{n-1}{2}} \left(4n\pi\right) \cos\left(\frac{n\pi y}{2b}\right) \cosh\left(C_1\right)}{n^2\pi^2 + 4C_1^2} \tag{C-12}$$

for $-b < y < b$. Equation (C-12) is also valid if y, b, and n are replaced by z, a, and m, respectively.

In order to make further use of the results of this section, it is necessary to investigate the convergence of the series in equations (C-5) and (C-12). According to Churchill (55), if the function is continuous on the interval (-a, a), if its derivative is sectionally continuous on this interval, and if f(-a)=f(a), then the convergence of the Fourier series representation of the function on this interval is absolute and uniform with respect to the variable z on that interval. For equation (C-5), the function f(z)=1 is obviously continuous on (-a, a), its derivative is also continuous on (-a, a), and f(-a)=f(a)=1. Since the hypotheses of the theorem are met, it follows that the series of equation (C-5) converges uniformly to the function f(z)=1. For equation (C-12), the function $f(y)=\cosh(C_1 y/b)$ satisfies all of the hypotheses of the theorem on the interval (-b, b) so that the uniform convergence of the series to the function it represents is assured.

It is now desired to integrate the series of interest term by term. From the properties of Fourier series, the term-by-term integration is valid as long as the function expressed by the series is sectionally continuous (55). All series of interest have this property. Thus

$$\int_{-a}^{a} 1\,dz = \sum_{m\ \text{odd}}^{\infty} \frac{4}{\pi} \int_{-a}^{a} \frac{(-1)^{\frac{m-1}{2}}}{m} \cos\left(\frac{m\pi z}{2a}\right) dz \qquad \text{(C-13)}$$

which reduces to

$$\frac{\pi^2}{8} = \sum_{m \text{ odd}}^{\infty} \frac{1}{m^2} = \sum_{n \text{ odd}}^{\infty} \frac{1}{n^2} \qquad \text{(C-14)}$$

Similarly

$$\int_{-b}^{b} \cosh\left(C_1 \, y/b\right) dy = 4\pi \sum_{n \text{ odd}}^{\infty} \frac{(-1)^{\frac{n-1}{2}} \cosh(C_1)\, n}{n^2\pi^2 + 4C_1^2} \int_{-b}^{b} \cos\left(\frac{n\pi y}{2b}\right) dy \qquad \text{(C-15)}$$

which reduces to

$$\frac{2b}{C_1} \sinh(C_1) = 16b \cosh(C_1) \sum_{n \text{ odd}}^{\infty} \frac{1}{n^2\pi^2 + 4C_1^2}$$

or

$$\sum_{n \text{ odd}}^{\infty} \frac{1}{n^2\pi^2 + 4C_1^2}^2 = \frac{\tanh(C_1)}{8C_1} \qquad \text{(C-16)}$$

The convergence of the series in (C-14) and (C-16) follows directly by the comparison test using the convergent series

$$T_1 = \sum_{m \text{ odd}}^{\infty} \frac{1}{m^{3/2}} \qquad \text{(C-17)}$$

as the test series.

It is also necessary to investigate the convergence of the series contained in F_1 and F_2 (Equations (19) and (20)). To prove convergence of the series in F_1,

it is first noted that

$$\frac{\cosh\left[\frac{\pi}{2\gamma}\left(D^2+m^2\right)^{\frac{1}{2}}\, y/b\right]}{\cosh\left[\frac{\pi}{2\gamma}\left(D^2+m^2\right)^{\frac{1}{2}}\right]} < 1 \qquad \text{(C-18)}$$

since $-b < y < b$, and that

$$\cos\left(\frac{m\pi z}{2a}\right) < 1 \qquad \text{(C-19)}$$

for $-a < z < a$.

Also,

$$m(m^2 + D^2) \geq m^3 \qquad \text{(C-20)}$$

or

$$\frac{1}{m(m^2 + D^2)} \leq \frac{1}{m^3} \qquad \text{(C-21)}$$

Thus

$$\frac{(-1)^{\frac{m-1}{2}} \cos\left(\frac{m\pi z}{2a}\right) \cosh\left[\frac{\pi}{2\gamma}\left(D^2+m^2\right)^{\frac{1}{2}}\, y/b\right]}{m(m^2 + D^2)\cosh\left[\frac{\pi}{2\gamma}\left(D^2+m^2\right)^{\frac{1}{2}}\right]} \leq \frac{1}{m^3} \qquad \text{(C-22)}$$

Now the series

$$\sum_{m \text{ odd}}^{\infty} \frac{1}{m^3}$$

converges and since it dominates the series of equation (C-22), this series must converge also. Furthermore, this series converges uniformly on the intervals

$-b < z < a$. This property of uniform convergence will be used extensively in the evaluation of I_1 and I_2 where differentiation and integration of the series are required.

Convergence of the series of equation (20) is established by noting that

$$\tanh\left[\frac{\pi}{2\gamma}\left(D^2 + m^2\right)^{\frac{1}{2}}\right] < 1 \tag{C-23}$$

and that

$$m^2(m^2 + D^2)(m^2 + D^2)^{\frac{1}{2}} \geq m^5 \tag{C-24}$$

or

$$\frac{1}{m^2(m^2 + D^2)(m^2 + D^2)^{\frac{1}{2}}} \leq \frac{1}{m^5} \tag{C-25}$$

Now, the series

$$\sum_{m \text{ odd}}^{\infty} \frac{1}{m^5}$$

converges and thus the series of equation (20) converges also. Convergence of the series involved in calculating the velocity profile therefore has been established.

APPENDIX D

EVALUATION OF I_1 AND I_2

For ease of calculation, the following relationships are introduced:

$$C = \frac{\pi}{2} D = \left[(\beta a)^2 + Ha^2\right]^{\frac{1}{2}} \tag{D-1}$$

$$A = (D^2 + m^2)^{\frac{1}{2}} \tag{D-2}$$

$$B = \frac{\pi}{2\gamma}(D^2 + m^2)^{\frac{1}{2}} = \frac{\pi}{2\gamma}(A) \tag{D-3}$$

With these relationships, (19) and (20) may be written

$$F_1 = \frac{1}{C^2}\left(\frac{\cosh(C\,z/a)}{\cosh(C)} - 1\right) + \frac{16}{\pi^3}\sum_{m\ \text{odd}}^{\infty} \frac{(-1)^{\frac{m-1}{2}} \cos\left(\frac{m\pi z}{2a}\right)\cosh(B\,y/b)}{mA^2\cosh(B)} \tag{19}$$

and

$$F_2 = \frac{1}{C^2}\left(\frac{\tanh(C)}{C} - 1\right) + \frac{32}{\pi^4}\sum_{m\ \text{odd}}^{\infty} \frac{\tanh(B)}{mA^2B} \tag{20}$$

Using these equations, it is possible to calculate the values of the parameters I_1 and I_2 from (33) and (34).

The first term that may be evaluated is the constant $F_1|_o$, which represents the value of F_1 at the centerline of the duct. Substituting y=0 and z=0 into (19) yields

$$F_1|_o = \frac{1}{C^2}\left(\frac{1}{\cosh(C)} - 1\right) + \frac{16}{\pi^3} \sum_{m\ \text{odd}}^{\infty} \frac{(-1)^{\frac{m-1}{2}}}{mA^2 \cosh(B)} \tag{D-4}$$

Further evaluation is not necessary and $F_1|_o$ may be treated as a constant in subsequent calculations.

To calculate $I_1(\beta)$, it is first necessary to obtain the value of F_1^2. This operation gives

$$F_1^2 = \frac{1}{C^4}\left(\frac{\cosh^2(Cz/a)}{\cosh^2 C} - \frac{2\cosh(Cz/a)}{\cosh(C)} + 1\right) + \frac{2}{C^2}\left(\frac{\cosh(Cz/a)}{\cosh(C)} - 1\right)$$

$$\cdot \frac{16}{\pi^3} \sum_{m\ \text{odd}}^{\infty} \frac{(-1)^{\frac{m-1}{2}} \cos\left(\frac{m\pi z}{2a}\right)\cosh(By/b)}{m A^2 \cosh(B)}$$

$$+ \left(\frac{256}{\pi^6}\right)\left(\sum_{m\ \text{odd}}^{\infty} \frac{(-1)^{\frac{m-1}{2}} \cos\left(\frac{m\pi z}{2a}\right)\cosh(By/b)}{m^2 A^2 \cosh(B)} \right)^2 \tag{D-5}$$

This expression must now be integrated across the channel. The values of the integrals are:

$$\int_{-a}^{a}\int_{-b}^{b} \frac{1}{C^4} \frac{\cosh^2(Cz/a)}{\cosh^2(C)}\, dydz = \frac{2ba}{C^5 \cosh^2(C)}\left(\frac{\sinh(2c)}{2} + C\right) \tag{D-6}$$

$$\int_{-a}^{a}\int_{-b}^{b} \frac{2}{C^4} \frac{\cosh(Cz/a)}{\cosh(C)}\, dydz = \frac{8ab}{C^5} \tanh(C) \tag{D-7}$$

$$\int_{-a}^{a}\int_{-b}^{b}\frac{1}{C^4}\,dydz=\frac{4ab}{C^4} \tag{D-8}$$

$$\int_{-a}^{a}\int_{-b}^{b}\frac{32}{\pi^3C^2}\,\frac{\cosh(Cz/a)}{\cosh(C)}\sum_{m\ odd}^{\infty}\frac{(-1)^{\frac{m-1}{2}}\cos\left(\frac{m\pi z}{2a}\right)\cosh(By/b)}{mA^2\cosh(B)}\,dydz$$

$$=\frac{512a^2}{C^2\pi^5}\sum_{m\ odd}^{\infty}\frac{\tanh(B)}{A^5} \tag{D-9}$$

$$\int_{-a}^{a}\int_{-b}^{b}\frac{32}{\pi^3C^2}\sum_{m\ odd}^{\infty}\frac{(-1)^{\frac{m-1}{2}}\cos\left(\frac{m\pi z}{2a}\right)\cosh(By/b)}{mA^2\cosh(B)}\,dydz$$

$$=\frac{512a^2}{C^2\pi^5}\sum_{m\ odd}^{\infty}\frac{\tanh(B)}{m^2A^3} \tag{D-10}$$

Special attention is necessary to evaluate the last integral. This integral involves the square of a series. If the series is expanded and then multiplied by itself (i.e., squared), there results terms containing $\cos^2\left(\frac{m\pi z}{2a}\right)$ and terms containing $\cos\left(\frac{m\pi z}{2a}\right)\cos\left(\frac{n\pi z}{2a}\right)$ where $m \neq n$. On integrating the squared series from -a to a, it is noted that those terms involving $\cos\left(\frac{m\pi z}{2a}\right)\cos\left(\frac{n\pi z}{2a}\right)$ drop out since $\cos\left(\frac{m\pi z}{2a}\right)$ is orthogonal on the interval (-a, a). Thus a reduction in the series is accomplished. The integral may be written

$$\int_{-a}^{a} \int_{-b}^{b} \left(\frac{256}{\pi^6}\right) \sum_{m\ odd}^{\infty} \frac{\cos^2\left(\frac{m\pi z}{2a}\right) \cosh^2(By/b)}{\left(mA^2 \cosh(B)\right)^2} \, dydz$$

$$= \frac{256ab}{\pi^6} \sum_{m\ odd}^{\infty} \frac{1}{m^2 A^4 B} \left(\tanh(B) + \frac{B}{\cosh^2(B)}\right) \qquad \text{(D-11)}$$

By using (D-6, 7, 8, 9, 10, and 11), the integral of F_1^2 is

$$\int_A F_1^2 \, dA = \frac{2ab}{C^5 \cosh(C)} \left(\frac{\sinh(2c)}{2} + C\right) - \frac{8ab}{C^5} \tanh(C)$$

$$+ \frac{4ab}{C^4} + \frac{512a^2}{C^2 \pi^5} \sum_{m\ odd}^{\infty} \frac{\tanh(B)}{A^5} - \frac{512a^2}{C^2 \pi^5} \sum_{m\ odd}^{\infty} \frac{\tanh(B)}{m^2 A^3}$$

$$+ \frac{256}{\pi^6} \sum_{m\ odd}^{\infty} \frac{1}{m^2 A^4 B} \left(\tanh(B) + \frac{B}{\cosh^2(B)}\right) \qquad \text{(D-12)}$$

If now (D-12) is substituted into (33) after combination of terms and $I_1'(\beta)$ is introduced as

$$I_1'(\beta) = \frac{I_1(\beta)}{a^2 \bar{U}^2} \qquad (40)$$

then

$$I_1'(\beta) = \left(\frac{1}{F_2^2}\right)\left[\frac{2}{\gamma C^4}\left(2 + \frac{1}{\cosh^2(C)} - \frac{3\tanh(C)}{C}\right)\right.$$

$$- \frac{1536}{\pi^7} \sum_{m\ \text{odd}}^{\infty} \frac{\tanh(B)}{m^2 A^5} + \frac{256}{\pi^6 \gamma} \sum_{m\ \text{odd}}^{\infty} \frac{1}{m^2 A^4 \cosh^2(B)}$$

$$\left. - \frac{2}{\gamma}\left(F_1|_o\right)^2\right] \qquad \text{(D-13)}$$

This is the expression that was used to evaluate $I_1'(\beta)$ in the calculation of x'.

To evaluate $I_2(\beta)$ from (34), it is necessary to find $\nabla^2 F_1$, where ∇^2 is the Laplacian operator. Differentiating F_1 twice with respect to y yields

$$\frac{\partial^2 F_1}{\partial y^2} = \frac{16}{\pi^3} \sum_{m\ \text{odd}}^{\infty} \frac{(-1)^{\frac{m-1}{2}} \cos\left(\frac{m\pi z}{2a}\right)\left(\frac{B^2}{b^2}\right)\cosh(By/b)}{m A^2 \cosh(B)} \qquad \text{(D-14)}$$

Evaluating at the centerline leads to

$$\left.\frac{\partial^2 F_1}{\partial y^2}\right|_o = \frac{4}{\pi \gamma^2 b^2} \sum_{m\ \text{odd}}^{\infty} \frac{(-1)^{\frac{m-1}{2}}}{m \cosh(B)} \qquad \text{(D-15)}$$

Similarly, on differentiating with respect to z twice, the result is

$$\frac{\partial^2 F_1}{\partial z^2} = \frac{\cosh(Cz/a)}{a^2 \cosh(C)} - \frac{4}{\pi a^2} \sum_{m \text{ odd}}^{\infty} \frac{(-1)^{\frac{m-1}{2}} m \cos\left(\frac{m\pi z}{2a}\right) \cosh(By/b)}{A^2 \cosh(B)} \quad \text{(D-16)}$$

Evaluated at the centerline, (D-16) is

$$\frac{\partial^2 F_1}{\partial z^2}\Big|_o = \frac{1}{a^2 \cosh(C)} - \frac{4}{\pi a^2} \sum_{m \text{ odd}}^{\infty} \frac{(-1)^{\frac{m-1}{2}} m}{A^2 \cosh(B)} \quad \text{(D-17)}$$

Integrating (D-14), (D-15), (D-16), and (D-17) over the cross section, the results are

$$\int_{-a}^{a} \int_{-b}^{b} \frac{\partial^2 F_1}{\partial y^2} dydz = \frac{64}{\pi^3} \sum_{m \text{ odd}}^{\infty} \frac{\tanh B}{m^2 A} \quad \text{(D-18)}$$

$$\int_{-a}^{a} \int_{-b}^{b} \frac{\partial^2 F_1}{\partial y^2}\Big|_o dydz = \frac{16}{\pi\gamma} \sum_{m \text{ odd}}^{\infty} \frac{(-1)^{\frac{m-1}{2}}}{m \cosh(B)} \quad \text{(D-19)}$$

$$\int_{-a}^{a} \int_{-b}^{b} \frac{\partial^2 F_1}{\partial z^2} dydz = \frac{4 \tanh(C)}{C\gamma} \frac{64}{\pi^3} \sum_{m \text{ odd}}^{\infty} \frac{\tanh(B)}{A^3} \quad \text{(D-20)}$$

$$\int_{-a}^{a} \int_{-b}^{b} \frac{\partial^2 F_1}{\partial z^2}\Big|_o dydz = \frac{4}{\gamma \cosh(C)} - \frac{16}{\gamma\pi} \sum_{m \text{ odd}}^{\infty} \frac{(-1)^{\frac{m-1}{2}} m}{A^2 \cosh(B)} \quad \text{(D-21)}$$

The other terms appearing in (34) may be found easily. Since $F_1|_o$ is a constant,

$$\int_{-a}^{a} \int_{-b}^{b} F_1|_o \, dydz = 4ab \, F_1|_o \tag{D-22}$$

Also

$$\int_{-a}^{a} \int_{-b}^{b} F_1 \, dydz = 4ab\left[\frac{1}{C^2}\left(\frac{\tanh(C)}{C} - 1\right) + \frac{32}{\pi^4} \sum_{m \text{ odd}}^{\infty} \frac{\tanh(B)}{m^2 A^2 B}\right] \tag{D-23}$$

But the quantity inside the braces of (D-23) is, from (20), identically F_2. Thus

$$\int_{-a}^{a} \int_{-b}^{b} F_1 \, dydz = 4abF_2 \tag{D-24}$$

On substituting (D-18), (D-19), (D-20), (D-21), (D-22), and (D-23) into (34) introducing

$$I_2'(\beta) = \nu \bar{U} I_2(\beta) \tag{41}$$

and combining terms, the result is

$$I_2'(\beta) = F_2\left[\frac{64}{\pi^3} \sum_{m \text{ odd}}^{\infty} \frac{\tanh(B)}{A}\left(\frac{1}{m^2} - \frac{1}{A^2}\right) + \frac{4}{C\gamma}\left(\tanh(C) - \frac{C}{\cosh(C)}\right)\right.$$

$$\left. - \frac{16}{\pi\gamma} \sum_{m \text{ odd}}^{\infty} \frac{(-1)^{\frac{m-1}{2}}}{\cosh(B)}\left(\frac{1}{m} - \frac{m}{A^2}\right) - \frac{4Ha^2}{\gamma}\left(F_2 - F_1|_o\right)\right]^{-1} \tag{D-25}$$

This equation has been used to evaluate $I_2'(\beta)$ in the x′ calculation.

APPENDIX E

COMPUTER PROGRAM

```
        B 5 5 0 0    F O R T R A N    C O M P I L A T I O N       X.10,   SATURDAY,  2/28/70, 00143 H.

CCOMPILE BIN1021/TECH   *FORTRAN        .11S800015   *1021 FLEGAL W M            R  0000
CPROCESS=       00000001310=    00000003,                                        R  0000
CDATA,                                                                           R  0000
CDATA ABC.                                                                       R  0000
C                                                                                R  0000
FILE  5=ABC,UNIT=READER                                                          R  0000
FILE  6=DEF,UNIT=PRINTER                                                         R  0000
C   NUMERICAL SOLUTION FOR FINITE WIDTH CHANNEL                                  R  0000
                                                          START OF SEGMENT ********** 1
   49  REAL I1PRIM, I2PRIM, I1INT, I2INT                                         R  0000
   50  DIMENSION  BETAA(35),Z(10),Y(10),A(200),B(200),XPRIME(35)                 R  0000
   52     AR =1.0/6.0                                                           R  0000
   53  HA=0.0                                                                   R  0005
   54  I1INT=2.0/AR                                                             R  0006
   55  I2INT=0.0                                                                R  0009
   56  READ (5,57)  (BETAA(N),N=1,35)                                           R  0010
   57  FORMAT (10F7.2)                                                          R  0027
   58  READ (5,59)  (Z(J),J=1,10)                                               R  0027
   59  FORMAT (10F5.2)                                                          R  0044
   60  READ (5,61)  (Y(I),I=1,10)                                               R  0044
   61  FORMAT (10F5.2)                                                          R  0061
   70  WRITE (6,71)                                                             R  0061
   71  FORMAT (1H1,8X,1HZ,9X,1HY,6X,5HBETAA,7X,2HF3,4X6HXPRIME//)                R  0064
   80  J=1                                                                      R  0064
   81  I=1                                                                      R  0065
   82  N=1                                                                      R  0066
   83  AREA=0.0                                                                 R  0067
   84  PI=3.1459265                                                             R  0068
   89  DO 213 N=1,35                                                            R  0071
   90  C=SQRT(BETAA(N)**2 + HA**2)                                              R  0077
   99  DO 102  M=1,199,2                                                        R  0081
  100  C1=M                                                                     R  0088
  101  A(M)= SQRT(C1**2 +(4.0/PI**2)*C**2)                                      R  0089
  102  B(M)= (PI/(2.0*AR))*A(M)                                                 R  0096
  109  SUM1=0.0                                                                 R  0102
  110  DO 113 M=1,199,2                                                         R  0103
  111  C1=M                                                                     R  0110
  112  TERM=TANH(B(M))/(((C1**2)*(A(M)**2)*B(M))                                R  0111
  113  SUM1=SUM1 + TERM                                                         R  0117
  114  F2=(TANH(C)/C -1.0)/C**2 + (32.0/PI**4)*SUM1                             R  0119
  119  SUM2= 0.0                                                                R  0128
  120  DO 126 M=1,199,2                                                         R  0129
  121  C1=M                                                                     R  0136
  122  ZPRIME=(C1*PI*Z(J))/2.0                                                  R  0137
  123  YPRIME= B(M)*Y(I)                                                        R  0142
  124  IF (B(M)-66.0) 125,125,127                                               R  0145
  125  TERM=(((-1.0)**((M-1)/2))*COS(ZPRIME)*COSH(YPRIME))/(C1*A(M)**2          R  0151
     1 *COSH(B(M)))                                                            R  0158
  126  SUM2=SUM2 + TERM                                                         R  0162
  127  F1=(COSH(Z(J)*C)/COSH(C) -1.0)/C**2 +(16.0/PI**3)*SUM2                   R  0164
  128  F3=F1/F2                                                                 R  0175
  130  IF(J.GT.1.OR.I.GT.1) GO TO 205                                           R  0177
  131  F10=F1                                                                   R  0181
  140  SUM3=0.0                                                                 R  0182
  141  DO 144 M=1,199,2                                                         R  0183
  142  C1=M                                                                     R  0190
  143  TERM=(TANH(B(M))/A(M))*(1.0/C1**2 - 1.0/A(M)**2)                         R  0191
  144  SUM3=SUM3 + TERM                                                         R  0202
  150  SUM4=0.0                                                                 R  0204
  151  DO 155 M=1,199,2                                                         R  0205
```

```
152   C1=M                                                                  R  0212
153   IF (B(M)-66.0) 154,154,156                                            R  0213
154   TERM=((-1.0)**((M-1)/2)/COSH(B(M)))*(1.0/C1 - C1/A(M)**2)             R  0219
155   SUM4=SUM4 + TERM                                                      R  0231
156   CONTINUE                                                              R  0233
160   SUM5=0.0                                                              R  0233
161   DO 164 M=1,199,2                                                      R  0234
162   C1=M                                                                  R  0241
163   TERM= TANH(B(M))/((A(M)**5)*(C1**2))                                  R  0242
164   SUM5= SUM5 + TERM                                                     R  0248
170   SUM6=0.0                                                              R  0250
171   DO 175 M=1,199,2                                                      R  0251
                                                        SEGMENT    1 IS  256 LONG
                                                  START OF SEGMENT **********  2
172   C1=M                                                                  R  0004
173   IF (B(M)-66.0) 174,174,176                                            R  0005
174   TERM= 1.0/((C1**2)*(A(M)**4)*((COSH(B(M)))**2))                       R  0011
175   SUM6=SUM6 +TERM                                                       R  0019
176   CONTINUE                                                              R  0021
200   I1PRIM= ((2.0/(AR*C**4))*(2.0+1.0/((COSH(C))**2 -3.0*TANH(C)/C)       R  0021
     1 -((512.0*3.0)/PI**7)*SUM5+(256.0/(AR*PI**6))*SUM6                    R  0034
     1 -(2.0/AR)*(F10**2))/F2**2                                            R  0047
203   I2PRIM=F2/((4.0/(C*AR))*(TANH(C)-C/COSH(C))-(64.0/PI**3)*SUM3         R  0054
     1 -(16.0/(PI*AR))*SUM4-((4.0 *HA**2)/AR)*(F2-F10))                     R  0063
204   XPRIME(N)=(I2PRIM+I2INT)*(I1PRIM-I1INT)/2.0 + AREA                    R  0074
205   WRITE (6,206)  Z(J),Y(I), BETAA(N), F3,XPRIME(N)                      R  0081
206   FORMAT(2F10.2,F10.3,F10.4,E13.5)                                      R  0102
207   IF(J.GT.1.OR.I.GT.1) GO TO 213                                        R  0102
210   AREA=XPRIME(N)                                                        R  0106
211   I1INT=I1PRIM                                                          R  0108
212   I2INT=I2PRIM                                                          R  0109
213   CONTINUE                                                              R  0110
300   IF (J.EQ.10) GO TO 400                                                R  0111
301   J=J+1                                                                 R  0114
302   GO TO 69                                                              R  0116
400   CONTINUE                                                              R  0117
      STOP                                                                  R  0117
      END                                                                   R  0118
                                                        SEGMENT    2 IS  140 LONG
```

```
                                        SEGMENT     3 IS    20 LONG
                                        SEGMENT     4 IS   138 LONG
                                START OF SEGMENT **********    5
                                        SEGMENT     5 IS    13 LONG

NUMBER OF SYNTAX ERRORS DETECTED = 0.
PRT SIZE = 67)  TOTAL SEGMENT SIZE = 567 WORDS)  DISK SIZE = 27 SEGS)  NO. PRGM. SEGS = 32.
ESTIMATED CORE STORAGE REQUIREMENT = 2880 WORDS)  COMPILATION TIME = 47 SECS)  NO. CARDS = 96.
```

APPENDIX F

ERROR ANALYSIS

Properties

The density was the only property measured experimentally. The error in determining the volume was $\pm$ 0.5 cc out of 100cc or $\pm$ 0.5 per cent and in the weight it was $\pm$ 0.0001gm out of 10gm or $\pm$ 0.1 per cent. Thus, the error in density was estimated at $\pm$ 0.5 per cent. The corresponding error in the molar concentration was estimated at less than 5 per cent. This led to an estimated error of less than 0.5 per cent in the viscosity if it is taken from tabulated data. The estimated error in taking the electrical conductivity from the tabulated data was less than 4 per cent.

Flow Rate

The flow rate was determined from the orifice pressure drop readings. These readings were possible to $\pm$ .1 in. of Hg. This inaccuracy introduced an error of from 1 to 4 per cent in the determination of the flow rate, the larger percentage error occurring for the lower values of the pressure drop. The average velocity was known to an accuracy of between 1 and 4 per cent. Thus, the error in the Reynolds number was between 1.5 and 4 per cent, and the error in x' was of the same order of magnitude.

Velocity

The error in the velocity of the probe in the calibrator was estimated at less than 1.5 per cent. The accuracy in reading the bridge voltage was $\pm$ 1 per cent. Taking into consideration the scatter in the calibration data, it was estimated that the velocity taken from the calibration curve was accurate to within $\pm$ 3 per cent. The non-dimensional velocity was therefore accurate to within 3 to 5 per cent.

Magnetic Field

The magnetic field was found to an estimated accuracy of 4 per cent. Consequently, the Hartmann number was known to within 5 per cent when the accuracy of the electrical conductivity data was considered.

Probe Position

The probe position was known to within 0.001". The channel width was also known to within 0.001". Thus the uncertainty in the value of the non-dimensional coordinate was less than 0.5 per cent.

LITERATURE CITED

1. E. Hagenback, "On the Determination of the Viscosity of a Fluid by Flow Experiments through Tubes," Pogg. Ann. 109, 385 (1860).

2. M. J. Boussinesq, "Sur la maniere dont le vitesse, dans un tube cylindrique de section circulaire, evase a son entree, se destribuent depuis cette entree jusqu'aux endroits ou se trouve etabli un regime uniforme," Compte Rendus 113, 9-15 (1890), 49-51 (1891).

3. L. Schiller, "The Development of the Laminar Velocity Profile and its Importance for Viscosity Measurement," Zeitschrift fur angewandte Mathematik und Mechanik, 2, pp. 96 (1922).

4. R. Siegel, "The Effect of Heating on Boundary Layer Transition for Liquid Flow in a Tube," DSc Thesis, M.I.T., 1953.

5. A. H. Shapiro, R. Siegel, and S. J. Kline, "Friction Factor in the Laminar Entry Region of a Smooth Tube," Proceedings of 2nd U.S. Congress of Applied Mechanics, pp. 733 (1954).

6. W. D. Campbell and J. C. Slattery, Transactions of ASME, Journal of Basic Engineering, 85, pp. 41 (1963).

7. R. C. Gupta, "Flow Development in the Hydrodynamic Entrance Region of a Flat Duct," AIChE Journal 11, 1149 (1965).

8. S. T. McComas, "Hydrodynamic Entrance Lengths for Ducts of Arbitrary Cross Section," Trans. ASME, Journal of Basic Engineering 89, 847-850 (1967).

9. W. C. Moffatt, "Analysis of MHD Channel Entrance Flows Using the Momentum Integral Method," AIAA Journal, Vol. 2, pp. 1495 (1964).

10. A. Maciulaitis and A. L. Loeffler, "A Theoretical Investigation of MHD Channel Entrance Flows," AIAA Journal 2, pp. 2100 (1964).

11. C. W. Tan, "Laminar MHD Channel Entrance Flows," AIAA Journal 3, p. 1369 (1965).

12. R. Zalosh, "Comparison of Velocity Profiles in MHD Entrance Channel Flows," AIAA Student Journal 4, pp. 20-23, (1966).

13. R. E. Schwirian, "A New Momentum - Integral Method for Treating MHD and Simple Hydrodynamic Entrance Flows," NASA TN D-5215 (1969).

14. J. B. Heywood and W. C. Moffatt, "Validity of Integral Methods in MHD Boundary-Layer Analyses," AIAA Journal 3, pp. 1565 (1965)

15. H. Schilichting, "Laminar Channel Entrance Flow," Zeitschrift fur angewandte Mathematik und Mechanik, 14, pp. 368 (1934).

16. M. Collins and W. R. Schowalter, "Laminar Flow in the Inlet Region of a Straight Channel," Physics of Fluids 5, pp. 1122 (1962).

17. M. Roidt and R. D. Cess, "An Approximate Analysis of Laminar Magnetohydrodynamic Flow in the Entrance Region of a Flat Duct," Journal of Applied Mechanics 29, 171-176 (1962).

18. H. L. Langhaar, "Steady Flow in the Transition Length of a Straight Tube," Journal of Applied Mechanics 9, 55-58 (1942).

19. L. S. Han, "Hydrodynamic Entrance Lengths for Incompressible Laminar Flow in Rectangular Ducts," Journal of Applied Mechanics 27, 403-409 (1960).

20. E. M. Sparrow, S. H. Lin, and T. S. Lundgren, "Flow Development in the Hydrodynamic Entrance Region of Tubes and Ducts," Physics of Fluids 7, 338 (1964).

21. D. P. Fleming, "Laminar Flow in the Hydrodynamic Entrance Region of Non-Circular Ducts," Ph.D. Thesis, University of Minnesota (1968).

22. W. T. Snyder, "Magnetohydrodynamic Flow in the Entrance Region of a Parallel-Plate Channel," AIAA Journal 3, pp. 1833 (1965).

23. E. E. Goins, Jr., "The Influence of the Initial Velocity Profile on Magnetohydrodynamic Flow Development in the Entrance Region of a Parallel Plate Channel," M.S. Thesis, University of Tennessee (1965).

24. W. T. Snyder and A. H. Eraslan, "The Influence of Hall Effect and Initial Velocity on MHD Flow in the Entrance Region of a Parallel Plate Channel," AEDC-TR-67-79 (1967).

25. J. R. Bodia and J. F. Osterle, "Finite Difference Analysis of Plane Poiseuille and Couette Flow Developments," Applied Sci. Res., Section A 10, 265-276 (1961).

26. Y. S. Wang and P. A. Longwell, "Laminar Flow in the Inlet Section of Parallel Plates," AIChE Journal 10, pp. 323 (1964).

27. J. S. Shohet, J. F. Osterle, and F. J. Young, "Velocity and Temperature Profiles for Laminar Magnetohydrodynamic Flow in the Entrance Region of a Plane Channel," Physics of Fluids 5, 545-549 (1962).

28. C. L. Hwang and L. T. Fan, "A Finite Difference Analysis of Laminar Magnetohydrodynamic Flow in the Entrance Region of a Flat Rectangular Duct," Applied Scientific Research B10, pp. 329 (1963).

29. A. Brandt and J. Gillis, "Magnetohydrodynamic Flow in the Inlet Region of a Straight Channel," Physics of Fluids 9, pp. 690 (1966).

30. C. L. Hwang, K. C. Li, and L. T. Fan, "Magnetohydrodynamic Channel Entrance Flow with Parabolic Velocity at the Entry," Physics of Fluids 9, pp. 1134 (1966).

31. J. A. Shercliff, "Entry of Conducting and Non-Conducting Fluids in Pipes," Proceedings of the Cambridge Philosophical Society 52, pp. 573 (1956).

32. F. J. Hale and J. C. Kerrebrock, "Insulator Boundary Layers in Magnetohydrodynamic Channels," AIAA Journal 2, pp. 461 (1964).

33. U. P. Hwang, L. T. Fan, and C. L. Hwang, "Compressible Laminar MHD Flow inside a Flat Duct with Heat Transfer," AIAA Journal, Vol. 5, p. 2113 (1967).

34. L. Schiller and H. Kirsten, "Die Entwicklung der Geschwendigkeitsverteilung bei der Turbulent Rohrstromung," Zeitschrift für Technische Physik 10, pp. 268 (1929).

35. A. H. Shapiro and R. D. Smith, "Friction Coefficients in the Inlet Length of Smooth, Round Tubes," NACA TN 1785 (1948).

36. R. G. Deissler, "Analytical and Experimental Investigation of Adiabatic Turbulent Flow in Smooth Tubes," NACA TN 2138 (1950).

37. J. Kaye, G. A. Brown, J. J. Dieckmann, and E. A. Sziklas, "Experimental Velocity Profiles for Supersonic Flow of Air in a Tube with and without Heat Transfer," Proceedings of the U. S. Congress of Applied Mechanics, pp. 787 (1954).

38. T. F. Irvine, Jr., and E. R. G. Eckert, "Comparison of Experimental Entrance Pressure Drops in Ducts with Rectangular and Triangular Cross Sections," Journal of Applied Mechanics 25, pp. 288 (1958).

39. R. M. Olsen and E. M. Sparrow, "Measurements of Turbulent Flow Development in Tubes and Annuli with Square or Rounded Entrances," AIChE Journal 9, pp. 766 (1963).

40. S. T. McComas and E. R. G. Eckert, "Laminar Pressure Drop Associated with the Continuum Entrance Region and for Slip Flow in a Circular Tube," Journal of Applied Mechanics, Vol. 32, 765 (1965).

41. N. S. Berman and V. A. Santos, "Laminar Velocity Profiles in Developing Flows Using a Laser Doppler Technique," AIChE Journal 15, pp. 383 (1969).

42. B. Atkinson, Z. Kemblowski, and J. M. Smith, "Measurements of Velocity Profiles in Developing Liquid Flows," AIChE Journal 13, pp. 17 (1967).

43. E. M. Sparrow, C. W. Hixon, and G. Shavit, "Experiments on Laminar Flow Development in Rectangular Ducts," Journal of Basic Engineering, Transactions of ASME 89, pp. 116 (1967).

44. R. J. Goldstein and D. K. Kreid, "Measurement of Laminar Flow Development in a Square Duct Using a Laser-Doppler Flowmeter," Journal of Applied Mechanics, Transactions of ASME 89, pp. 813 (1967).

45. J. Hartmann and F. Lazarus, "Experimental Investigations of the Flow of Mercury in a Homogeneous Magnetic Field," Danske Videnshabernes Seskab, Mathematisk-Fysiske Meddeleser 15, No. 7 (1937).

46. W. Murgatroyd, "Experiments on MHD Channel Flows," Philosophical Magazine 44, pp. 1348 (1953).

47. A. Maciulaitis, A. L. Loeffler, and P. J. Calcanes, "Experimental Investigation of MHD Flows through Circular Pipes at High Hartmann and Reynolds Numbers," Electricity From MHD, Vol. 2, International Atomic Energy Agency, pp. 879 (1966).

48. A. I. Khozahainov, "Experimental Study of the Initial Region of a Square Magnetohydrodynamic Channel Taking Account of the Inhomogeneity of the Magnetic Field in the Longitudinal Direction," Soviet Physics - Technical Physics 10. pp. 1213 (1966).

49. Handbook of Chemistry and Physics, 50th Edition, Chemical Rubber Co., Cleveland, (1969).

50. R. H. Stokes and R. Mills, Viscosity of Electrolytes and Related Properties, Oxford: Pergamon Press, (1965).

51. R. A. Robinson and R. H. Stokes, Electrolyte Solutions, Academic Press, Inc., New York (1959).

52. G. W. Sutton and A. Sherman, Engineering Magneto hydrodynamics, McGraw-Hill Co., Inc., New York, (1965).

53. R. C. Fisher and A. D. Zieber, Calculus and Analytic Geometry, Prentice-Hall, Inc., Englewood Cliffs, New Jersey, p. 638 (1962).

54. S. Eskinazi, Principles of Fluid Mechanics, Allyn and Bacon, Inc., Boston, pp. 361-365 (1962).

55. R. V. Churchill, Fourier Series and Boundary Value Problems, McGraw-Hill, Inc., New York, pp. 102-109 (1963).

VITA

William Malcolm Flegal was born in Chattanooga, Tennessee, on June 11, 1945. He is the son of Mr. and Mrs. Harry Flegal of Rossville, Georgia.

He was educated in the public schools of Rossville, Georgia, graduating from Rossville High School as its valedictorian in 1962. He entered the Georgia Institute of Technology where he received a Bachelor of Mechanical Engineering degree with honor in 1966. During his undergraduate studies, he was elected to Tau Beta Pi engineering honorary fraternity, Pi Tau Sigma mechanical engineering honorary fraternity, and Phi Kappa Phi. He entered the Graduate Division of the Georgia Institute of Technology in September, 1966, and received the Master of Science in Mechanical Engineering degree in 1968.

On October 5, 1968, he was married to Prentiss Lee Irwin of Decatur, Georgia.